DEVELOPING A CORTICALLY-BASED VISUAL PROSTHESIS

FOR THE BLIND IN A CHRONIC NONHUMAN

PRIMATE MODEL

by

Tyler Scott Davis

A dissertation submitted to the faculty of
The University of Utah
in partial fulfillment of the requirements for the degree of

Doctor of Philosophy

Department of Bioengineering

The University of Utah

May 2013

The University of Utah Graduate School

STATEMENT OF DISSERTATION APPROVAL

The dissertation of   **Tyler Scott Davis**

has been approved by the following supervisory committee members:

Bradley Greger	, Chair	**12/7/2012**
		Date Approved
Richard Normann	, Member	**12/7/2012**
		Date Approved
Paul House	, Member	**12/7/2012**
		Date Approved
John White	, Member	**12/7/2012**
		Date Approved
Alessandra Angelucci	, Member	**12/7/2012**
		Date Approved

and by   **Patrick Tresco**   , Chair of

the Department of   **Bioengineering**

and by Donna M. White, Interim Dean of The Graduate School.

ABSTRACT

This dissertation provides an in-depth evaluation of microstimulation of the primary visual cortex (V1) using chronically implanted Utah Electrode Arrays (UEAs) in macaque monkeys for use as a visual prosthesis.

Within the scope of this dissertation are several significant contributions. First, a minimally invasive and robust device for head fixation was developed. In comparison to other available designs, this device improved long-term outcomes by providing a stronger, less invasive interface that reduced the risk of infection. This device made it possible to acquire chronic microstimulation data in macaque monkeys. It has been tested on three animals and has provided a stable interface for over two years.

Second, this dissertation is the first to describe the factors influencing the performance and safety of microstimulation of V1 with the UEA. Two UEAs were implanted in V1 of two macaque monkeys, and experiments were performed several months following implantation. The electrical and recording properties of the electrodes and the high-resolution visuotopic organization of V1 were measured. In addition, threshold stimulation levels that evoked behavioural responses using single electrodes were determined. Periodic microstimulation at currents up to 96 μA did not impair the ability to record neural signals and did not affect the animal's vision where the UEAs were implanted. It was discovered, however, that microstimulation at these levels evoked behavioural responses on only 8 of 82 systematically stimulated electrodes. It was

suggested that the ability to evoke behavioral responses may depend on the location of the electrode tips within the cortical layers of V1, the distance of the electrode tips to neuronal somata, and the inability of nonhuman primates to recognize and respond to a generalized set of evoked percepts.

Finally, this dissertation is the first to describe the spatial and temporal characteristics of microstimulation of V1 with the UEA over chronic time periods. Two years after implantation, it was found that consistent behavioural responses could be evoked during simultaneous stimulation of multiple contiguous electrodes. Saccades to electrically-evoked targets using groups of nine electrodes showed that the animal could discriminate spatially distinct percepts with a resolution comparable to the current epi-retinal prostheses. These results demonstrate chronic perceptual functionality and provide evidence for the feasibility of a UEA-based visual prosthesis for the blind.

TABLE OF CONTENTS

LIST OF FIGURES

CHAPTER 1

INTRODUCTION

Profound blindness is a prevalent cause of disability and poses extraordinary

challenges to individuals in our predominantly sight reliant society. Living with acquired

blindness lowers the quality of life and results in large societal costs due to increased

healthcare burden and the loss of productivity. Globally, in the year 2002, 36 million

people were classified as blind [1]. Despite large efforts to prevent blindness, this number

has increased to 39 million in 2010 [2]. In the United States alone, the annual economic

impact was found to be $5.5 billion spent for medical care and a loss of more than

209,000 quality-adjusted life years [3]. A significant percentage of blindness is caused by

diseases such as glaucoma and age-related macular degeneration [2]. Other causes

include traumatic injury to the eye and its connections to the brain. Currently, there are

no effective treatments for these causes of blindness. While genetic and regenerative

interventions can provide therapeutic solutions to some of these conditions, such

approaches are only recently being investigated with limited success. Further, it is

unknown how these approaches could restore functional vision when the retina and the

initial visual pathways are fully degenerate or destroyed. In contrast, neural prosthetic

approaches have already allowed thousands of deaf patients to hear sounds and acquire

language abilities [4-6]. These observations provide compelling reasons to pursue the

development of neural prosthetic systems to restore some level of useful vision in the profoundly blind.

The concept of restoring sight to individuals with profound blindness by electrical stimulation at a location along the visual pathway has existed for many years. Groups have explored stimulation of visual areas including the retina, optic nerve, lateral geniculate nucleus (LGN), and the primary visual cortex (V1) [7-18]. Each of these approaches employs a similar device concept, which involves electrical stimulation of the visual system using groups of electrodes to generate patterns of useful visual percepts. For many of these approaches, a video camera could be used to capture the visual scene in front of a blind subject. The video stream would then be converted into a spatio-temporal pattern of electrical pulses and delivered to the implanted electrodes to generate a two-dimensional representation of the visual scene that could be used by the subject for reading and navigation. A conceptual image of a V1-based prosthesis that uses Utah Electrode Arrays (UEAs) is shown in Figure 1.1.
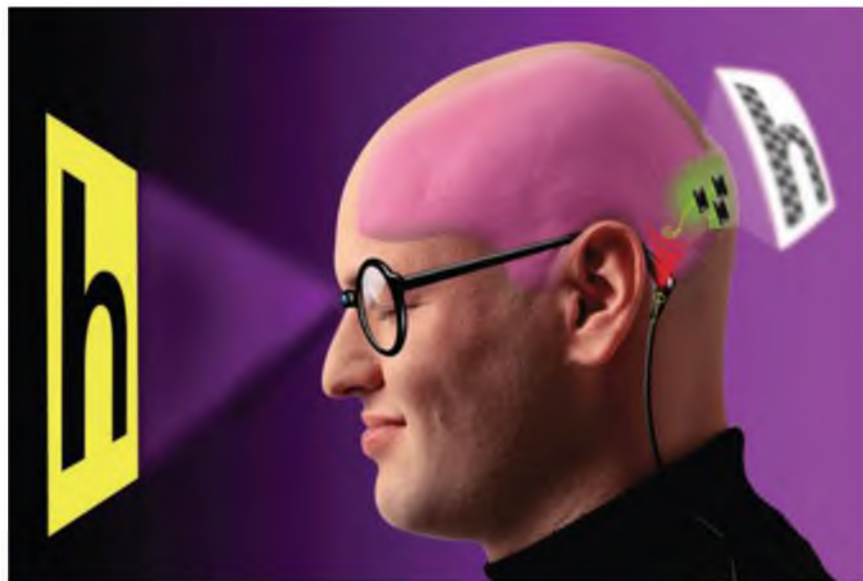
Figure 1.1. Conceptual image of a UEA-based visual prosthesis.

Recent technological advancements and the work of groups worldwide have turned concept into reality. Focus has changed from whether it is possible to evoke visual percepts during electrical stimulation of the visual pathways to questions of how to optimize these percepts for maximum benefit. Groups are interested in ways to improve biocompatibility and stability, as well as, the quality and resolution of the evoked percepts. Researchers are trying to understand the minimum requirements for a useful prosthesis. One study attempted to quantify the minimum resolution needed for a prosthesis to be useful. In this study, subjects navigated an obstacle course and read text while wearing a phosphene simulator that pixelated their vision. It was determined that 625 electrodes implanted in a 1 cm^2 area near the foveal representation in V1 could produce a phosphene image that would restore an acuity of 20/30 and allow reading of fixed text at a rate of 100 words/min [19-21]. Many of the devices that are being tested today, however, contain much fewer than 625 electrodes. The Argus II epiretinal prosthesis from Second Sight, for example, contains an array of only 60 electrodes, but has been shown to provide significant improvements in several tasks of daily living [7, 10, 22]. Increasing electrode density and, subsequently, the resolution of the system is only one of many factors influencing the usefulness of a visual prosthesis. Other factors include surgical accessibility, stability and nature of stimuli, and target population. Each of the previously mentioned approaches addresses these factors differently and come with a unique set of advantages and disadvantages.

Background

Some groups have targeted the optic nerve or the LGN as potential sites for a visual prosthesis. One group has implanted a cuff electrode on the optic nerve of a human patient with Retinitis Pigmentosa and has demonstrated a limited degree of pattern recognition and orientation discrimination [16, 17, 23]. Another group has provided proof-of-concept for a LGN prosthesis by measuring saccades to phosphenes during electrical stimulation via electrodes in the LGN in behaving monkeys [11]. Each of these approaches, however, target structures that contain a representation of visual space in compact and difficult to access regions of the brain. The optic nerve carries the entire representation of visual space within a ~3 mm diameter structure that contains approximately 1.2 million axons [24]. Interfacing with such a densely consolidated structure to provide the complex patterns of focal stimulations that are needed for a useful prosthesis poses a challenge. Further, interventions at both the optic nerve and LGN require intact retinal ganglion cells (RGCs) and are, therefore, limited to treating blindness caused by diseases of the retina. Diseases such as glaucoma that damage the axons of RGCs or traumatic injury to the eye and its connections to the visual cortex can only be treated with a cortically-based visual prosthesis.

Due to the challenges of the optic nerve and LGN approaches, recent effort has focused on the retinal and V1 approaches for a visual prosthesis. Several groups worldwide are pursuing prostheses based upon retinal stimulation and are developing sophisticated microelectronic interfaces in the hopes of restoring functional vision [13, 23, 25-28]. To date, over 20 different devices are under development, and at least five groups are pursuing human clinical trials either with acute or chronic implantation of

neurostimulating devices [12, 25, 27]. Retinal microstimulation via arrays of stimulating electrodes has allowed subjects to recognize individual alphanumeric characters and to achieve limited visual navigation [18, 22, 29-31]. The Second Sight Argus II System is the world's first commercially available visual prosthesis. For this device, an RF inductive coil link is used to transmit power and data from an externally worn video camera to an internally placed stimulator that consists of an array of 60 epiretinal microelectrodes. In a single-arm, prospective, multicenter clinical trial, 30 patients were implanted with the device, and subjects were found to performed statistically better with the system on versus off. This device was shown to provide a 96% improvement in object localization, 57% improvement in motion discrimination and a 23% improvement in discrimination of oriented gratings. The best recorded visual acuity was 20/1260 [10]. Another group has developed a subretinal prosthesis that consists of an array of 1500 active microphotodiodes that control the stimulus level of adjacent microelectrodes. With this device, the visual scene is projected naturally onto the microphotodiodes through the lens of the eye, resulting in light-dependent control of the level of stimulation. This device was implanted in several human patients in a recent investigational study. One of the patients was able to perform object identification, navigate an unfamiliar environment, and read large print letters with a visual acuity of 20/1000 [18]. The level of visual restoration achieved by these two studies has been the result of over a decade of research and development.

Advanced forms of retinal blindness lead to extensive remodeling of the retina and its neural connections to the brain [32]. This remodeling of the neural architecture could disrupt the way that information from stimulation is transmitted to higher areas of

the brain and may pose a challenge to the retinal approach of vision restoration. Additionally, some causes of blindness involve damage to the retina itself or its connections via the optic nerve to the LGN and the visual cortex. Glaucoma is an example of a disease that causes this type of blindness by damaging the axons of the RGCs as they exit the eye via the optic disc. This disease is prevalent worldwide and was estimated to cause bilateral blindness in approximately 8.4 million people in 2010 [33]. Because degeneration or damage to these early visual pathways does not appear to affect higher visual centers [34, 35], a cortical approach to a visual prosthesis could provide a viable option for sight restoration to a broader range of blinding conditions. Further, a cortical prosthesis has the potential to provide a higher resolution interface since a given region of visual space is represented by a larger area of neural tissue. This cortical magnification of the visual field could provide a solution to limitations related to electrode density and stimulation overlap. As with each of the approaches, however, a cortically-based prosthesis faces a unique set of challenges that will be discussed in detail throughout the remainder of this dissertation.

Since the early twentieth century, it has been known that electrical stimulation of V1 produces percepts in the form of Gaussian-shaped points of light called phosphenes [36]. Researchers in the late 60's and early 70's demonstrated that stimulating an array of subdural surface electrodes placed over the visual cortex of human subjects could produce crude spatial patterns of phosphenes [37-39]. These electrodes consisted of relatively large platinum discs (~1-9 mm^2) that were placed on the surface of V1 on top of the pia arachnoid, a structure that covers the underlying functional cortical tissue. As a result, it was discovered that large currents (~1-3 mA) were needed to generate

phosphenes when stimulating V1 with surface electrodes. These large currents were found to produce highly nonlinear interactions between the phosphenes of closely spaced electrodes, leading to unpredictable patterns during multiple electrode stimulation. Further, the high stimulus levels occasionally led to seizures in some subjects.

More recent work using microelectrodes has created renewed interest in the idea of a cortically-based artificial vision system. Using small clusters of penetrating microelectrodes to excite more focal regions of the cortex, researchers demonstrated that phosphenes could be evoked with currents an order of magnitude smaller than those used with surface electrodes [14, 40]. It was also shown that stimulation of multiple closely spaced electrodes in a human subject could produce simple patterns of phosphenes such as two separate phosphenes or a line of phosphenes [14].

Studies using macaque monkeys further support the idea of a cortically-based artificial vision system using penetrating microelectrodes. These studies have shown that sighted monkeys can be trained to indicate percepts in their field of view during microstimulation of V1 and have demonstrated that these animals, in particular rhesus macaques, can serve as a good model for understanding the psychophysics of microstimulation-evoked phosphenes [8, 35, 41-43]. Using macaque monkeys, one group quantified several parameters of stimulation and their effect on phosphene detection thresholds for single or pairs of acutely implanted microelectrodes [35, 41]. Thresholds as a function of stimulus amplitude, duration and frequency were measured. Amplitudes ranging from 10's to 100's of microamps, pulse durations of approximately 200 μs, and frequencies of 50-200 Hz were found to be effective. It was shown that small changes, as low as 10 percent, in both frequency and amplitude could be detected during continuous

stimulation. It was also shown that thresholds varied as a function of electrode depth within cortex. The lowest thresholds occurred when the electrode tips resided in layers 3 and 4A, and the highest thresholds were found in layers 4C and 6. In a more recent study, macaque monkeys were used to quantify the sizes, contrasts, and colors of phosphenes evoked during stimulation of single microelectrodes in V1 [42]. It was found that percepts ranged from 9 to 26 minutes of arc in diameter with contrasts from 2.6 to 10 percent. It was also found that percepts were composed of a range of low-contrast colors, mostly with whitish tints, but some with red, yellow, and bluish tints. One of the very few studies that looked at the chronic capabilities of multiple microelectrodes in V1 for use as a visual prosthesis was performed by Bradley and colleagues [8]. In this 16 month study, a total of 152 microelectrodes in the form of 2 and 8-pin clusters were implanted into V1 of a single behaving macaque monkey. Responses to stimulation were recorded by measuring the animal's saccades to the evoked phosphenes. It was found that the animal could make reliable saccades to locations in visual space that corresponded to the expected locations of phosphenes based on previously determined receptive field maps. Approximately 32 of the 152 electrodes were stimulated, however, and only a subset of those 32 were found to evoke consistent responses over the duration of the study. Many of the spatial and temporal characteristics of chronic microstimulation were not fully addressed.

In spite of the significant body of work on the subject of microstimulation in V1, none of the human or animal studies to date have resulted in the development of a functional cortically-based visual prosthesis.

Challenges

There are several critical challenges to developing a cortically-based neural prosthesis for vision restoration. These challenges include: 1) Optimizing the neural interface design for the complex three dimensional structure of primary visual cortex; 2) Understanding the interactions of spatio-temporal patterns of microstimulations and determining if subjects can discriminate such patterns; and 3) Demonstrating long-term function of a cortically-based neural prosthesis in a model system that approaches real-world conditions. The work presented in this dissertation addresses the third challenge.

Approach

In order to characterize the long-term function of a cortically-based vision prosthesis, a model was implemented that closely resembled a potential clinical application in a blind human subject. As part of this model, the established rhesus macaque system was used. These NHPs have visual systems similar to humans and have been shown to accurately report phosphenes during electrical stimulation of V1 [8, 35, 41-44]. For stimulation delivery, Utah Electrode Arrays (UEAs) were used, which are high-count fixed-geometry arrays of microelectrodes that can be implanted into the visual pathways to allow periodic injections of electrical currents at many closely spaced sites. The large number and regular pattern of electrodes in these arrays make it possible to generate the complex spatio-temporal stimulation patterns needed for studying patterned perceptions. Further, these arrays provide a multichannel interface to the visual cortex that can be used for both neural recording and microstimulation and could, eventually, form the cornerstone of a visual neuroprosthetic system. They have been successfully implanted and used for research applications in the motor cortex [45-48], auditory cortex

[49, 50], auditory nerve [51-53], sciatic nerve [54], and visual cortex [55, 56] of various animal models. Moreover, they have been acutely implanted in the middle temporal gyrus of epilepsy patients undergoing temporal lobectomy surgery [57-62] and chronically implanted in the motor cortex of paralyzed human patients [63-67]. While these studies have demonstrated the utility of the UEA in a number of research and motor prosthetic applications, the work presented herein is the first to show the chronic capability of UEA-based microstimulation for sensory prosthetic applications.

Overview

This dissertation contains three main sections. The first discusses the design and implementation of a robust, yet minimally invasive device for chronic head fixation in macaques. Such a device was needed for the successful completion of the chronic stimulation experiments that followed. This section was published in the Journal of Neuroscience Methods in 2009, and the contributing authors were TS Davis, K Torab, PA House, and B Greger. The second and third sections of this dissertation contain an in depth discussion of the safety and chronic functionality of a UEA-based vision prosthesis system. Understanding the behavior of such a system under conditions approaching the real-world is a necessary step in the development of a cortically-based visual prosthesis capable of restoring functional vision to the blind. These two sections were published in the Journal of Neural Engineering in 2011 and 2012, respectively. The contributing authors for the second section were K Torab, TS Davis (co-first author), DJ Warren, PA House, RA Normann, and B Greger. The contributing authors for the third section were TS Davis, RA Parker, PA House, E Bagley, S Wendelken, RA Norman, and B Greger.

References

[1]   *Global Data on Visual Impairments*, World Health Organization, 2002.

[2]   *Global Data on Visual Impairments*, World Health Organization, 2010.

[3]   K. D. Frick *et al.*, "Economic impact of visual impairment and blindness in the United States," *Archives of ophthalmology,* vol. 125, no. 4, pp. 544-50, Apr, 2007.

[4]   J. Maurer *et al.*, "Reliability of cochlear implants," *J. Otolaryngol. Head Neck Surg.,* vol. 132, no. 5, pp. 746-50, May, 2005.

[5]   C. Pantev *et al.*, "Dynamics of auditory plasticity after cochlear implantation: a longitudinal study," *Cerebral cortex,* vol. 16, no. 1, pp. 31-6, Jan, 2006.

[6]   P. Chang, "Implantable hearing devices--beyond hearing aids," *Australian family physician,* vol. 34, no. 3, pp. 157-61, Mar, 2005.

[7]   M. P. Barry, and G. Dagnelie, "Use of the Argus II retinal prosthesis to improve visual guidance of fine hand movements," *Invest. Ophthalmol. Visual Sci.,* vol. 53, no. 9, pp. 5095-101, Aug, 2012.

[8]   D. C. Bradley *et al.*, "Visuotopic mapping through a multichannel stimulating implant in primate V1," *J. Neurophysiol.,* vol. 93, no. 3, pp. 1659-70, Mar, 2005.

[9]   T. S. Davis *et al.*, "Spatial and temporal characteristics of V1 microstimulation during chronic implantation of a microelectrode array in a behaving macaque," *J. Neural. Eng.,* vol. 9, no. 6, pp. 065003, Dec, 2012.

[10]   M. S. Humayun *et al.*, "Interim results from the international trial of Second Sight's visual prosthesis," *Ophthalmology,* vol. 119, no. 4, pp. 779-88, Apr, 2012.

[11]   J. S. Pezaris, and R. C. Reid, "Demonstration of artificial visual percepts generated through thalamic microstimulation," *Proc. Natl. Acad. Sci.,* vol. 104, no. 18, pp. 7670-5, May 1, 2007.

[12]   J. F. Rizzo, 3rd, "Update on retinal prosthetic research: the Boston Retinal Implant Project," *J. Neuroophthalmol.,* vol. 31, no. 2, pp. 160-8, Jun, 2011.

[13]   J. F. Rizzo, 3rd *et al.*, "Perceptual efficacy of electrical stimulation of human retina with a microelectrode array during short-term surgical trials," *Invest. Ophthalmol. Visual Sci.,* vol. 44, no. 12, pp. 5362-9, Dec, 2003.

[14]   E. M. Schmidt *et al.*, "Feasibility of a visual prosthesis for the blind based on intracortical microstimulation of the visual cortex," *Brain,* vol. 119 (Pt 2), pp. 507-22, Apr, 1996.

[15] K. Torab *et al.*, "Multiple factors may influence the performance of a visual prosthesis based on intracortical microstimulation: nonhuman primate behavioural experimentation," *J. Neural. Eng.*, vol. 8, no. 3, pp. 035001, Jun, 2011.

[16] C. Veraart *et al.*, "Visual sensations produced by optic nerve stimulation using an implanted self-sizing spiral cuff electrode," *Brain Res.*, vol. 813, no. 1, pp. 181-6, Nov 30, 1998.

[17] C. Veraart *et al.*, "Pattern recognition with the optic nerve visual prosthesis," *Artificial organs*, vol. 27, no. 11, pp. 996-1004, Nov, 2003.

[18] E. Zrenner *et al.*, "Subretinal electronic chips allow blind patients to read letters and combine them to words," *Proc. R. Soc.*, vol. 278, no. 1711, pp. 1489-97, May 22, 2011.

[19] K. Cha *et al.*, "Simulation of a phosphene-based visual field: visual acuity in a pixelized vision system," *Ann. Biomed. Eng.*, vol. 20, no. 4, pp. 439-49, 1992.

[20] K. Cha *et al.*, "Mobility performance with a pixelized vision system," *Vision Res.*, vol. 32, no. 7, pp. 1367-72, Jul, 1992.

[21] K. Cha *et al.*, "Reading speed with a pixelized vision system," *J. Opt. Soc. Am.*, vol. 9, no. 5, pp. 673-7, May, 1992.

[22] A. K. Ahuja *et al.*, "Blind subjects implanted with the Argus II retinal prosthesis are able to improve performance in a spatial-motor task," *Br. J. Ophthalmol.*, vol. 95, no. 4, pp. 539-43, Apr, 2011.

[23] C. Veraart *et al.*, "Vision rehabilitation in the case of blindness," *Expert review of medical devices*, vol. 1, no. 1, pp. 139-53, Sep, 2004.

[24] J. B. Jonas *et al.*, "Human optic nerve fiber count and optic disc size," *Investigative ophthalmology & visual science*, vol. 33, no. 6, pp. 2012-8, May, 1992.

[25] G. Dagnelie, "Visual prosthetics 2006: assessment and expectations," *Expert review of medical devices*, vol. 3, no. 3, pp. 315-25, May, 2006.

[26] J. Dowling, "Artificial human vision," *Expert review of medical devices*, vol. 2, no. 1, pp. 73-85, Jan, 2005.

[27] I. Wickelgren, "Biomedical engineering. A vision for the blind," *Science*, vol. 312, no. 5777, pp. 1124-6, May 26, 2006.

[28] E. Zrenner, "Will retinal implants restore vision?," *Science*, vol. 295, no. 5557, pp. 1022-5, Feb 8, 2002.

[29] A. Caspi *et al.*, "Feasibility study of a retinal prosthesis: spatial vision with a 16-electrode implant," *Arch. Opthalmol.*, vol. 127, no. 4, pp. 398-401, Apr, 2009.

[30] S. H. Greenwald *et al.*, "Brightness as a function of current amplitude in human retinal electrical stimulation," *Invest. Ophthalmol. Visual Sci.*, vol. 50, no. 11, pp. 5017-25, Nov, 2009.

[31] A. Horsager *et al.*, "Spatiotemporal interactions in retinal prosthesis subjects," *Invest. Ophthalmol. Visual Sci.*, vol. 51, no. 2, pp. 1223-33, Feb, 2010.

[32] B. W. Jones *et al.*, "Retinal remodeling triggered by photoreceptor degenerations," *J. Comp. Neurol.*, vol. 464, no. 1, pp. 1-16, Sep 8, 2003.

[33] H. A. Quigley, and A. T. Broman, "The number of people with glaucoma worldwide in 2010 and 2020," *Br. J. Ophthalmol.*, vol. 90, no. 3, pp. 262-7, Mar, 2006.

[34] R. A. Normann *et al.*, "Toward the development of a cortically based visual neuroprosthesis," *J. Neural. Eng.*, vol. 6, no. 3, pp. 035001, Jun, 2009.

[35] J. R. Bartlett *et al.*, "Psychophysics of electrical stimulation of striate cortex in macaques," *J. Neurophysiol.*, vol. 94, no. 5, pp. 3430-42, Nov, 2005.

[36] W. Penfield, and T. Rasmussen, "The Cerebral Cortex of Man," p. 248, New York: Macmillan, 1950.

[37] G. S. Brindley, and W. S. Lewin, "The visual sensations produced by electrical stimulation of the medial occipital cortex," *J. Physiol.*, vol. 196, no. 2, pp. 479-93, Feb, 1968.

[38] W. H. Dobelle, and M. G. Mladejovsky, "Phosphenes produced by electrical stimulation of human occipital cortex, and their application to the development of a prosthesis for the blind," *J. Physiol.*, vol. 243, no. 2, pp. 553-76, Dec, 1974.

[39] D. A. Pollen, "Some perceptual effects of electrical stimulation of the visual cortex in man," *The Nervous System*, vol. 2, pp. 519-28, 1975.

[40] M. Bak *et al.*, "Visual sensations produced by intracortical microstimulation of the human occipital cortex," *Med. Biol. Eng. Comput.*, vol. 28, no. 3, pp. 257-9, May, 1990.

[41] E. A. DeYoe *et al.*, "Laminar variation in threshold for detection of electrical excitation of striate cortex by macaques," *J. Neurophysiol.*, vol. 94, no. 5, pp. 3443-50, Nov, 2005.

[42] P. H. Schiller *et al.*, "New methods devised specify the size and color of the spots monkeys see when striate cortex (area V1) is electrically stimulated," *Proc. Natl. Acad. Sci. USA*, vol. 108, no. 43, pp. 17809-14, Oct 25, 2011.

[43]   E. J. Tehovnik, and W. M. Slocum, "Depth-dependent detection of microampere currents delivered to monkey V1," *Eur. J. Neurosci.*, vol. 29, no. 7, pp. 1477-89, Apr, 2009.

[44]   E. J. Tehovnik *et al.*, "Phosphene induction and the generation of saccadic eye movements by striate cortex," *J. Neurophysiol.*, vol. 93, no. 1, pp. 1-19, Jan, 2005.

[45]   J. Baker *et al.*, "Multi-scale recordings for neuroprosthetic control of finger movements," *Conf. Proc. IEEE Eng. Med. Biol. Soc.*, pp. 4573-7, 2009.

[46]   N. Hatsopoulos *et al.*, "Cortically controlled brain-machine interface," *Conf. Proc. IEEE Eng. Med. Biol. Soc.*, vol. 7, no. 1, pp. 7660-3, 2005.

[47]   M. D. Linderman *et al.*, "Neural recording stability of chronic electrode arrays in freely behaving primates," *Conf. Proc. IEEE Eng. Med. Biol. Soc.*, vol. 1, pp. 4387-91, 2006.

[48]   M. Velliste *et al.*, "Cortical control of a prosthetic arm for self-feeding," *Nature*, vol. 453, no. 7198, pp. 1098-101, Jun 19, 2008.

[49]   S. J. Kim *et al.*, "Electrophysiological mapping of cat primary auditory cortex with multielectrode arrays," *Ann. Biomed. Eng.*, vol. 34, no. 2, pp. 300-9, Feb, 2006.

[50]   P. J. Rousche, and R. A. Normann, "Chronic recording capability of the Utah Intracortical Electrode Array in cat sensory cortex," *J. Neurosci. Methods*, vol. 82, no. 1, pp. 1-15, Jul 1, 1998.

[51]   T. Hillman *et al.*, "Cochlear nerve stimulation with a 3-dimensional penetrating electrode array," *Otol. Neurotol.*, vol. 24, no. 5, pp. 764-8, Sep, 2003.

[52]   S. J. Kim *et al.*, "Selective activation of cat primary auditory cortex by way of direct intraneural auditory nerve stimulation," *Laryngoscope*, vol. 117, no. 6, pp. 1053-62, Jun, 2007.

[53]   J. C. Middlebrooks, and R. L. Snyder, "Intraneural stimulation for auditory prosthesis: modiolar trunk and intracranial stimulation sites," *Hear. Res.*, vol. 242, no. 1-2, pp. 52-63, Aug, 2008.

[54]   D. McDonnall *et al.*, "Selective motor unit recruitment via intrafascicular multielectrode stimulation," *Can. J. Physiol. Pharmacol.*, vol. 82, no. 8-9, pp. 599-609, Aug-Sep, 2004.

[55]   E. M. Maynard *et al.*, "A technique to prevent dural adhesions to chronically implanted microelectrode arrays," *J. Neurosci. Methods*, vol. 97, no. 2, pp. 93-101, Apr 15, 2000.

[56]   D. J. Warren *et al.*, "High-resolution two-dimensional spatial mapping of cat striate cortex using a 100-microelectrode array," *Neuroscience,* vol. 105, no. 1, pp. 19-31, 2001.

[57]   P. A. House *et al.*, "Acute microelectrode array implantation into human neocortex: preliminary technique and histological considerations," *Neurosurg. Focus,* vol. 20, no. 5, pp. 1-4, 2006.

[58]   C. J. Keller *et al.*, "Heterogeneous neuronal firing patterns during interictal epileptiform discharges in the human cortex," *Brain,* vol. 133, no. Pt 6, pp. 1668-81, Jun, 2010.

[59]   C. A. Schevon *et al.*, "Propagation of epileptiform activity on a submillimeter scale," *J. Clin. Neurophysiol.,* vol. 27, no. 6, pp. 406-11, Dec, 2010.

[60]   C. A. Schevon *et al.*, "Microphysiology of epileptiform activity in human neocortex," *J. Clin. Neurophysiol.,* vol. 25, no. 6, pp. 321-30, Dec, 2008.

[61]   C. A. Schevon *et al.*, "Spatial characterization of interictal high frequency oscillations in epileptic neocortex," *Brain,* vol. 132, no. Pt 11, pp. 3047-59, Nov, 2009.

[62]   A. Waziri *et al.*, "Initial surgical experience with a dense cortical microarray in epileptic patients undergoing craniotomy for subdural electrode implantation," *Neurosurgery,* vol. 64, no. 3, pp. 540-5, Mar, 2009.

[63]   L. R. Hochberg *et al.*, "Neuronal ensemble control of prosthetic devices by a human with tetraplegia," *Nature,* vol. 442, no. 7099, pp. 164-71, Jul 13, 2006.

[64]   S. P. Kim *et al.*, "Neural control of computer cursor velocity by decoding motor cortical spiking activity in humans with tetraplegia," *J. Neural Eng.,* vol. 5, no. 4, pp. 455-76, Dec, 2008.

[65]   C. L. Ojakangas *et al.*, "Decoding movement intent from human premotor cortex neurons for neural prosthetic applications," *J. Clin. Neurophysiol.,* vol. 23, no. 6, pp. 577-84, Dec, 2006.

[66]   W. Truccolo *et al.*, "Primary motor cortex tuning to intended movement kinematics in humans with tetraplegia," *J. Neurosci.,* vol. 28, no. 5, pp. 1163-78, Jan 30, 2008.

[67]   C. E. Vargas-Irwin *et al.*, "Decoding complete reach and grasp actions from local primary motor cortex populations," *J. Neurosci.,* vol. 30, no. 29, pp. 9659-69, Jul 21, 2010.

CHAPTER 2

A MINIMALLY INVASIVE APPROACH TO LONG-TERM HEAD

FIXATION IN BEHAVING NONHUMAN PRIMATES[1]

Abstract

We have designed a device for long-term head fixation for use in behaving

nonhuman primates that is robust yet minimally invasive and simple to use. This device

is a modified version of the halo system that is used in humans for cervical traction and

stabilization after spinal column injuries. This device consists of an aluminum halo with

four titanium skull pins offset from the halo by aluminum posts. The titanium pins insert

onto small segments of cranially reinforcing titanium plate, which are attached to the

skull with titanium cortex screws. The surgery involves four scalp incisions, placement of

the reinforcing plates, insertion of the pins for attachment of the halo, and incision

closure. After the halo is attached, the animal's head can be fixed to a primate chair using

a custom-built attachment arm that provides three degrees of adjustability for proper

positioning during behavioral tasks. We have installed this device on two Macaque

monkeys weighing 7 and 10 kg. The halos have been in place on these animals for up to 8

months without signs of discomfort or loss of fixation. Using this method of head

fixation, we have been able to track the animals' eye positions with an accuracy of less

than two visual degrees while they perform behavioral tasks.

<u>Introduction</u>

Experiments in behaving nonhuman primates often require head fixation for accurate tracking of eye movements and stable neural recordings [1-3]. Many methods of head fixation have been developed, each with a particular set of advantages and disadvantages. Evarts and Mountcastle [1, 2] were among the first to use head fixation in nonhuman primates to improve the outcome of behavioral experiments. Mountcastle [2] used a device that involved the placement of stainless steel bolts into the frontal and parietal regions of the animal's skull. These bolts served as fixation points for an acrylic head cap that attached to a primate chair to provide immobilization of the animal's head. This design has been extensively used for chronic head fixation in behaving primates, but is associated with several drawbacks. Attachment of this device requires a large incision to be made sagittally across the superior portion of the scalp and displacement of the skin in this area to make room for the acrylic cap. The invasiveness of this surgery can lead to chronic infections and prolonged discomfort for the animal. In addition, extended use of this device leads to bone necrosis around the implanted bolts and eventual failure. A failed head cap is traumatic to the animal, requires immediate surgical intervention, and results in a long-term interruption of behavioral experiments. Foeller and Tychsen [4] used this method of head fixation on 20 animals and observed an average time to failure of 11 months (range 5 months to 2 years) over the course of experimentation. Betelak [5] made improvements to this original design by using titanium endosseus implants for fixation, instead of stainless steel bolts, and allowing osteointegration to occur before the final attachment of the acrylic head cap. This method resulted in a more stable interface with the animal's skull that nearly eliminated the occurrence of failure. The attachment

procedure, however, took up to 6 months to complete and required the use of specialized dental equipment, making the overall implementation of this device more difficult.

Several researchers have proposed design alternatives to the acrylic head cap. These newer methods of head fixation have been created to address some of the problems that are associated with the original design, such as the complexity and invasiveness of the attachment surgery. These methods, however, introduce new problems like device instability and device complexity. Pigarev [6] built a device consisting of a multifaceted aluminum frame that surrounds the head of the animal and holds 8 opposing posts. The posts are attached to the frame using dental cement and make contact with the skull surface through skin incisions. The posts, however, are not anchored directly to the bone. This device provided a stable interface for up to 2 years, and allowed for adjustability during growth. It was tested and used in a smaller species of Macaque monkey (*Macaca fascicularis*), but was never tested on larger monkeys like the *Macaca mulatta*. Since this device does not make a rigid connection with the bone, problems of strength and stability might arise when used with larger monkeys. Also, this device is composed of many angles and connections, making it more complex to build and implement.

In the early 1970s, Friendlich [7] developed a design for head fixation that was modeled after a system used in human orthopedics for cervical stabilization after spinal column injury [8]. Later, Isoda [9] implemented a similar design with some minor modifications. Their design consisted of an aluminum ring or halo, four aluminum posts that attached to the halo at four fixed locations, and four stainless steel skull pins. The skull pins were threaded into the ends of each post, and the tips of the pins were held by pressure against the surface of the skull. This design was tested on two *Macaca fuscata*

weighing approximately 5 kg and provided a stable interface for up to 18 months. Both Friendlich [7] and Isoda [9], however, discovered problems with loosening over time due to bone necrosis at the skull/pin interface. Friendlich [7] found that maintaining a stable attachment required regular tightening of the skull pins and eventual relocation of these pins to different areas of the skull.

We began the development of our head fixation device by replicating the design proposed by Isoda [9]. We encountered similar problems with bone necrosis and loosening over time. As a result, we made several modifications to improve stability and minimize loosening. Our final design requires a minimally invasive surgery for attachment, is simple to construct, and has been stable for use in experiments lasting several months in larger Macaque monkeys. Since more mature and experienced monkeys are typically larger, this device will be useful for experiments that implement complex behavioral tasks requiring years of training. Because this device is minimally invasive, it is anticipated that the long-term risk of infection will be reduced. We have added several modifications to the design by Isoda [9]. We have changed the main halo frame to include multiple holes for adjustability during the placement and alignment of the posts and skull pins. We have modified the posts to include a tab that adds a second point of attachment to the frame for increased strength against torsional forces. We have added reinforcing titanium plates, which attach to the skull with titanium cortex screws and strengthen the skull against penetrating and translational forces. By distributing the force of each skull pin over a larger surface area, the plates should minimize bone necrosis and erosion at the skull/pin interface, allowing for a more stable and long-term connection.

Methods

Overview

This device consists of an aluminum halo frame, four titanium skull pins offset from the halo by aluminum posts, and four pieces of cranially reinforcing titanium plate with titanium bone screws. The halo serves as a rigid support for the attachment of the posts and skull pins. The posts serve as an offset for the attachment of the skull pins to the frame, allowing the frame to rest above the ears and supraorbital ridge of the animal and out of its visual field. The reinforcing titanium plates and screws are attached to the surface of the skull at each pin location to add stability against translational and penetrating forces.

Halo

To build the halo frame, a three-dimensional model was created using AutoCAD software. This model was then used to cut the frame from 3/8 in. 6061 aluminum alloy plate using a computer numerical control (CNC) mill (Haas Automation, Inc., Oxnard, CA). The frame has a thickness of 3/8 in., and the inner dimensions of the frame measure 4.95/4.40 in. (major axis/minor axis). The frame was designed with 30 equally spaced holes at 12-degree increments around its perimeter. Twenty-seven of these 30 holes were made to accept #10–32 recessed machine bolts to allow for variability in post and pin placement. The remaining three holes were given standard 1/4 in.-20 threads to serve as attachment points to the attachment arm on the primate chair (Figure 2.1(a)).

Offset posts

Each post was manually cut from 3/8 in. 6061 aluminum alloy plate using a standard milling machine (Clausing Industrial, Inc., Kalamazoo, MI). At the base of each post, a tab was made that bolts to the halo frame to prevent rotation about its axis during pin insertion and tightening. At the end of the tab, a 0.2 in. diameter slot was created to allow for a small amount of rotation when aligning the skull pins with the skull surface. A 1/4 in.-28 tapped hole was placed at the end of each post to accept the corresponding skull pin. Each post has a thickness of 3/8 in. and comes in a variety of lengths ranging from 0.85 to 1.1 in. (Figure 2.1(b)).

Skull pins

The 1/4 in.-28×2.5 in. long titanium skull pins were purchased from PMT Corporation (Chanhassen, MN), and the tips were modified on a metal lathe to provide a more stable interface with the skull and titanium reinforcement plates (Figure 2.1(c)). The small diameter portion of the tip matches the diameter of the holes in the reinforcement plates. The large diameter portion of the tip is made smooth to minimize the risk of infection at the device/skin interface.

Reinforcement plates

Titanium MatrixMIDFACE adaption plates (0.8mm thickness) and 1.5mm×4mm long titanium self-tapping cortex screws were purchased from a medical device company (Synthes, Inc., Monument, CO). These plates and attachment screws were used to hold the tip of the skull pin to the skull surface and to reinforce the bone against penetrating and translational forces. The plates were cut to a length of 3 or 4 holes (~13-18mm)
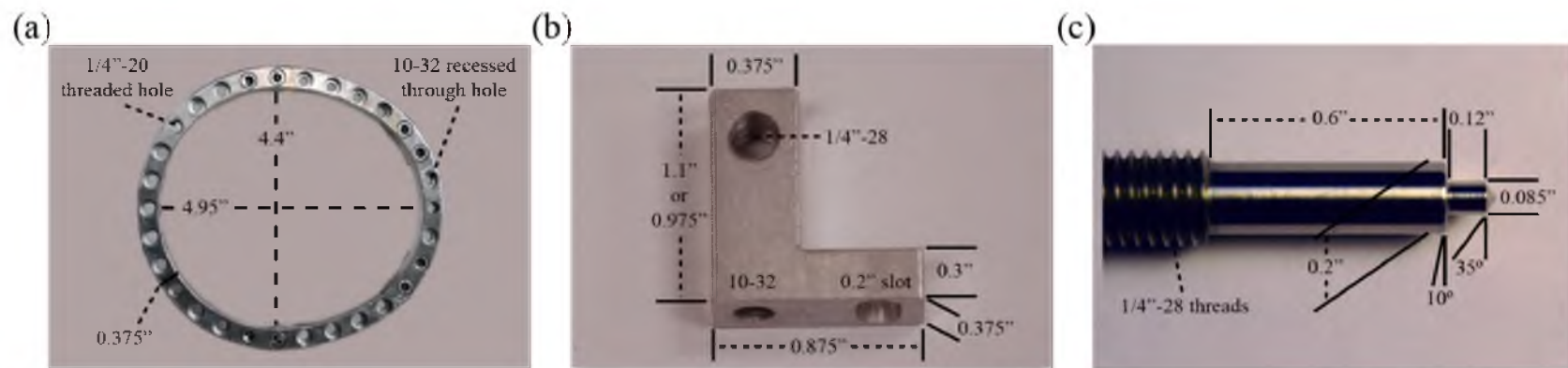
Figure 2.1. Device components with dimensions: (a) halo frame; (b) offset post; (c) modified titanium skull pin.

during the surgery and attached by predrilling holes into the outer cortex of the skull and inserting the cortical screws at both ends of the plate. Holes were drilled using a Synthes 1.1mm×4mm long drill bit.

Primate chair

To complete the head fixation system, a Macaque chair (Primate Products, Inc.,Woodside, CA) was modified to create an attachment arm to provide a connection between the chair and the halo frame during behavioral tasks (Figure 2.2). This attachment arm was created from pipes and connectors that were purchased from a modular framing company (80/20, Inc., Columbia City, IN). An attachment plate, which is bolted to this arm, was cut from 3/8 in. 6061 aluminum alloy plate using a CNC mill and was made to include a groove to match and accept the outer contour of the halo frame.
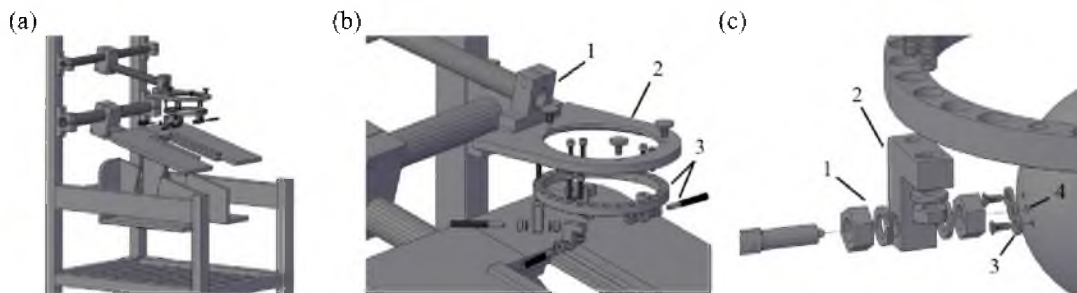
Figure 2.2. (a) Overall view of primate chair with halo device. (b) Exploded view of the attachment arm (1), attachment plate (2), and halo frame with posts and skull pins (3). (c) Enlarged view showing insertion path of skull pin. The pin passes through stainless steel nuts and washers (1), an aluminum offset post (2), a titanium plate that is attached to the skull with titanium cortex screws (3), and into a predrilled hole in the skull surface (4).

Device alignment and set-up

Before the surgical attachment procedure, the device is assembled and placed on a model Macaque skull to ensure the proper positioning of each skull pin. Each post is attached to the halo with 2 #10-32 machine bolts and rotated to provide a perpendicular interface between the pin and skull surface. The posts and pins are arranged so that the halo is centered above the skull (Figure 2.3(c)) and each pin tip contacts the correct skull location. The front pins should ideally be located on the temporal bone slightly anterior to the auditory canal and superior enough to minimize contact of the halo with the animal's ears (Figure 2.3(a)). These pins should be placed close to the anterior portion of the ear because the bone in this area is thicker. The back pins should be placed slightly superior to the superior nuchal line on the occipital bone (Figure 2.3(b)). As much as possible, all pins should contact the skull at a perpendicular angle and be rotated to provide counter-balanced forces during tightening. Holes 8 and 13 for the front and the back pins, respectively (counting from the most anterior hole in a clockwise or counterclockwise direction), were found to provide a centered fit of the halo and correct positioning of each

Figure 2.3. Fixation device positioned on Macaque skull. (a) Anterior view of device showing halo frame (1), offset post (2), and skull pin (3). The skull pin is placed in temporal bone superior and slightly anterior to the auditory canal. (b) Posterior view of device showing post with skull pin and an enlarged image of the titanium reinforcement plate with cortex screws (4). The posterior pin is placed slightly superior to the superior nuchal line. (c) Superior view of device showing pin position and angle with respect to cranial suture lines.

pin tip at the skull surface.

<u>Attachment procedure</u>

All procedures were carried out following an IACUC approved protocol. The device is attached with the animal under general anesthesia using a sterile technique. To begin the procedure, anesthesia is induced with an injection of ketamine 10 mg/kg intramuscularly while the animal is in the primate chair. The animal is then carried to the surgery table, intubated, and placed under general anesthesia using 2–5% isoflurane, a tidal volume of 150 mL, and a respiratory rate of 10. Vitals are monitored continuously during the procedure to maintain an adequate heart rate, temperature, and oxygen saturation.

The animal is then placed in a stereotaxic frame. Stabilization bars are attached to the eye sockets and upper jaw to prevent rotation of the head around the ear bars during surgery. Ophthalmological salve is placed in the eyes to prevent drying, and intravenous fluids are initiated to maintain hydration. A prophylactic injection of the antibiotic enrofloxacin (5 mg/kg i.m.) is given at this time. Clippers are used to trim the hair around the four pin sites, and the animal and the stereotaxic frame are prepped and draped in a sterile manner.

Before any incisions are made, the device is positioned on the animal's head in the desired location. Each pin is hand tightened to mark the skin locations where incisions are to be made. The pins are then loosened, and the device is removed. A scalpel is used to make incisions in the skin at the marked locations. Blunt dissection is performed through subcutaneous tissue and muscle to expose the skull surface. A

periosteal elevator is used to expose and clean enough bone surface to ensure proper positioning and attachment of the reinforcement plates.

The device is repositioned on the animal's head so that the halo rests out of the animal's field of view and above the ears. Each pin location is verified to ensure proper positioning. The pins are hand tightened onto the skull surface to temporarily keep the device in place. Once the device is properly positioned, one pin is removed and replaced with the threaded drill guide. The drill guide is used to ensure correct alignment and stability during drilling. It also acts as a stop to provide safety by limiting drilling depth (Figure 2.4(a)). A 2mm drill bit is used to drill a hole 3mm deep into the skull surface where the tip of the skull pin will contact the surface of the skull. The drill and drill guide are then removed. A piece of titanium plate is cut to a length of 3 or 4 holes. The plate is bent to fit the curvature of the skull surface. The skull pin is then threaded through the offset post with nuts and lock washers on both sides. The pin is threaded so that the tip passes through the middle hole in the reinforcement plate and into the drilled hole in the surface of the skull. The pin is tightened by hand. With the plate now held in place by the pin, it is rotated about its axis to best fit the curvature of the skull surface and also to allow room for placement of the titanium screws. Pilot holes are drilled in the bone underlying the remaining holes in the plate using the Synthes 1.1mm×4mmlong drill bit. The two 4mm long self-tapping titanium screws are placed into these holes to complete the attachment of the plate to the skull (Figures 2.4(b) and 2.4(c)). This process is then repeated for each of the remaining pin sites. After all four plates and skull pins have been placed, the pins are tightened in an alternating pattern by hand using an Allen wrench. Prior to the addition of the titanium reinforcement plates in this procedure, we found that

Figure 2.4. (a) Drill guide used to align the drill bit during the attachment procedure. (b) Reinforcement plate for the temporal pin with titanium cortex screws at each end. (c) Reinforcement plate for the occipital pin with the pin threaded through the plate and into the predrilled hole in the skull surface. The predrilled hole was made using the drill guide.

an applied torque of 2 in.-pounds, as measured using a torque screwdriver, was sufficient to cause fracturing of the underlying bone. Care must be taken to avoid over tightening. Each lock nut is then tightened on both sides of the pin to prevent loosening. Wounds are rinsed with sterile saline, infused with antibiotics, and closed using a nonabsorbable monofilament suture. The animal's hair and skin are cleansed to remove the povidone-iodine solution, and neomycin ointment is applied to the wounds. Anesthesia is discontinued, and the animal is extubated. Postsurgical injections of ketoprofen (2 mg/kg i.m.) and buprenorphine (0.01mg/kg i.m.) are administered at this time. Postoperative medications include enrofloxacin (5 mg/kg i.m. daily for 5 days), ketoprofen (2 mg/kg i.m. daily for 5 days), and buprenorphine (0.02 mg/kg i.m. twice a day for 2 days). Additionally, for the duration of the device attachment, pin sites are cleaned at least once a week with cotton swabs soaked in hydrogen peroxide.

Results

We have installed this device on two Macaque monkeys weighing 7 and 10 kg. Previously trained behavioral tasks were resumed 3 days after surgery. Tasks requiring

eye tracking and head fixation were started 2 weeks after surgery. These animals have shown no signs of discomfort or pain while in their cages or during training. Shortly after attachment, these animals learned to include the device in the scheme of their body and were rarely found to catch the protruding edges on their cages or the primate chair. Because this device was designed to be lightweight (~0.5 pounds), it does not appear to be cumbersome to the animals or inhibit normal movement in their cages. Our animals are pair-housed and have access to an activity module to provide an enriched social environment. This device does not appear to alter the social or behavioral interactions of these monkeys with the other monkeys in the cage. The wounds at each pin site have healed with minimal scarring and show little or no edema or erythema (Figure 2.5(a)). One animal has been performing behavioral tasks requiring head fixation for 8 months and has experienced only a superficial infection at a temporal pin site. This infection was treated with daily cleansing using a combination of chlorhexidine solution and hydrogen peroxide. The other animal has been performing behavioral tasks for 5months with no signs of infection or complications. The device has remained stable on both animals since the initial attachment procedure, and the skull pins have not required tightening during this time.

We have tracked the eyes of each animal with an accuracy of less than 2 visual degrees during a behavioral task involving threshold detection of photic stimuli. Experiments were conducted in a dark chamber with a background luminance below 0.0001 cd/m^2. The animal was dark adapted and then trained to place its hands on proximity sensors and to fixate within a central region (2.6° in diameter) of a CRT monitor. Fixation positions were randomly alternated among five locations during the

progression of the task. A gaussian-shaped stimulus (1° in diameter) was then displayed

on the screen for 500ms at a fixed location with varying intensities. Following an

auditory cue, the animal would indicate if it saw the stimulus by raising either its right or

left hand (Figure 2.5(b)). Catch trials were inserted at random intervals, and the monkey

was rewarded with a squirt of juice from a tube by answering correctly. Eye positions

were sampled at 1 kHz using the EyeLink 1000 infrared eye tracking system (SR

Research, Ltd., Ontario, Canada) and plotted in Figures 2.5(c) and 2.6 to demonstrate the

accuracy and overall stability of the device.

Discussion

This method of head fixation for nonhuman primate research offers a simple

design that is easy to implement and less invasive than other methods of head fixation.

This system is also very stable and appears to avoid the loosening and bone necrosis

issues that have been experienced with other similar designs. The open structure of this

device would allow room for recording chambers and external connectors with

placements over many areas of the skull. The addition of reinforcing titanium plates to

this design allows for easy removal for imaging purposes and later reattachment at the

same location. Since these plates and the corresponding cortex screws are permanently

attached to the skull, however, they may cause small distortion artifacts and be

problematic for some studies. If imaging is required for a study, the reinforcement plates

can be placed at specific locations to minimize distortion over the area of interest. If head

fixation is necessary during the imaging process, this device can be constructed of

magnetic resonant compatible materials. The halo frame and posts can easily be

machined from high performance plastics like polyetherimide, and the titanium skull pins

Figure 2.5. (a) Enlarged image of the right occipital pin site 5 months after surgery. (b) Head-fixed animal performing a behavioral task requiring eye fixation. Eye positions were sampled at 1 kHz using the EyeLink 1000 infrared eye tracking system (SR Research, Ltd., Ontario, Canada). (c) Graph of recorded eye positions in units of visual degrees. For each trial, the animal was required to fixate within an area of diameter 2.6° (1) while a stimulus (2) was presented and a response was acquired. If the animal looked outside of the defined area, the trial was aborted and no reward was received. A total of 118 trials were completed, each requiring a fixation duration of 1250 ms. Eye position data is plotted in red (3). Fixation positions were randomly alternated among five locations [(0,0); (5,0); (0,5); (−5,0); (0,−5)] during the task and are represented by the five clusters of eye position data. The central cluster of data follows a gaussian distribution with $2\sigma \approx 0.8°$.
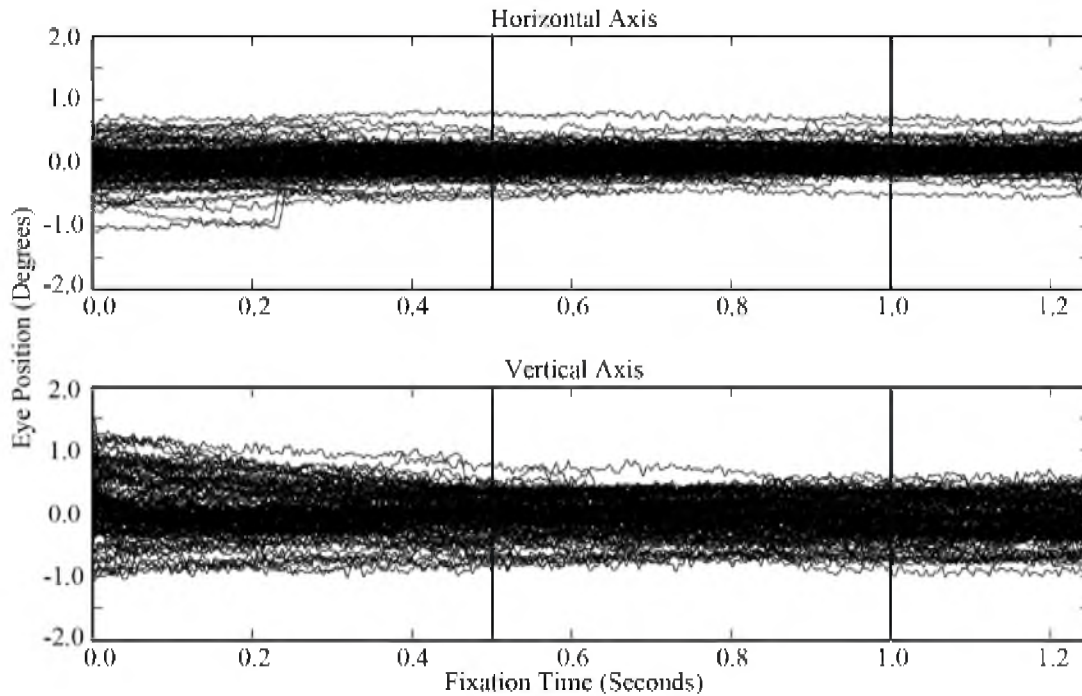
Figure 2.6. Eye position data recorded at 1 kHz using the Cerebus data acquisition system (Blackrock Microsystems, Salt Lake City, UT). Plots show superimposed eye positions along the horizontal and vertical axis for 118 trials of the behavioral task described in Figure 2.5. Stimulus onset and offset are indicated by vertical lines. Individual tracings reveal small noise fluctuations on the order of minutes of visual angle. The smoothness of the tracings demonstrate the stability of this head fixation system while tracking eye movements with the EyeLink 1000 infrared eye tracking system (SR Research, Ltd., Ontario, Canada).

can be replaced with their ceramic counterparts [10, 11]. This device performed well for

behavioral tasks that require accurate tracking of the eyes. We expect that it would also

provide sufficient stability to perform neural recordings from isolated neurons using

single or multiple electrodes.

<u>Acknowledgements</u>

References

[1] E. V. Evarts, "Relation of pyramidal tract activity to force exerted during voluntary movement," *J Neurophysiol.*, vol. 31, no. 1, pp. 14-27, Jan, 1968.

[2] V. B. Mountcastle *et al.*, "Posterior parietal association cortex of the monkey: command functions for operations within extrapersonal space," *J. Neurophysiol.*, vol. 38, no. 4, pp. 871-908, Jul, 1975.

[3] D. A. Robinson, "A Method of Measuring Eye Movement Using a Scleral Search Coil in a Magnetic Field," *IEEE Trans. Biomed. Eng.*, vol. 10, pp. 137-45, Oct, 1963.

[4] P. Foeller, and L. Tychsen, "Eye movement training and recording in alert macaque monkeys: 1. Operant visual conditioning; 2. Magnetic search coil and head restraint surgical implantation; 3. Calibration and recording," *Strabismus*, vol. 10, no. 1, pp. 5-22, Mar, 2002.

[5] K. F. Betelak *et al.*, "The use of titanium implants and prosthodontic techniques in the preparation of non-human primates for long-term neuronal recording studies," *J. Neurosci. Methods*, vol. 112, no. 1, pp. 9-20, Nov 15, 2001.

[6] I. N. Pigarev *et al.*, "A reversible system for chronic recordings in macaque monkeys," *J. Neurosci. Methods*, vol. 77, no. 2, pp. 157-62, Dec 1, 1997.

[7] A. R. Friendlich, "Primate head restrainer using a nonsurgical technique," *J. Appl. Physiol.*, vol. 35, no. 6, pp. 934-5, Dec, 1973.

[8] U. Vieweg, and R. Schultheiss, "A review of halo vest treatment of upper cervical spine injuries," *Arch. Orthop. Trauma Surg.*, vol. 121, no. 1-2, pp. 50-5, 2001.

[9] M. Isoda *et al.*, "Design of a head fixation device for experiments in behaving monkeys," *J. Neurosci. Methods*, vol. 141, no. 2, pp. 277-82, Feb 15, 2005.

[10] D. J. Dubowitz *et al.*, "Direct comparison of visual cortex activation in human and non-human primates using functional magnetic resonance imaging," *J. Neurosci. Methods*, vol. 107, no. 1-2, pp. 71-80, May 30, 2001.

[11] M. A. Pinsk *et al.*, "Methods for functional magnetic resonance imaging in normal and lesioned behaving monkeys," *J. Neurosci. Methods*, vol. 143, no. 2, pp. 179-95, Apr 30, 2005.

CHAPTER 3

MULTIPLE FACTORS MAY INFLUENCE THE PERFORMANCE

OF A VISUAL PROSTHESIS BASED ON INTRACORTICAL

MICROSTIMULATION: NONHUMAN PRIMATE

BEHAVIOURAL EXPERIMENTATION[1]

Abstract

We hypothesize that a visual prosthesis capable of evoking high-resolution visual perceptions can be produced using high-electrode-count arrays of penetrating microelectrodes implanted into the primary visual cortex of a blind human subject. To explore this hypothesis, and as a prelude to human psychophysical experiments, we have conducted a set of experiments in primary visual cortex (V1) of non-human primates using chronically implanted Utah Electrode Arrays (UEAs). The electrical and recording properties of implanted electrodes, the high-resolution visuotopic organization of V1, and the stimulation levels required to evoke behavioural responses were measured. The impedances of stimulated electrodes were found to drop significantly immediately following stimulation sessions, but these post-stimulation impedances returned to pre-stimulation values by the next experimental session. Two months of periodic microstimulation at currents of up to 96 µA did not impair the mapping of receptive fields from local field potentials or multi-unit activity, or impact behavioural visual thresholds

of light stimuli that excited regions of V1 that were implanted with UEAs. These results demonstrate that microstimulation at the levels used did not cause functional impairment of the electrode array or the neural tissue. However, microstimulation with current levels ranging from 18 to 76 μA (46 $\pm$ 19 μA, mean $\pm$ std) was able to elicit behavioural responses on eight out of 82 systematically stimulated electrodes. We suggest that the ability of microstimulation to evoke phosphenes and elicit a subsequent behavioural response may depend on several factors: the location of the electrode tips within the cortical layers of V1, distance of the electrode tips to neuronal somata, and the inability of nonhuman primates to recognize and respond to a generalized set of evoked percepts.

Introduction

The concept of a visual prosthesis to restore vision to individuals with profound blindness by electrically stimulating primary visual cortex (V1) was initially explored with experiments conducted in human patients [1-3]. These studies demonstrated that individual points of light, known as phosphenes, could be evoked by stimulating the surface of V1 via an array of macroelectrodes. Using this technique, they confirmed the global visuotopic organization of V1, and that subjects could assimilate spatial patterns of phosphenes with simultaneous stimulation via multiple macroelectrodes. However, large currents, in the milliampere range, were required to evoke individual phosphenes. Such large currents, when passed through groups of neighbouring electrodes, caused nonlinear interactions between the location and character of the evoked phosphenes and resulted in seizures in at least one patient [4]. Other researchers found that using penetrating intracortical microelectrodes to stimulate V1 in human patients evoked phosphenes at currents a few orders of magnitude lower than those required for surface stimulation

using macroelectrodes [5, 6]. These studies demonstrated the ability of electrical stimulation of V1 to evoke subjective visual perceptions in human patients, but were constrained by the difficulty of performing research in human patients and the technological limitations of the time.

Additional insight into intracortical microstimulation of V1 has come from acute studies performed in nonhuman primates (NHPs). It was demonstrated that NHPs could be trained on a reaction time task using photic stimulation and continue to perform the task in response to intracortical microstimulation of visual cortex. This reaction time task was used to optimize microstimulation parameters for evoking behavioural responses [7]. Another extensive study explored the effectiveness of various V1 intracortical microstimulation parameters in evoking phosphenes [8]. However, these acute studies did not address the chronic performance and stability of V1 microstimulation, factors important in the eventual development of a human visual prosthesis. In a contemporaneous study [9], V1 of NHPs were chronically implanted with a large number of microelectrodes. NHPs made saccades to phosphenes evoked by microstimulation via these electrodes. Additionally, the spatial location of the phosphene was similar to the spatial location of the receptive field (RF) mapped from neurons recorded on that electrode. These studies showed that NHPs, in particular macaque monkeys, can serve as a good animal model for studying the psychophysics of microstimulation-evoked phosphenes.

Several human studies have examined using a fixed geometry penetrating intracortical microelectrode array, such as the Utah Electrode Array (UEA), for motor prosthetic applications [10-15]. However, none of the human or NHP studies to date have

characterized the chronic safety and efficacy of microstimulation via such an array for sensory prosthetic applications. In moving towards this goal, we obtained high-resolution visuotopic mapping of V1 by measuring the RFs of both the multi-unit activity (MUA) and local field potentials (LFPs) across UEAs over periods of several months. The *in vivo* impedances and the quality of the recorded neural signals and RFs were measured over time to examine the functionality of the UEAs and the implanted neural tissue. We found that microstimulation at levels required to evoke behavioural responses in the NHPs did not result in functional impairment of the UEAs or the neural tissue. However, stimuli delivered via only a small number of electrodes were able to evoke phosphenes to which the NHPs would respond. We discuss several potential challenges of using intracortical microstimulation as the basis of a visual prosthesis and the use of NHPs as a model for a human visual prosthesis.

Methods

All surgical and experimental procedures were performed in accordance with the guidelines of the US Department of Agriculture and were approved by the University of Utah's Institutional Animal Care and Use Committee.

Instrumentation

Visual stimuli were generated using a real-time visual stimulator (ViSaGe, Cambridge Research Systems, Rochester, Kent, England) and displayed on a CRT monitor (G90fb, ViewSonic, Walnut, CA). The NHPs were head-fixed using a minimally invasive technique [16] and their eye positions were tracked with an infrared camera (1 kHz sampling rate, EyeLink 1000, SR Research, Mississauga, ON, Canada). Hand

position was monitored and behavioural responses were registered with capacitive switches, which detected the presence of the NHP's hand when it was within a few millimeters of the sensor.

Behavioural tasks

The NHP was placed in a primate chair inside of a dark chamber to dark adapt. After 25 to 35 min, it was required to place each of its hands on a capacitance switch, one to its left and the other to its right. A small crosshair would then appear in the centre of the CRT screen. Once the NHP directed its gaze within 1° of the centre of the crosshair, the crosshair would change to a 0.1×0.1 visual degrees box indicating the start of the trial. The NHP had to maintain its gaze within 1° of the centre of the box, or the trial was aborted.

For photic and electric stimulation tasks, stimuli were presented after fixation was maintained for a randomized duration (400-800 ms). Photic stimuli were round, monochromatic Gaussian shapes with a diameter of 1 visual degree. Luminance levels were varied between 0 and 10 000 μcd m^{-2} with step sizes adapted in order to obtain several data points on the psychometric curve. The parameters of electrical microstimulation are described in the methods section. Stimulus presentation was followed by a second randomized hold duration, and then an auditory cue was given indicating that the NHP should now make its response. The NHP would then respond by removing its right hand to indicate that it did not perceive, or its left hand to indicate that it did perceive, a stimulus. Photic threshold trials were rewarded with a bolus of juice 50% of the time regardless of the answer. Microstimulation trials were sparsely introduced into an ongoing photic task and were rewarded with juice 100% of the time

regardless of the answer. Clearly visible or invisible catch photic trials were used to ensure that the animal was responding truthfully and it was rewarded only if the correct response was made without any of the task constraints being violated. Using this forced-choice detection task, the NHP was required to indicate whether or not it perceived visual stimuli of varying luminance values, and phosphenes evoked by varying current amplitudes. Five or more responses to stimuli presented at a minimum of three intensity levels that spanned threshold (i.e. a minimum of 15 total responses) were considered to be valid or consistent behavioural response. Psychometric data were fit using a Weibull cumulative distribution function, which was used to estimate response thresholds (intensity value at 50% probability of detection).

For the RF mapping task, the NHP had to maintain fixation while visual stimuli were presented. The animal was rewarded as long as it continued to maintain fixation and none of the task constraints were violated.

Subjects and surgery

Two adult male rhesus macaques (*Macaca mulatta*) were used in these experiments and they are referred to as NHP1 and NHP2 in the subsequent text. We followed human protocols during the surgeries and post-operative care. Two Cereport arrays were implanted (Figure 3.1(a)) in V1 of each NHP using a pneumatic inserter [17]. Reference wires were placed in the subdural space. For NHP1, array1 was implanted anterior to the calcarine fissure and lateral to the sagittal sulcus. Array2 was implanted anterior to the first array and lateral to the sagittal sulcus. This anatomical area was expected to represent the lower right visual quadrant of the visual field close to the
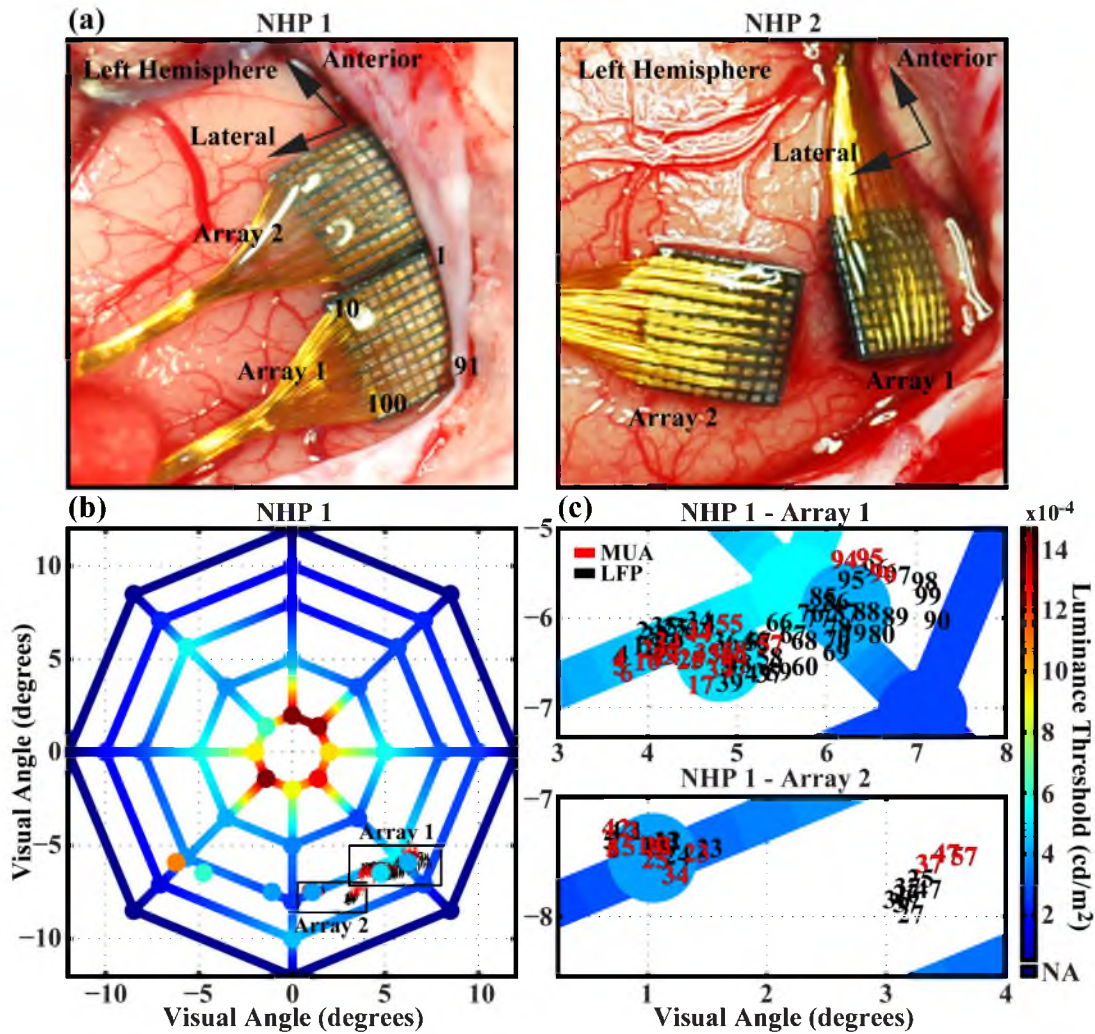
Figure 3.1. Comparison of the anatomic and visuotopic locations of the electrode arrays and the spatial distribution of luminance thresholds across visual space for a behaving non-human primate. (a) Placement of arrays in a cortex for NHP1 and NHP2. Arrays were placed in the left occipital cortex near the calcarine fissure and lateral to the sagittal sulcus for both animals. Electrode numbering scheme (with respect to lead wire location) is shown and is the same for all arrays. (b) Luminance threshold values obtained from NHP1 for points across visual space. Values for spatial locations at the vertices of the plot were obtained before implantation of the arrays. Values located in the lower left and lower right quadrants of the plot that are not located at the vertices were obtained after the completion of all microstimulation experiments more than 290 days post-implantation. The centre of the plot represents the fixation point. MUA-RF and LFP-RF centre locations on each array are superimposed with the number indicating the electrode upon which they were recorded. (c) Enlarged views of the boxed regions in (b) showing RF centre locations. Data were obtained from an experimental session 5 months post-implantation.

vertical meridian at about 8° of eccentricity [18]. For NHP2, array1 was implanted anterior to the calcarine fissure and lateral to the sagittal sulcus, and array2 was implanted lateral to array1. This anatomical area was expected to represent the visual field near the horizontal meridian from 2.5° to 9° of eccentricity.

After a week of data collection, NHP2 damaged its connectors. Limited data were collected from this animal and are included in Figure 3.6(a). NHP1 was implanted with two arrays (array1 and array2), but the quality of the recordings from array2 was poor and, with the exception of data in Figures 3.4(c) and 3.6(c), it was not included in this work. Neither one of the NHPs exhibited any observable signs of neurological deficiencies throughout the course of the experiments.

Microelectrode arrays

Fixed-geometry arrays of penetrating microelectrodes were used for neural recording and microstimulation (Cereport Array (UEA), Blackrock Microsystems, Salt Lake City, UT). These arrays have been successfully implanted in the motor cortex [19-22], the auditory cortex [23, 24], the auditory nerve [25-27], the sciatic nerve [28], and the visual cortex [29, 30] of various animal models. Moreover, these electrodes have been acutely implanted in the middle temporal gyrus of epilepsy patients undergoing temporal lobectomy surgery [31-36] and chronically implanted in the motor cortex of paralyzed human patients [10-15].

Each array consisted of one hundred 1 mm long microelectrodes arranged in a 10 × 10 grid spaced 400 μm apart. The length of the electrode was chosen so that the electrode tip would reside approximately in layer 4 A/B of V1 [37, 38]. Each electrode base is electrically isolated from its neighbouring electrodes with glass and the rest of the

electrode, with the exception of the iridium-oxide tip, is insulated with a 2 μm coat of parylene-C. Each electrode tip is metalized with sputtered iridium-oxide film (SIROF) for better charge injection capacity. The electrodes have been manufactured to have an exposed tip length of 60 ± 40 μm, resulting in an active geometrical surface area of 500-4000 μm^2 (Personal communication, Blackrock Microsystems, Salt Lake City, UT). The electrode impedances ranged from 40 to 80 kΩ before implantation as measured with a 1 kHz sine-wave constant current signal (Cerebus, Blackrock Microsystems, Salt Lake City, UT). Median impedances were used for analysis after outliers (i.e. impedances greater than 2 MΩ) were discarded.

Data collection

MUA, LFPs, and behavioural data were recorded using a 128-channel data acquisition system (Cerebus, Blackrock Microsystems, Salt Lake City, UT). The continuous signal was sampled at 30 kHz and band-pass filtered with cutoff frequencies of 0.3 and 7500 Hz. This signal was digitally lowpass filtered at 250 Hz and was used for LFP analysis. It was digitally high-pass filtered at 250 Hz, and a threshold value of -3.5 RMS times the noise was used to obtain MUAs.

Microstimulation

For microstimulation experiments, we used a system capable of delivering electrical currents to 96 electrodes (RX7, Tucker-Davis Technologies, Alachua, FL). The stimulator battery had a compliance voltage of ±24 V (NC48, Tucker-Davis Technologies, Alachua, FL). The stimulators were capable of delivering currents up to 100 μA to each electrode.

Constant-current pulses were delivered to V1 through the individual electrodes on the UEA. Each pulse consisted of a cathodic-first symmetric biphasic square wave with no interphase interval and a phase width of 200 μs. Pulses were delivered at 200 Hz for a duration of 200 ms. Current amplitudes ranged from 0 to 96 μA. At these stimulation levels, 1.0-19.2 nC/phase was delivered to the tissue through each electrode. The charge density for each electrode ranged from 50 to 960 μC cm^{-2} for an electrode tip geometrical surface area of 2000 μm^2. Similar stimulation parameters evoked phosphenes in a human patient [6] and behavioural responses in macaque monkeys [9].

Systematic microstimulation was performed on a subset of 37 electrodes on array1 and 45 electrodes on array2 in NHP1. Initially, electrodes that were chosen for microstimulation were evenly distributed across the arrays. Later, more electrodes were selected for microstimulation based on their ability to record neural signals. Since these electrodes were not part of the initial subset, the total number of electrodes that were stimulated is different for each array.

Receptive field mapping

For RF mapping, the display was calibrated with a photometer (L203, Macam Photometrics LTD, Tranent, East Lothian, England) so that the white intensity level was set to 84.2 cd m^{-2} and the background level was set to 41.9 cd m^{-2}. The RF properties of each electrode were measured by flashing a small (0.45 × 0.45 visual degrees) white square at random locations on the screen against a grey background. The stimulus was flashed every 100 ms for a trial duration of 1000 or 2000 ms. RF maps from MUA (MUA-RF) were generated by reverse correlation of the visual stimuli with action potential event times [39] for 21 temporal offsets (0, 5, 10, …, 100 ms). The amplitude of

the RF response for each offset was calculated by dividing the value of the peak response by the mean of the background. The five largest RF responses of the 21 temporal offsets were averaged to create the RF map. From this RF map, responses with amplitudes greater than 10 are defined as large. RF maps were also generated from stimulus-evoked LFPs by forward correlation of the stimulus presentations to the response of the LFP signal. Specifically, for each location at which a stimulus was presented, the average evoked LFP response was integrated from 0 to 200 ms after stimulus onset. The LFP-RF was defined as the distribution of the integrated LFP responses for all spatial locations at which stimuli were presented.

Analysis of visuotopic organization

The conformal nature of the visuotopic organization of V1 was estimated. A non-linear, least-mean-square method was used to minimize the distances between the actual RF centres and the coordinate transforms of each array into visual space. The coordinate transformation allowed for five degrees of freedom: magnification along both sides of the array, rotation of the array, and translation along both the horizontal and vertical axes [30]. The degree of conformality was estimated as the average length of the vector connecting each RF centre to the transformed location of the electrode on which the RF was measured.

Results

We examined a number of physiological and device performance factors that could influence the development of a high-resolution cortically based visual prosthesis.

Validation of primate behaviour and functional status of implant sites

To ensure that the NHPs could correctly report visual percepts and to verify that their visual systems remained functional post-implantation, they were trained on a forced-choice photic detection task prior to implantation. The NHPs were required to indicate whether they were able to perceive photic stimuli at various luminance intensities. Threshold values that were obtained from the NHPs were compared to those obtained from human subjects. The visual detection thresholds for five human subjects for a stimulus located in the right visual hemisphere at an eccentricity of 2° along the horizontal meridian ranged from 520 to 1750 μcd m^{-2} (946 ± 493 μcd m^{-2}, mean ± std). Using the same task and stimuli, the thresholds obtained for NHP1 and NHP2 were 960 and 1480 μcd m^{-2}, respectively, indicating that the NHPs were able to perform the detection task at a level comparable to human subjects. For NHP1, luminance thresholds were also obtained for visual stimuli that were evenly distributed across a circular region spanning 24° of visual space (Figure 3.1(b)). Threshold values were in agreement with the spatial density distribution of rods and cones on the human [40] and macaque [41] retinas.

Prior to array implantation, luminance thresholds were measured for the stimuli presented in the approximate location of the visual space representing the region of cortex in which the arrays were later implanted. These values ranged from 250 to 550 μcd m^{-2} and 250 to 715 μcd m^{-2} for NHP1 and NHP2, respectively. At greater than 290 days post-implantation and after 2 months of periodic microstimulation using currents up to 96 μA, the photic thresholds for the visual field locations represented by the cortex where the arrays were implanted were measured and ranged from 410 to 890 μcd m^{-2}. For the

same spatial location in the opposite visual field, represented by unimplanted V1, thresholds ranged from 390 to 1080 μcd m^{-2} (Figure 3.1(b)). These values confirm that cortical function had not been impaired by the implantation and the chronic presence of the UEA.

Electrode impedances

Electrode impedances were measured multiple times each week over the course of 8 months. In NHP1, the median pre-implantation impedances were 46 kΩ for array1 and 67.4 kΩ for array2 and the first post-implantation impedances, taken 3 weeks after the surgery, were 192 kΩ for array1 and 396 kΩ for array2. In NHP2, the median pre-implantation impedances were 44 kΩ for array1 and 46 kΩ for array2 and the first post-implantation measurements, taken 3 weeks after the surgery, were 170 kΩ for array1 and 113 kΩ for array2. Over time, we observed a gradual drop in impedances down to near pre-implantation values. In NHP1, the median impedances taken 8 months after surgery were 105 kΩ for array1 and 121.5 kΩ for array2. This drop in impedances occurred on both stimulated and non-stimulated electrodes and was not significantly different between the two groups (p>0.34, Kolmogorov–Smirnov). Since NHP2 damaged its connectors shortly after surgery, impedances were not measured over a long enough period of time to observe a similar drop. Electrode impedances greater than 2 MΩ were not included in these analyses. We also measured electrode impedances before and after each stimulation session. After stimulation sessions, a significant drop (p<0.01, Kolmogorov-Smirnov) in impedance was observed for all electrodes that were stimulated (Figure 3.2(a)). Impedances on the stimulated electrodes increased by the next stimulation session and

(a) Electrode Impedances After Stimulation Sessions

(b) Electrode Impedances Before Stimulation Sessions
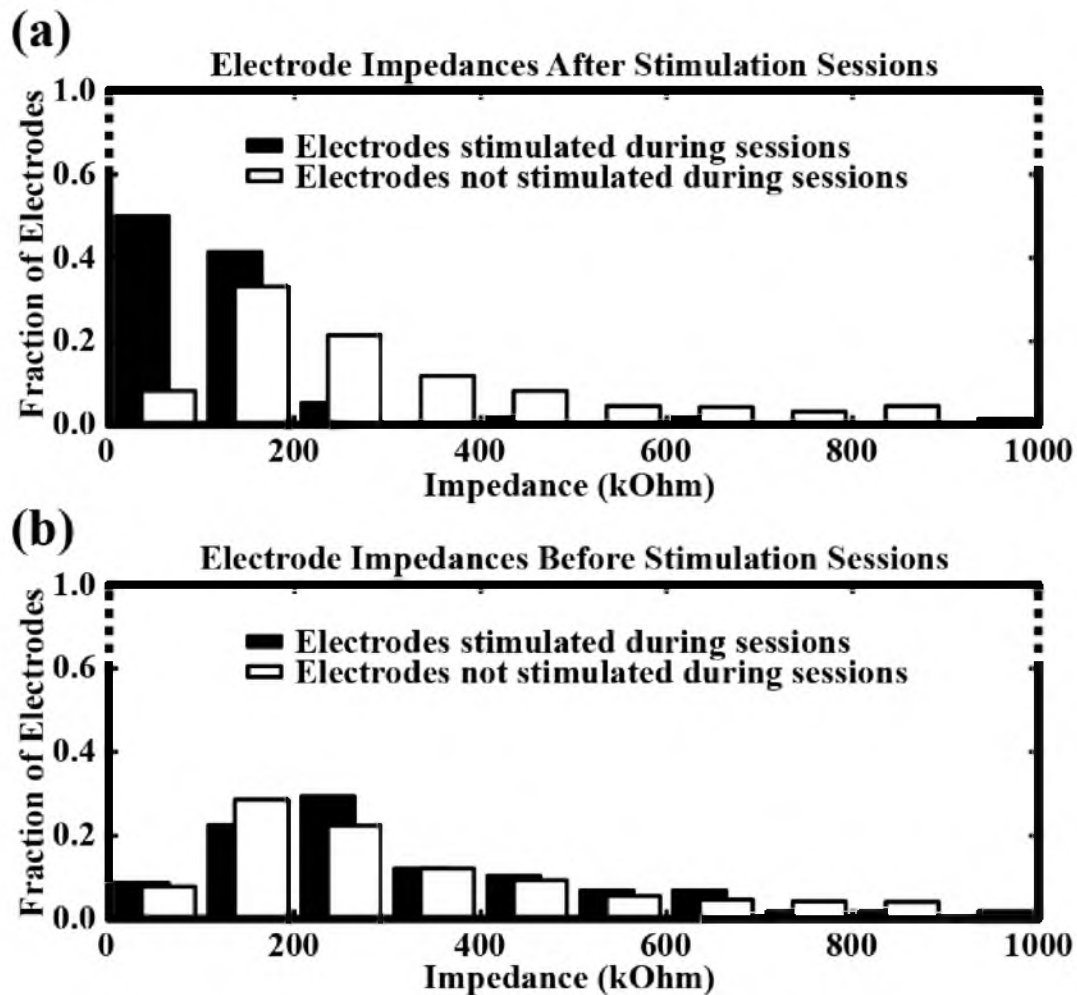
Figure 3.2. Stimulated electrodes show a consistent drop in impedance after stimulation sessions. (a) Distribution of impedances after each stimulation session for electrodes that were stimulated (black) and those that were not stimulated (white). A significant decrease in impedance was observed for electrodes that were stimulated when compared to electrodes that were not stimulated. Data were taken from eight sessions and consisted of 58 stimulated and 710 non-stimulated electrodes. (b) Post-stimulation impedances increased by the next stimulation session and the distribution of impedances was not significantly different when compared to impedances from electrodes that were never stimulated.

their distribution was not significantly different (p>0.36, Kolmogorov-Smirnov) when compared to the distribution of the non-stimulated electrodes (Figure 3.2(b)).

MUA and LFP recording and mapping

Throughout 7 months of experimentation, full-bandwidth data were recorded on every electrode for both arrays in NHP1. On array1 of NHP1, when using a threshold value of -3.5 RMS times the noise, the MUA was detected on every electrode. Twenty-eight electrodes recorded a large MUA, defined as mean waveforms with a peak-to-peak amplitude greater than 125 μV, across 19 recording sessions spanning 6 months (Figure 3.3(a)). The activity on these channels was not consistent over time, i.e. large MUA was observed to appear and disappear across sessions for individual electrodes. The region of the array with a large MUA was consistent over time. RFs were mapped using MUA. Twenty-five electrodes exhibited large MUA-RF responses (methods section). Sixteen of these responses came from electrodes that recorded a large MUA. Electrodes exhibiting large MUA-RFs were generally clustered in the upper-middle region of the array where large MUA was recorded (Figure 3.3(b)).

Over 3 months of experimentation, visually evoked LFP were recorded on most electrodes on array1 of NHP1. Fifty-two of these electrodes exhibited large responses, defined as average LFP waveforms with a peak-to-peak amplitude greater than 75 μV. For this array, a phase reversal in the amplitude of the responses was observed across the electrodes. Approximately half of the visually evoked responses manifested a prominent negative-going average waveform, and the other half showed a prominent positive-going waveform (Figure 3.4(a)). Every electrode on this array that recorded evoked responses also exhibited an LFP-RF. Moreover, the positive-going and negative-going evoked
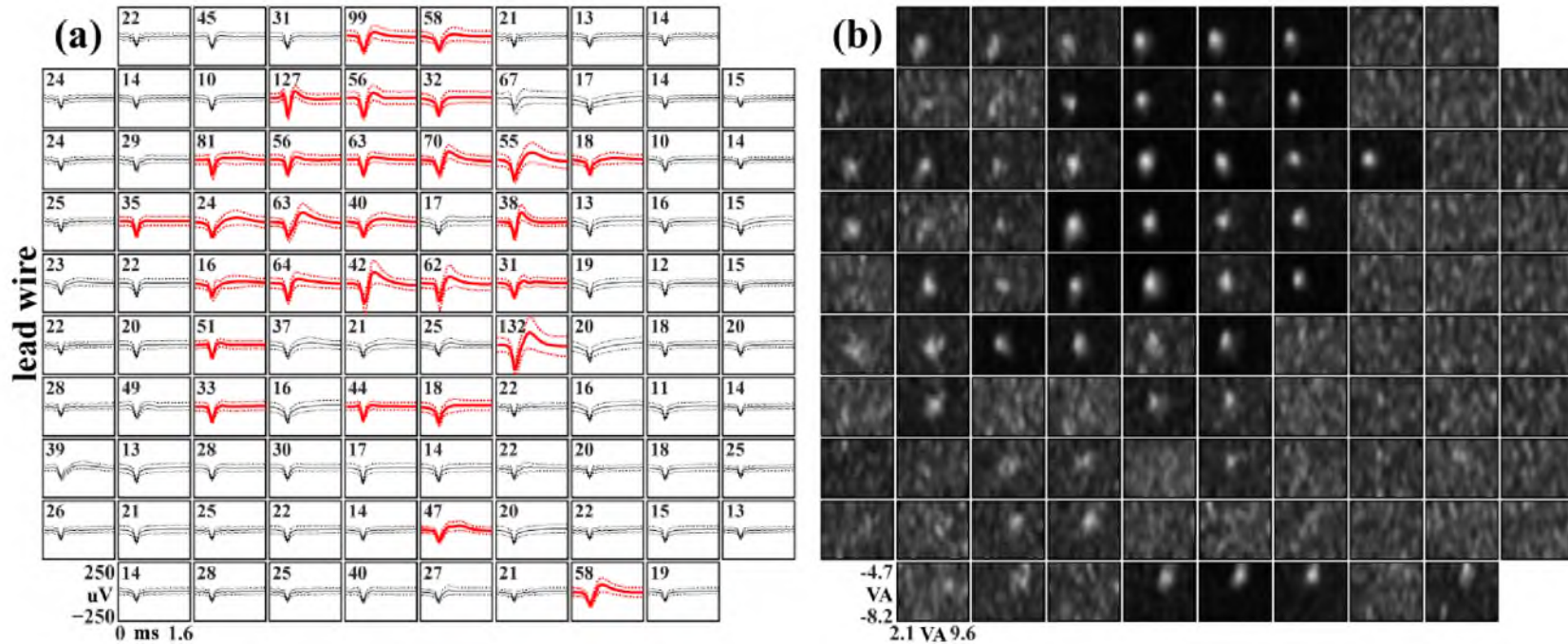
Figure 3.3. Across multiple recording sessions, the largest MUA was mostly localized to the upper-middle region of the array. This region correlated with the region where robust MUA-RFs were observed. (a) Largest MUA for each electrode compiled from 19 recording sessions spanning 6 months. Waveforms were extracted from full-bandwidth (30 kS s^{-1}), high-pass filtered (250 Hz) neural recordings using a 100 µV threshold crossing. The mean waveform for each electrode was then calculated from these extracted waveforms. Mean waveforms with a peak-to-peak amplitude greater than 125 µV are shown in bold red. Firing rate in Hertz is shown in the upper left corner of each box. (b) RFs generated using reverse correlation. Each box represents a region of visual space vertically from -4.7 to -8.2 visual degrees and horizontally from 2.1 to 9.6 visual degrees with the fixation point near the upper left corner. Data came from an experimental session 5 months post-implantation in NHP1 array1.

Figure 3.4. Visually evoked LFP recordings and LFP-RFs demonstrated an amplitude phase reversal across the array. The region of the array with negative-going LFP responses correlated with the region where the largest MUA was observed. (a) Largest visually evoked LFP for each electrode compiled from ten recording sessions spanning 3 months. Each waveform represents the average of ~50 LFP responses to a visual stimulus. Responses with a peak-to-peak amplitude greater than 75 µV are shown in bold red. Stimulus onset occurred at time zero. A shift from a positive to a negative-going response can be seen when moving diagonally across the array. (b) Each box represents a region of visual space vertically from -4.7 to -8.2 visual degrees and horizontally from 2.1 to 9.6 visual degrees with the fixation point near the upper left corner. Pixel intensities represent the area under the evoked LFP response for a stimulus at that location in visual space. White RFs were generated from positive-going LFP responses and black RFs from negative-going responses. (c) LFP-RFs across array2. An amplitude phase reversal was not observed for this array. (d) LFP-RF sizes for array1 compiled from ten recording sessions over 3 months and separated into black (negative-going LFP) versus white (positive-going LFP) responses. RFs were fit to a Gaussian curve, and the radius represents the standard deviation of the fit. Black RFs were significantly smaller than white RFs.
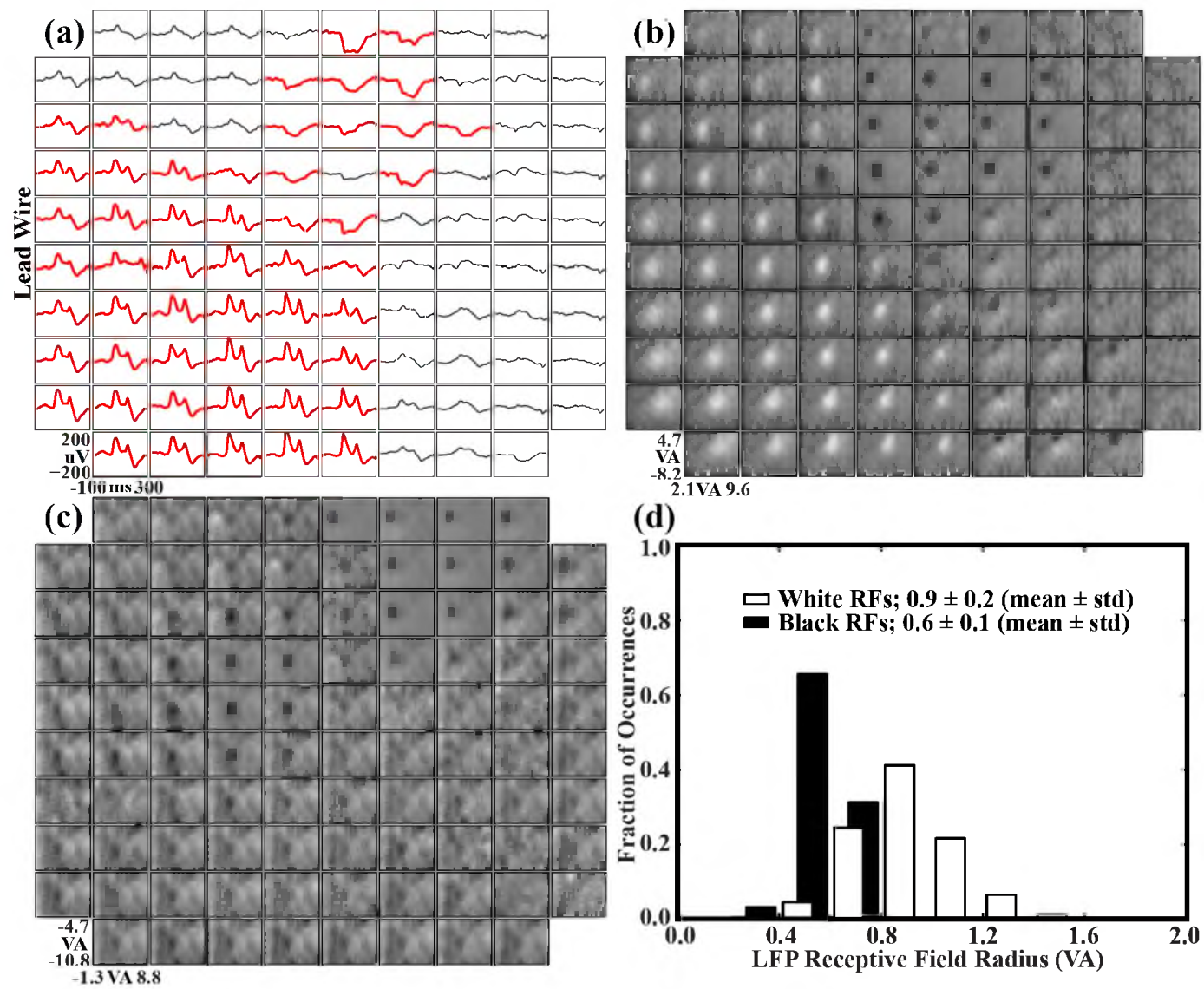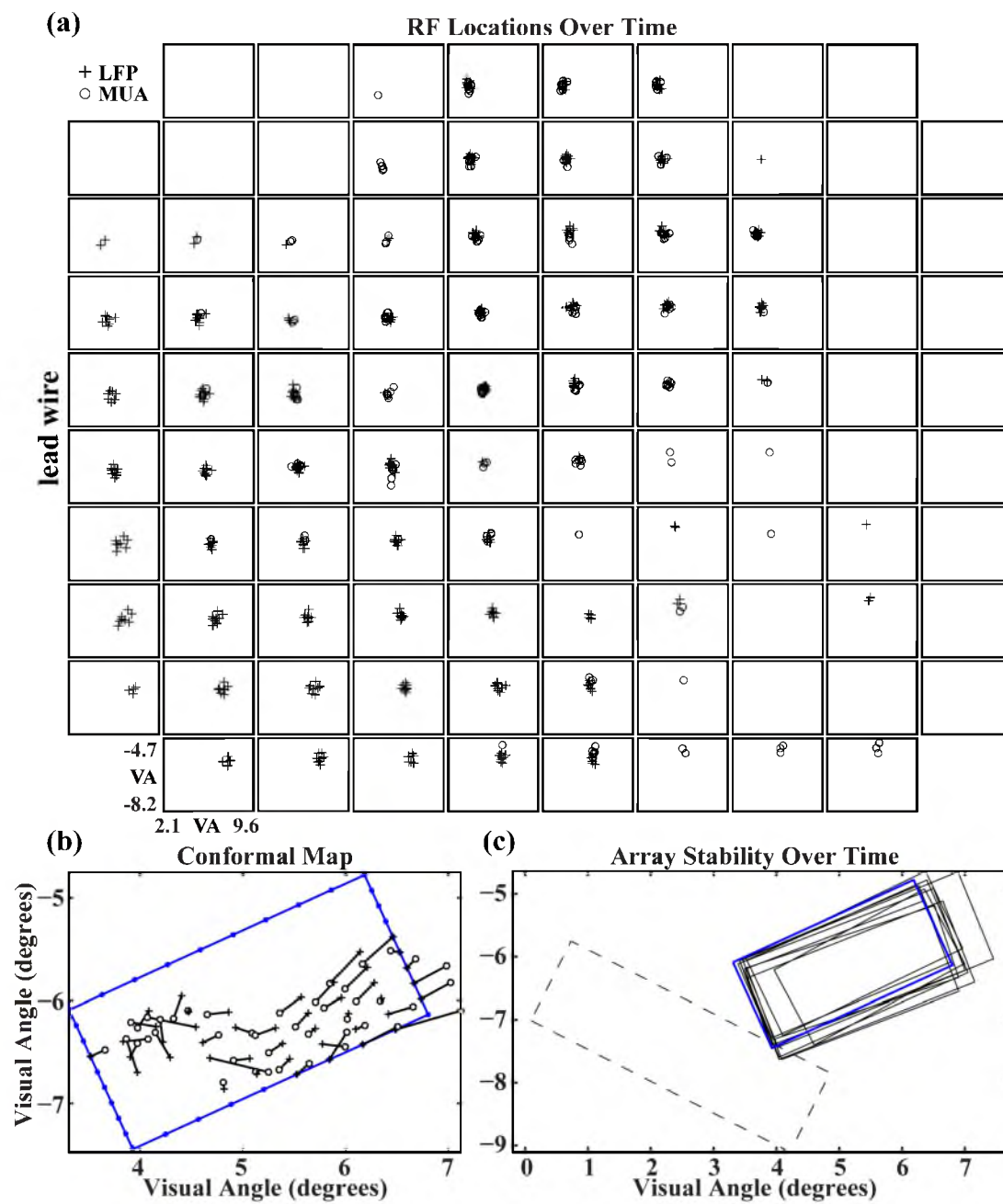
response waveforms yielded significantly different RF diameters (p<0.05, Kolmogorov–Smirnov) for the positive (0.9 ± 0.2 visual degrees, mean ± std) and the negative (0.6 ± 0.1 visual degrees, mean ± std) RFs (Figure 3.4(d)). LFPs, but not MUA, were also recorded on array2. Similar to the findings on array1, any electrode that exhibited an evoked LFP response to visual stimuli also yielded an LFP-RF. However, all of the evoked responses on this array were negative going (Figure 3.4(c)).

MUA and LFP visuotopy

The spatial locations of both MUA-RFs and LFP-RFs were measured during ten recording sessions over a 97 day period. The mean spatial separation for all RF centres during this time was 0.2 ± 0.1 (mean ± std) visual degrees. The mean spatial separation between MUA-RF and LFP-RF centres, for those electrodes and experimental sessions on which both were simultaneously recorded, was 0.3 ± 0.2 (mean ± std) visual degrees (Figure 3.5(a)). The global visuotopic organization of RFs across the array was further analyzed by applying a least-mean-squared-error fit to a conformal transformation of the electrode array geometry to the locations of the RF centres associated with their respective electrodes [30]. The least-mean-squared-error fit minimizes the length of vectors connecting each transformed electrode location and its respective RF centre. This calculation was performed independently for MUA-RF and LFP-RF centres. As calculated from LFP-RF centres, array1 spanned approximately 1.5° by 3.0° of visual field (Figure 3.5(b)), while array2 spanned 1.5° by 4° of visual field. Repeated calculations of the global visuotopic organization were made and found to be consistent across the 97 day time period (Figure 3.5(c)). There was some movement of the array outline across time, limited to around 1/3 of a degree of visual angle, but there was no

Figure 3.5. RF centres are stable over time and occupy distinct regions of visual space for different electrodes across the array. The location of the array in visual space remains stable over time. (a) MUA-RF and LFP-RF centres for each electrode taken from ten recording sessions spanning 97 days. The spatial variance for all MUA and LFP centres is 0.2 ± 0.1 (mean ± std) visual degrees. (b) Least-mean-squared-error fit of a conformal transformation of the electrode array geometry to the locations of the RF centres associated with their respective electrodes. Data were collected 148 days after implantation in NHP1 on array1. The blue rectangular outline with small, filled circles represents the electrode array as mapped into visual space with each symbol indicating the location of an electrode along the periphery of the array. The large filled diamond and filled square on the left corners of this outline represent electrode sites at the most anterolateral and anteromedial corners of the array, respectively. Crosses represent the conformal geometry of the electrode array transformed into a visual space representation. Each cross is connected to an open circle that represents the mapped RF centre of that electrode. (c) Solid outlines represent array1 position in visual space over 97 days of recording. Outlines were generated from LFP-RF data using the method described in (b). The blue outline represents the fit from the data shown in (b). The dashed outline shows the position of array2 for a single recording session.

(a)

RF Locations Over Time

+ LFP
○ MUA

-4.7
VA
-8.2

2.1 VA 9.6

lead wire

(b)

Conformal Map

Visual Angle (degrees)

Visual Angle (degrees)

(c)

Array Stability Over Time

Visual Angle (degrees)

long-term trend apparent in this movement. The mean vector length is an estimate of the difference between the conformal representation of the array in visual space and the observed RF locations and can be used as a method of quantifying visuotopic scatter. The mean vector lengths were 1.97 ± 0.34 and 0.94 ± 0.18 visual degrees (mean $\pm$ std) for LPF and MUA calculated RF centres, respectively, and are comparable to the values previously obtained from cats [30].

Microstimulation

For NHP1, systematic stimulation via 37 electrodes of array1 and 45 electrodes of array2 was performed. By varying the stimulation current, psychometric curves were obtained for all electrodes that elicited a consistent behavioural response (Figure 3.6(a)). Prior to the connector failure in NHP2, one electrode in array1 was stimulated and elicited consistent behavioural responses. For NHP1, 5 of the 37 stimulated electrodes on array1 and 3 of the 45 stimulated electrodes on array 2 elicited consistent behavioural responses from which psychometric curves were generated. These electrodes were clustered in the upper-middle region of the array1. Threshold values for all electrodes for which psychophysical curves could be generated ranged from 18 to 76 µA (46 ± 19 µA mean $\pm$ std) (Figure 3.6(b)). Out of the 37 systematically stimulated electrodes in array1, 32 did not elicit consistent behavioural responses when systematically stimulated over multiple days using currents up to 96 µA (Figure 3.6(b)). Similar results are shown for stimulating electrodes on array2 (Figure 3.6(c)).

After repeated stimulation via individual electrodes during a session, we qualitatively observed a decrease in the ability of the NHP to detect phosphenes. When an electrode was stimulated above its threshold level repeatedly over a short period of
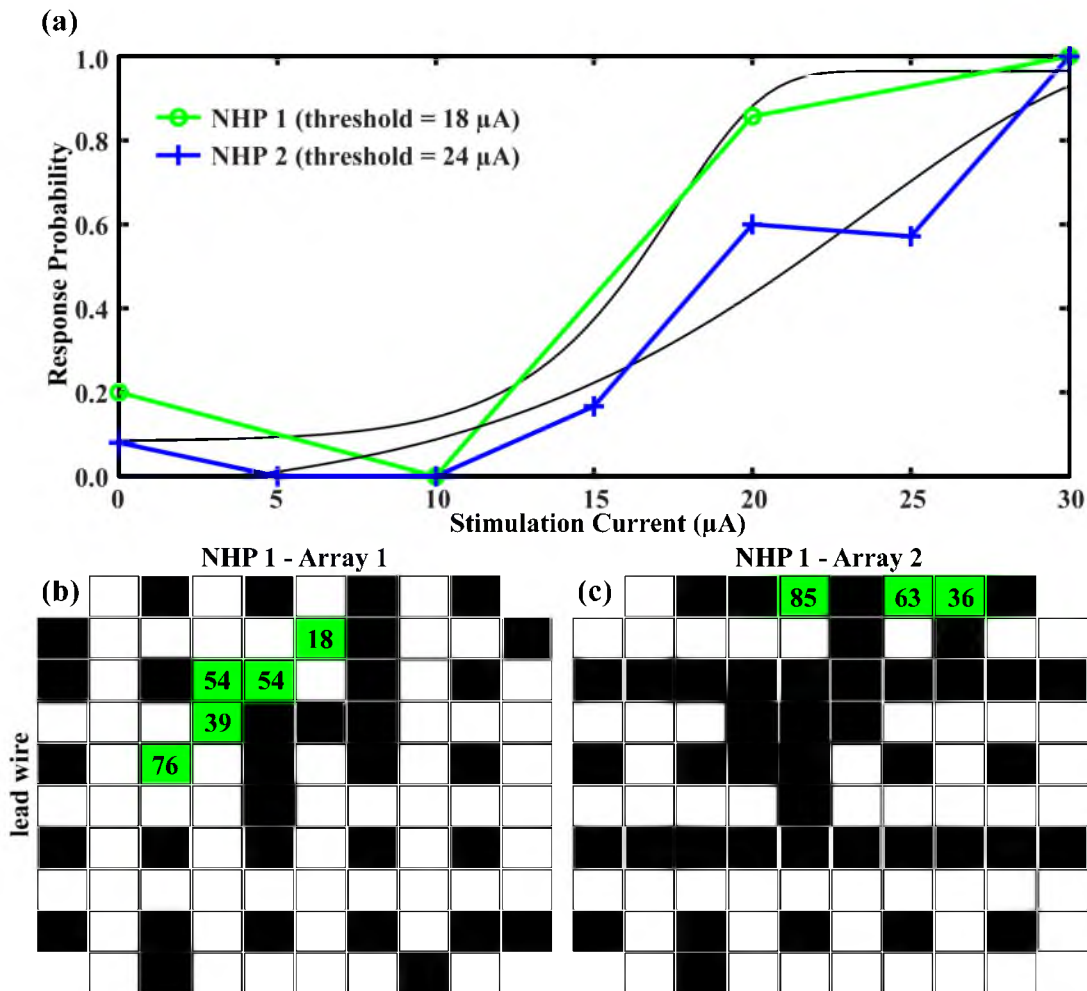
Figure 3.6. Effective microstimulation occurred on electrodes in the same region of the array where the largest MUA and the negative-going visually evoked LFP responses were recorded. (a) Behavioural responses to microstimulation of a single electrode in each of two NHPs. Each data point represents the average of approximately five yes/no responses to that level of stimulation. Stimulation parameters for both animals consisted of a train of 40 cathodic-first pulses of width 200 µs and frequency 200 Hz. The green psychometric curve was generated from data collected from NHP1 by stimulation via electrode 15 on array1. The blue psychometric curve was generated from data collected from NHP2 by stimulation via electrode 56 on array1. Black curves are the nonlinear fits of the Weibull function to the data. Thresholds are taken at the 50% response probability. (b) Distribution of stimulated electrodes and the resulting behavioural responses across array1 for NHP1. Black boxes represent electrodes that were stimulated up to 96 µA and did not elicit a behavioural response. Green boxes show electrodes that generated psychometric curves in response to stimulation. The numbers in each box represent the lowest current threshold acquired for that electrode. White boxes were never stimulated. (c) Same plot as (b) for NHP1 array2.

time (i.e. minutes), increasingly higher levels of stimulation were required for the NHP to indicate detection. As a workaround to this, we increased the time between repeated stimulations of the same electrode by introducing photic stimuli interleaved with an occasional electrical stimulus.

Discussion

In this work, we investigated the functional consequences of chronic implantation and periodic electrical stimulation via a fixed-geometry intracortical microelectrode array in NHP V1. Measurement of photic detection thresholds demonstrated that the NHPs' visual systems did not have deficits in visual or visually guided motor behaviour. Further, they have been successfully trained to perform the forced-choice photic and electric threshold tasks. NHP behaviour and attention can likely account for much of the variance observed across threshold detection data sets.

V1 of a behaving NHP was confirmed to be visuotopically organized, but only in a global sense. It was further demonstrated that maps of this organization using an array of penetrating microelectrodes were stable over the three months of experimentation. Although individual RFs did not follow a perfectly conformal map, when examining the global visuotopic organization across a large number of RFs the visuotopy agrees with previous findings [42]. As some electrodes did not provide an RF for all ten recording sessions, the variance seen in global organization could be simply one of the regression errors. Other sources of variance in the visuotopic organization could be due to micro-saccades and the limited resolution of the eye tracking system (0.25-0.5 visual degrees).

After several months of being implanted and undergoing multiple microstimulation sessions, electrodes were still able to record MUA and LFP signals.

This demonstrated that arrays could be subjected to physiologically effective (and higher) levels of microstimulation *in vivo* without functional degradation. Photic threshold values were similar before and after array implantation and microstimulation, confirming that the neural tissue was not functionally impaired.

Below we discuss some of the challenges involved with electrical microstimulation of macaque V1.

Quality of signals recorded

A large amplitude MUA was recorded on a small number of electrodes throughout seven months of recording. The same sparse action potential activity has been observed in arrays implanted in A1 and the parabelt cortex of macaque [43], while large well-isolated action potentials have consistently been recorded on similar arrays implanted in the primary motor cortex of macaques [19] and cats [44]. The cells in the middle layers of sensory cortices, where the electrode tips are targeted, are relatively small compared to the large pyramidal projection cells in the primary motor cortex. Such a difference in size may be a significant factor influencing the differential in the quality of recordings in sensory versus motor cortices. In acute or sub-chronic recording experiments with single microelectrodes, the electrode can be positioned to optimize the neuronal activity [45]. In the experiments reported herein, however, fixed-geometry electrode arrays were used as the basis for a visual prosthesis, and such flexibility in positioning electrodes was not available. Thus, only a few electrodes may have been close enough to neuronal somata to record a large MUA. However, LFPs were recorded on nearly all electrodes. LFPs are thought to be sampling neuronal signals over a larger electrode recording radius (several hundred μm) compared to MUA (~100 μm or less)

[46-48], which may explain why more electrodes recorded evoked LFP than MUA signals. Additionally, similar to reports by others, large MUA recordings were inconsistent on individual electrodes from recording session to recording session, while LFPs were consistently recorded during all sessions [29, 49].

Factors influencing microstimulation efficacy

Our ability to evoke phosphenes was limited during these experiments. Stimulation evoked consistent behavioural responses on five out of the 37 electrodes and three out of the 45 electrodes for the two arrays implanted in NHP1. Only one electrode on the arrays in NHP2 generated phosphenes, but these arrays were not systematically tested before their connectors were damaged. Our data suggest that the ability to reliably evoke phosphenes and thus elicit consistent behavioural responses may be influenced by several factors: changes in electrode impedance, the location of the electrode tips in cortical lamina and relative to cell bodies, and the inability of the NHP to generalize from the training on photic stimuli to responding to phosphenes generated by microstimulation.

Changes in electrode impedances. After array implantation, impedances increased, which presumably was due to the addition of tissue impedances and/or fibrous tissue encapsulation promoted by the foreign body response [50-53]. Over the course of the experiments, the impedance of all electrodes gradually dropped toward pre-implantation levels. This drop has also been reported by others [19, 24, 44]. After each microstimulation session, the impedance of stimulated electrodes dropped significantly. This post-stimulation impedance drop has been previously reported and termed 'rejuvenation'. It is thought to be due to removal of the cellular and acellular debris around the electrode site by a hydrous monolayer produced at iridium electrodes during

pulsing [52, 54]. When the impedance of an electrode drops during the microstimulation with a constant-current pulse, the voltage across the electrode will drop accordingly. The acute impedance drop and concomitant change in voltage may have influenced the ability to microstimulate to effect. However, the impedances remained within an acceptable range throughout the experiments, so that microstimulation does not appear to have functionally impaired the electrode tips.

Electrode tip location. Electrodes that evoked consistent behavioural responses to microstimulation were grouped in the upper-middle region of array1 in NHP1. This is the same region where the electrodes recorded the large MUA. This observation suggests that the distance from an electrode tip to neuronal somata may be an important factor influencing our ability to effectively evoke behavioural responses to microstimulation.

Previous findings demonstrate a complex temporal pattern in visually evoked LFP responses as a function of the laminar placement of the recording electrode tip [37, 55]. We observed that many of the visually evoked LFP responses manifested a positive-going waveform on contiguous electrodes, and that many other evoked responses manifested a negative-going waveform on a different set of contiguous electrodes. It has also been shown that the visual spread of RFs, generated with similar techniques used in this study, was related to the cortical lamina from which the recordings were made [48]. This study showed that this visual spread is smallest in layer 4C and increases in shallower and deeper layers. We observed that the sizes of LFP-RFs on electrodes recording negative-going waveforms were smaller than the sizes of the LFP-RFs on electrodes recording positive-going waveforms. Further, it has been shown that microstimulation detection thresholds vary as a function of the cortical lamina in which

the electrode tip is placed [37, 56]. These values tended to decrease with depth and the lowest threshold values were reported in layer 2/3 [37] or layer 5/6 [56]. The electrodes on array1 from NHP1 that elicited consistent behavioural responses were in the same region of the array as the electrodes which recorded negative-going LFPs and smaller LFP-RFs. Together, these findings suggest that the plane of the electrode tips of array1 in NHP1 was not parallel to the plane of the cortical lamina, so that the electrode tips straddle a sink-source current boundary. The electrodes which recorded negative-going LFP waveforms and small LFP-RFs were likely located in or close to layer 4C and in a layer with low thresholds, and were therefore more likely to elicit a behavioural response with microstimulation, while the electrodes which recorded positive-going LFP waveforms were likely located across a sink-source boundary in a layer with relatively high thresholds.

Our data are consistent with the results of others described above and suggest that the ability to evoke phosphenes and therefore elicit behavioural responses may be influenced by the proximity of the electrode tips to neuronal somata and their placement in cortical lamina.

Limitations of NHP experimentation. In previous human studies, phosphenes have been described as round Gaussian spots, clouds of smaller dots, and points of light with different colours and shapes [1, 6]. We trained the NHPs to indicate detection of round monochromatic Gaussian photic stimuli of a single size. Because the NHPs were only trained to respond to this simple, round Gaussian stimulus, and microstimulation may have generated more complex visual perceptions, it is possible that the NHPs were simply confused by some of the microstimulation-evoked percepts and therefore did not

respond. Increasing the level of microstimulation has also been shown to change the number of perceived phosphenes from one to two [6]. We found that RF centre locations of MUA and LFP signals of the same electrode did not perfectly overlap, so that it is unclear whether phosphenotopy will follow the visuotopic organization of the MUA-RFs or LFP-RFs. It is possible that at high stimulation levels two phosphenes, one located at the MUA-RF and another at the LFP-RF, were generated. This could also cause confusion in the NHPs and result in a lack of response.

The factors described above may account for the fact that only eight out of 82 systematically stimulated electrodes elicited behavioural responses. These results can be compared to the other studies of electrical stimulation via chronically implanted electrodes. In an NHP study, 12 of the 37 stimulated electrodes (144 total implanted electrodes) resulted in behavioural responses [9]. In a human patient who could easily understand and articulate responses to complex visual percepts, 34 of the 36 stimulated electrodes (38 implanted electrodes) elicited subjective visual perceptions [6].

Conclusion

We demonstrated that microstimulation of the primary visual cortex via a high-density array of penetrating microelectrodes is capable of evoking visual perceptions in NHPs. Continuous long-term microstimulation of neural tissue has been shown to produce neuronal cell loss within a small radius (~60-150 μm) of the stimulating electrodes [57]. Further, we acknowledge that any implanted system will evoke some degree of foreign body response. However, in our experiments, any such cell loss and foreign body response did not appear to functionally impair the NHP visual system or the electrode array. This was shown by (1) the similar photic threshold values before and

after the experiments and (2) the ability to record the large amplitude MUA and LFPs with spatially distinct RFs for different electrodes throughout the experiments. Electrode impedances dropped acutely in response to microstimulation, and, over time, the impedances of all electrodes in the array dropped towards the pre-implantation values. Impedance values, however, never indicated that a functional electrode failed during the experiments. While some further animal experimentation will be needed to determine factors such as optimal laminar placement of electrode tips and optimal stimulation parameters, these results support the move into human experiments where verbal feedback on the evoked visual perceptions will greatly accelerate our understanding of how the parameters of cortical microstimulation relate to subjective visual perception.

Acknowledgements

References

[1]   G. S. Brindley, and W. S. Lewin, "The visual sensations produced by electrical stimulation of the medial occipital cortex," *J. Physiol.*, vol. 196, no. 2, pp. 479-93, Feb, 1968.

[2]   W. H. Dobelle, and M. G. Mladejovsky, "Phosphenes produced by electrical stimulation of human occipital cortex, and their application to the development of a prosthesis for the blind," *J. Physiol.*, vol. 243, no. 2, pp. 553-76, Dec, 1974.

[3]   D. A. Pollen, "Some perceptual effects of electrical stimulation of the visual cortex in man," *The Nervous System*, vol. 2, pp. 519-28, 1975.

[4]   S. Kotler, "Vision quest," *Wired mag.*, pp. 10.09 (September), 2002.

[5]   M. Bak *et al.*, "Visual sensations produced by intracortical microstimulation of the human occipital cortex," *Med. Biol. Eng. Comput.*, vol. 28, no. 3, pp. 257-9, May, 1990.

[6]   E. M. Schmidt *et al.*, "Feasibility of a visual prosthesis for the blind based on intracortical microstimulation of the visual cortex," *Brain*, vol. 119 (Pt 2), pp. 507-22, Apr, 1996.

[7]   E. A. DeYoe, "An investigation in the awake macaque of the threshold for the detection of electrical currents applied to striate cortex: psychophysical properties and laminar differences," PhD Thesis, Rochester University, NY, USA, 1983.

[8]   J. R. Bartlett *et al.*, "Psychophysics of electrical stimulation of striate cortex in macaques," *J. Neurophysiol.*, vol. 94, no. 5, pp. 3430-42, Nov, 2005.

[9]   D. C. Bradley *et al.*, "Visuotopic mapping through a multichannel stimulating implant in primate V1," *J. Neurophysiol.*, vol. 93, no. 3, pp. 1659-70, Mar, 2005.

[10]   L. R. Hochberg *et al.*, "Neuronal ensemble control of prosthetic devices by a human with tetraplegia," *Nature*, vol. 442, no. 7099, pp. 164-71, Jul 13, 2006.

[11]   S. P. Kim *et al.*, "Neural control of computer cursor velocity by decoding motor cortical spiking activity in humans with tetraplegia," *J. Neural Eng.*, vol. 5, no. 4, pp. 455-76, Dec, 2008.

[12]   C. L. Ojakangas *et al.*, "Decoding movement intent from human premotor cortex neurons for neural prosthetic applications," *J. Clin. Neurophysiol.*, vol. 23, no. 6, pp. 577-84, Dec, 2006.

[13]   W. Truccolo *et al.*, "Primary motor cortex tuning to intended movement kinematics in humans with tetraplegia," *J. Neurosci.*, vol. 28, no. 5, pp. 1163-78, Jan 30, 2008.

[14]   C. E. Vargas-Irwin *et al.*, "Decoding complete reach and grasp actions from local primary motor cortex populations," *J. Neurosci.*, vol. 30, no. 29, pp. 9659-69, Jul 21, 2010.

[15]   J. Zhuang *et al.*, "Decoding 3-D reach and grasp kinematics from high-frequency local field potentials in primate primary motor cortex," *IEEE Trans. Biomed. Eng.*, vol. 57, no. 7, pp. 1774-84, Jul, 2010.

[16]   T. S. Davis *et al.*, "A minimally invasive approach to long-term head fixation in behaving nonhuman primates," *J. Neurosci. Methods*, vol. 181, no. 1, pp. 106-10, Jun 30, 2009.

[17]   P. J. Rousche, and R. A. Normann, "A method for pneumatically inserting an array of penetrating electrodes into cortical tissue," *Ann. Biomed. Eng.*, vol. 20, no. 4, pp. 413-22, 1992.

[18]   J. Kaas, and C. Collins, "The Primate Visual System," C. Press, ed., pp. 265-9, Boca Raton, FL: CRC Press, 2004.

[19]   J. Baker *et al.*, "Multi-scale recordings for neuroprosthetic control of finger movements," *Conf. Proc. IEEE Eng. Med. Biol. Soc.*, pp. 4573-7, 2009.

[20]   N. Hatsopoulos *et al.*, "Cortically controlled brain-machine interface," *Conf. Proc. IEEE Eng. Med. Biol. Soc.*, vol. 7, no. 1, pp. 7660-3, 2005.

[21]   M. D. Linderman *et al.*, "Neural recording stability of chronic electrode arrays in freely behaving primates," *Conf. Proc. IEEE Eng. Med. Biol. Soc.*, vol. 1, pp. 4387-91, 2006.

[22]   M. Velliste *et al.*, "Cortical control of a prosthetic arm for self-feeding," *Nature*, vol. 453, no. 7198, pp. 1098-101, Jun 19, 2008.

[23]   S. J. Kim *et al.*, "Electrophysiological mapping of cat primary auditory cortex with multielectrode arrays," *Ann. Biomed. Eng.*, vol. 34, no. 2, pp. 300-9, Feb, 2006.

[24]   P. J. Rousche, and R. A. Normann, "Chronic recording capability of the Utah Intracortical Electrode Array in cat sensory cortex," *J. Neurosci. Methods*, vol. 82, no. 1, pp. 1-15, Jul 1, 1998.

[25]   T. Hillman *et al.*, "Cochlear nerve stimulation with a 3-dimensional penetrating electrode array," *Otol. Neurotol.*, vol. 24, no. 5, pp. 764-8, Sep, 2003.

[26]   S. J. Kim *et al.*, "Selective activation of cat primary auditory cortex by way of direct intraneural auditory nerve stimulation," *Laryngoscope*, vol. 117, no. 6, pp. 1053-62, Jun, 2007.

[27]   J. C. Middlebrooks, and R. L. Snyder, "Intraneural stimulation for auditory prosthesis: modiolar trunk and intracranial stimulation sites," *Hear. Res.*, vol. 242, no. 1-2, pp. 52-63, Aug, 2008.

[28]   D. McDonnall *et al.*, "Selective motor unit recruitment via intrafascicular multielectrode stimulation," *Can. J. Physiol. Pharmacol.*, vol. 82, no. 8-9, pp. 599-609, Aug-Sep, 2004.

[29]   E. M. Maynard *et al.*, "A technique to prevent dural adhesions to chronically implanted microelectrode arrays," *J. Neurosci. Methods*, vol. 97, no. 2, pp. 93-101, Apr 15, 2000.

[30] D. J. Warren *et al.*, "High-resolution two-dimensional spatial mapping of cat striate cortex using a 100-microelectrode array," *Neuroscience,* vol. 105, no. 1, pp. 19-31, 2001.

[31] P. A. House *et al.*, "Acute microelectrode array implantation into human neocortex: preliminary technique and histological considerations," *Neurosurg. Focus,* vol. 20, no. 5, pp. 1-4, 2006.

[32] C. J. Keller *et al.*, "Heterogeneous neuronal firing patterns during interictal epileptiform discharges in the human cortex," *Brain,* vol. 133, no. Pt 6, pp. 1668-81, Jun, 2010.

[33] C. A. Schevon *et al.*, "Propagation of epileptiform activity on a submillimeter scale," *J. Clin. Neurophysiol.,* vol. 27, no. 6, pp. 406-11, Dec, 2010.

[34] C. A. Schevon *et al.*, "Microphysiology of epileptiform activity in human neocortex," *J. Clin. Neurophysiol.,* vol. 25, no. 6, pp. 321-30, Dec, 2008.

[35] C. A. Schevon *et al.*, "Spatial characterization of interictal high frequency oscillations in epileptic neocortex," *Brain,* vol. 132, no. Pt 11, pp. 3047-59, Nov, 2009.

[36] A. Waziri *et al.*, "Initial surgical experience with a dense cortical microarray in epileptic patients undergoing craniotomy for subdural electrode implantation," *Neurosurgery,* vol. 64, no. 3, pp. 540-5, Mar, 2009.

[37] E. A. DeYoe *et al.*, "Laminar variation in threshold for detection of electrical excitation of striate cortex by macaques," *J. Neurophysiol.,* vol. 94, no. 5, pp. 3443-50, Nov, 2005.

[38] S. Shushruth *et al.*, "Comparison of spatial summation properties of neurons in macaque V1 and V2," *J. Neurophysiol.,* vol. 102, no. 4, pp. 2069-83, Oct, 2009.

[39] D. Ringach, and R. Shapley, "Reverse correlation in neurophysiology," *Cogn. Sci.,* vol. 28, pp. 147-66, 2004.

[40] E. Hecht, "Optics," pp. (Reading, MA: Addison-Wesley), 2001.

[41] A. K. Goodchild *et al.*, "Comparison of photoreceptor spatial density and ganglion cell morphology in the retina of human, macaque monkey, cat, and the marmoset Callithrix jacchus," *J. Comp. Neurol.,* vol. 366, no. 1, pp. 55-75, Feb 26, 1996.

[42] R. B. Tootell *et al.*, "Functional anatomy of macaque striate cortex. II. Retinotopic organization," *J. Neurosci.,* vol. 8, no. 5, pp. 1531-68, May, 1988.

[43] E. Smith, and B. Greger, "Multiple, simultaneous recordings from auditory cortex in the awake, behaving macaque," *Neurosci. Annu. Meeting,* 2010.

[44]   R. A. Parker *et al.*, "The functional consequences of chronic, physiologically effective intracortical microstimulation," *Prog. Brain Res.*, vol. 194, pp. 145-65, 2011.

[45]   J. G. Cham *et al.*, "Semi-chronic motorized microdrive and control algorithm for autonomously isolating and maintaining optimal extracellular action potentials," *J. Neurophysiol.*, vol. 93, no. 1, pp. 570-9, Jan, 2005.

[46]   G. Buzsaki, "Large-scale recording of neuronal ensembles," *Nature Neurosci.*, vol. 7, no. 5, pp. 446-51, May, 2004.

[47]   S. Katzner *et al.*, "Local origin of field potentials in visual cortex," *Neuron*, vol. 61, no. 1, pp. 35-41, Jan 15, 2009.

[48]   D. Xing *et al.*, "Spatial spread of the local field potential and its laminar variation in visual cortex," *J Neurosci*, vol. 29, no. 37, pp. 11540-9, Sep 16, 2009.

[49]   X. Liu *et al.*, "Stability of the interface between neural tissue and chronically implanted intracortical microelectrodes," *IEEE Trans. Rehabil. Eng.*, vol. 7, no. 3, pp. 315-26, Sep, 1999.

[50]   S. F. Lempka *et al.*, "In vivo impedance spectroscopy of deep brain stimulation electrodes," *J. Neural Eng.*, vol. 6, no. 4, pp. 046001, Aug, 2009.

[51]   C. Newbold *et al.*, "An in vitro model for investigating impedance changes with cell growth and electrical stimulation: implications for cochlear implants," *J. Neural. Eng.*, vol. 1, no. 4, pp. 218-27, Dec, 2004.

[52]   K. J. Otto *et al.*, "Voltage pulses change neural interface properties and improve unit recordings with chronically implanted microelectrodes," *IEEE Trans. Biomed. Eng.*, vol. 53, no. 2, pp. 333-40, Feb, 2006.

[53]   J. C. Williams *et al.*, "Complex impedance spectroscopy for monitoring tissue responses to inserted neural implants," *J. Neural. Eng.*, vol. 4, no. 4, pp. 410-23, Dec, 2007.

[54]   P. G. Pickup, and V. I. Birss, "A model for anodic hydrous oxide growth at iridium," *J. Electroanal. Chem.*, vol. 220, pp. 83-100, 1987.

[55]   A. Maier *et al.*, "Distinct superficial and deep laminar domains of activity in the visual cortex during rest and stimulation," *Front. Syst. Neurosci.*, vol. 4, 2010.

[56]   E. J. Tehovnik *et al.*, "Phosphene induction and the generation of saccadic eye movements by striate cortex," *J. Neurophysiol.*, vol. 93, no. 1, pp. 1-19, Jan, 2005.

[57]   D. McCreery *et al.*, "Neuronal loss due to prolonged controlled-current stimulation with chronically implanted microelectrodes in the cat cerebral cortex," *J. Neural. Eng.*, vol. 7, no. 3, pp. 036005, Jun, 2010.

CHAPTER 4

SPATIAL AND TEMPORAL CHARACTERISTICS OF

V1 MICROSTIMULATION DURING CHRONIC

IMPLANTATION OF A MICROELECTRODE

ARRAY IN A BEHAVING MACAQUE[1]

Abstract

It has been hypothesized that a vision prosthesis capable of evoking useful visual

percepts can be based upon electrically stimulating the primary visual cortex (V1) of a

blind human subject via penetrating microelectrode arrays. As a continuation of earlier

work, we examined several spatial and temporal characteristics of V1 microstimulation.

An array of 100 penetrating microelectrodes was chronically implanted in V1 of a

behaving macaque monkey. Microstimulation thresholds were measured using a two-

alternative forced choice detection task. Relative locations of electrically-evoked percepts

were measured using a memory saccade-to-target task. The principal finding was that two

years after implantation we were able to evoke behavioural responses to electric

stimulation across the spatial extent of the array using groups of contiguous electrodes.

Consistent responses to stimulation were evoked at an average threshold current per

electrode of 204 ± 49 µA (mean $\pm$ std) for groups of four electrodes and 91 ± 25 µA for

groups of nine electrodes. Saccades to electrically-evoked percepts using groups of nine

electrodes showed that the animal could discriminate spatially distinct percepts with groups having an average separation of 1.6 ± 0.3 mm (mean $\pm$ std) in cortex and 1.0 ± 0.2 degrees in visual space. These results demonstrate chronic perceptual functionality and provide evidence for the feasibility of a cortically-based vision prosthesis for the blind using penetrating microelectrodes.

Introduction

Blindness is a prevalent cause of disability and poses extraordinary challenges to individuals in our society [1]. Although treatments exist for many causes of blindness, there is currently no effective treatment for those who are profoundly blind as a result of degeneration or damage to the retina and its connections to visual cortex.

Early studies have shown that surface stimulation of primary visual cortex (V1) in humans using an array of macroelectrodes (1-9 mm^2) can evoke points of light called phosphenes, and that subjects could assimilate simple spatial patterns of phosphenes with simultaneous stimulation of groups of electrodes [2-4]. These studies, however, encountered limitations in resolution as a result of electrode size, placement, and the large currents required to generate phosphenes. More recent studies in both humans and animals have shown that stimulation of V1 using penetrating microelectrodes resulted in improved resolution and a decreased amount of current needed to evoke phosphenes [5-7]. Several studies have explored the effectiveness of various stimulus parameters in evoking phosphenes using individual or pairs of microelectrodes in acute preparations [8-10]. Few studies, however, have looked at the performance and safety of microstimulation in V1 via chronically implanted arrays of microelectrodes.

To be useful, a visual prosthesis based on V1 microstimulation via an array of penetrating microelectrodes must provide reliable, targeted activation of the visual system over extended time periods. The array of implanted electrodes must retain the ability to evoke spatially distinct visual percepts, and the currents required to generate these percepts must remain stable and within a range that is safe to electrode and tissue throughout the life of the implant. Few studies have looked at the spatial and temporal characteristics of chronic V1 microstimulation. One study characterized the subjective perceptions of phosphenes evoked by stimulation of 38 microelectrodes in V1 of a blind human subject over a period of four months [6]. Initially, 34 of the 38 electrodes were found to evoke phosphenes using ~20 μA currents and ~2 mC cm^{-2} charge densities. The threshold current for one electrode was monitored and found to be relatively stable over time. However, the parameters of stimulation for this electrode were adjusted throughout the study to maximize perception, making it difficult to quantify this result. Additionally, many of the implanted electrodes were not monitored for the duration of the study due to mechanical failure of the wire leads, and the long-term performance of the implant was not fully characterized. Another study looked at the performance of electrical stimulation of chronically implanted microelectrodes in V1 of a macaque monkey [5]. In this 16 month study, the animal was implanted with 152 microelectrodes and trained to saccade to the phosphenes evoked during stimulation of individual electrodes. Of the 152 electrodes that were implanted, 32 were selected for stimulation. The stimulation levels required to evoke saccades to phosphenes were ~20 μA and ~1 mC cm^{-2}. These stimulation levels did not damage the tissue based on histological analysis of the implant sites. The stability of these levels over time, however, was not quantified, and the

functionality of the remaining 120 unstimulated electrodes was not discussed. Both of the above studies provided valuable insight into the feasibility of a visual prosthesis based on microstimulation of V1. However, several of the spatial and temporal characteristics of a chronic implant that are important to the future development of a prosthesis, such as the long-term reliability of all implanted electrodes, were not fully addressed.

The goal of the research reported herein is to develop a cortically-based neural prosthetic device that will restore functional vision to profoundly blind human individuals. This approach will work by electrically stimulating V1 via a number of Utah Electrode Arrays (UEAs) to produce useful visual percepts. During the first year of this study, we encountered a restricted ability to evoke percepts on many of the implanted electrodes [7]. Difficulty with reliably evoking percepts using arrays of microelectrodes implanted in cortex over extended time periods has been reported elsewhere [5, 6, 11]. Here, we present additional findings collected during the second year of implantation. We show that consistent visual percepts can be evoked via microstimulation of a UEA that has been implanted in V1 for two years. We found that we can evoke percepts for the majority of stimulated electrodes across the array by increasing the volume of stimulated cortical tissue through simultaneous stimulation of groups of electrodes. We also found that the threshold stimulus levels required to generate these percepts manifested a small, but significant increase with time. These levels, however, did not appear to cause any obvious damage to the system based on our ability to consistently evoke behavioural responses and the stability of the electrical properties of the implant over the course of experimentation. Two years after implantation, we show that the animal can discriminate percepts evoked by stimulation of separate regions of the UEA, thus providing evidence

of the functionality of an array of penetrating microelectrodes under chronic conditions for use as a visual prosthesis.

Methods

All surgical and experimental procedures were performed in accordance with the guidelines of the U. S. Department of Agriculture and were approved by the University of Utah's Institutional Animal Care and Use Committee.

Subject and surgery

In overview, two UEAs, a total of 192 electrodes, were implanted in V1 of a male rhesus macaque (Macaca mulatta) (Figure 4.1). Early experiments involved mapping visually responsive regions for each electrode and determining the minimum currents required to evoke behavioural responses during single electrode stimulation [7]. One of the UEAs was lost due to a superficial infection at the connector approximately 18 months after implantation, so the data presented in this study were collected using the more posterior functional array from 19 to 24 months post-implantation.
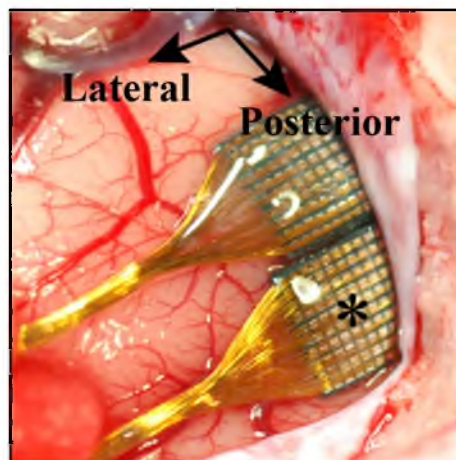

Figure 4.1. Surgical image of the implanted UEAs. Data for this study were collected using the posterior array indicated with the asterisk.

We followed human protocols during the surgery and post-operative care. The UEAs were implanted in V1 of the animal using a pneumatic inserter [12]. Reference wires were used as the current return path during microstimulation and were placed in the subdural space. The arrays were implanted anterior to the calcarine sulcus and lateral to the sagittal fissure. This anatomical location was expected to represent the lower right visual quadrant at about eight degrees of eccentricity [13]. The orientation of the posterior array in cortex is identified using the wire bundle and remains consistent in subsequent Figures. For a more detailed account of the surgery, see our companion work [7].

Microelectrode array

Fixed-geometry arrays of penetrating microelectrodes were used for neural recording and microstimulation (Cereport Array (UEA), Blackrock Microsystems, Salt Lake City, UT). These arrays were originally developed for a vision prosthesis [14, 15]. They have been successfully implanted in the motor cortex [16-19], the auditory cortex [20, 21], the auditory nerve [22, 23], the sciatic nerve [24], and the visual cortex [25, 26] of various animal models. Moreover, these electrodes have been acutely implanted in the middle temporal gyrus of epilepsy patients undergoing temporal lobectomy surgery [27-32] and chronically implanted in the motor cortex of paralyzed human patients [33-37]. Each array consisted of one hundred 1 mm long microelectrodes arranged in a 10×10 grid spaced 400 µm apart. The length of the electrode was chosen so that the electrode tip would reside approximately in layer 4 A/B of V1 [9, 38]. Each electrode base is electrically isolated from its neighbouring electrodes with glass, and the rest of the electrode, with the exception of the iridium-oxide tip, is insulated with a 2 µm coat of

parylene-C. Each electrode tip is metalized with a sputtered iridium-oxide film (SIROF) for better charge injection capacity [39]. The electrodes have been manufactured to have an exposed tip length of 60 ± 40 μm, resulting in an active geometrical surface area of 500–4000 μm^2. The electrode impedances ranged from 40 to 80 kΩ before implantation as measured with a 1 kHz sine-wave 10 nA constant current signal (Cerebus, Blackrock Microsystems, Salt Lake City, UT). Mean impedances were used for analysis after outliers (i.e. impedances greater than 2 MΩ) were discarded.

Instrumentation

The task control system, which handled the presentation of photic and electrical stimuli, consisted of custom software running on an embedded controller using a real-time operating system (National Instruments, Austin, TX). Visual stimuli were generated using a real-time visual stimulator (ViSaGe, Cambridge Research Systems, Rochester, Kent, England) and displayed on a CRT monitor (G90fb, ViewSonic, Walnut, CA). The animal was head-fixed using a minimally invasive technique [40] and eye positions were tracked with an infrared camera (1 kHz sampling rate, EyeLink 1000, SR Research, Mississauga, ON, Canada). Hand positions were monitored and behavioural responses registered with capacitive switches, which detected the presence of the animal's hand when it was within a few millimeters of the sensor. Physiological and behavioural data were recorded using a 128-channel data acquisition system (Cerebus, Blackrock Microsystems, Salt Lake City, UT). Data analysis was performed using Matlab technical computing software (MathWorks, Natick, MA).

Microstimulation

During the first year of experimentation, as reported in our previous work [7], we used a system that was capable of delivering a maximum of 100 µA to each electrode (RX7, Tucker-Davis Technologies, Alachua, FL). For microstimulation experiments reported here, we used a system that could deliver up to 300 µA across a 50 kΩ load to a total of 128 electrodes (IZ2, Tucker- Davis Technologies, Alachua, FL). The stimulator battery had a compliance voltage of ±15 V (LZ48-400, Tucker-Davis Technologies, Alachua, FL). Constant-current pulses without anodic bias were delivered to V1 through the individual electrodes on the UEA. Each pulse consisted of a cathodic-first symmetric biphasic square wave with an interphase interval of 100 µs and a phase width of 200 µs. Pulses were delivered at 200 Hz for a duration of 200 ms. Current amplitudes were varied up to 300 µA. At these levels, up to 60 nC phase^{-1} and 3 mC cm^{-2} was delivered to the tissue through each electrode for a typical electrode tip geometrical surface area of 2000 µm^2. Similar stimulation parameters evoked phosphenes in a human patient [6] and behavioural responses in a macaque monkey [5]. These parameters were used for all microstimulation experiments unless otherwise specified. For microstimulation experiments using groups of multiple contiguous electrodes, the reported currents were delivered to each of the individual electrodes of the group.

Threshold mapping

The animal's responses to stimuli of varying intensities were monitored to determine the minimum perceived intensity or threshold. The animal was placed in a primate chair inside a sound attenuated, dark chamber and was required to place each of its hands on a capacitance switch, one to its left and the other to its right. A small 0.1 ×

0.1 visual degrees fixation point then appeared in the centre of a CRT screen 34 cm in front of the animal. Once the animal directed its gaze within 1 degree of the centre of the point, the trial would start. The animal had to maintain its gaze within this defined region, or the trial was aborted. For both photic and electric trials, stimuli were presented after fixation was maintained for a randomized duration of 500 to 1000 ms. Stimulus presentation was followed by a second randomized hold duration, and then an auditory cue was given indicating that the animal should make a response. The animal would then respond by removing its right hand to indicate that it did not perceive or its left hand to indicate that it did perceive a stimulus. Photic stimuli were round, monochromatic Gaussian shapes with diameters that varied from 0.25 to 0.5 visual degrees and locations that were presented randomly in the lower right quadrant of visual space where the UEA was previously determined to be located [7]. These stimuli were white against a dark background, and the luminance levels were kept in a range that was clearly visible to the animal. Electric stimuli consisted of the passage of current simultaneously through one or more electrodes on the UEA using the parameters described in section 2.4. Microstimulation trials were sparsely introduced into an ongoing photic task and were rewarded with juice one hundred percent of the time regardless of the answer. Clearly visible photic trials and trials consisting of the absence of photic or electric stimuli were used as catch trials to ensure that the animal was responding truthfully. The animal was rewarded only if the correct response was made without any of the task constraints being violated. Using this forced-choice detection task, we were able to determine responses to electric stimulation at various amplitudes. Approximately five or more responses to electric stimuli presented at three or more current levels that spanned threshold (i.e. ~15

total responses) were considered to be a valid or consistent behavioural response. Psychometric data were fit using a Weibull cumulative distribution function, which was used to estimate response thresholds (current value at 50% probability of detection).

<u>Memory saccade mapping</u>

This task involved making saccades to the remembered spatial location of a previously presented photic or electric stimulus. The sequence of steps to complete a trial was similar to the threshold task described in section 2.5. To begin a trial, the animal was required to maintain fixation within 1 degree of a fixation point that was displayed at the centre of a CRT screen. After the start of the trial, a photic or electric stimulus was presented for 200 ms. The animal was required to maintain fixation during the presentation of the stimulus and for a random period of 500 to 1000 ms after the stimulus was removed. The animal was then required to saccade to the remembered location of the stimulus. For photic trials, round, monochromatic Gaussian shapes with a diameter of 0.25 visual degrees were presented, and the animal was required to saccade to within 1.5 degrees of the target location. Photic targets were distributed evenly across the lower right quadrant of visual space in the general location of the implanted electrodes. Targets that closely overlapped with the previously determined electrode locations were removed to avoid training the animal on photic saccade endpoints that closely resembled electric endpoints, making it difficult to distinguish the two types of saccades. For electric trials, a train of biphasic pulses (see section 2.4) were simultaneously delivered to one of three separate groups of nine contiguous electrodes. The animal was required to saccade to within a large region that encompassed the location of the implanted UEA in visual

space. This region had a diameter of eight visual degrees and extended beyond the limits of the UEA location by at least two degrees on all sides.

Feline microstimulation

To confirm the results observed during microstimulation in the macaque, microstimulation was also performed via a chronically implanted UEA in feline motor cortex. For this experiment, the animal was anesthetized with Telazol administered intramuscularly at 0.01 mg/kg. Sterile, clinical fine-wire electrodes (Chalgren Enterprises, Inc., Gilroy, CA) were placed in the triceps or extensor carpi muscle. Reference electrodes were placed subcutaneously near the intramuscular electrode. Microstimulation was then applied using the parameters described in section 2.4. Electromyographic (EMG) signals to evoked muscle twitches were recorded at a sampling rate of 25 kHz using a data acquisition board (RHA2000-EVAL, Intan Technologies, Los Angeles, CA). To determine the amplitude of the evoked response, the recorded EMG was filtered with a 100-1500 Hz bandpass elliptic filter of order 10, rectified and then convolved with a Gaussian window of standard deviation 10 ms. The peak response was defined as the difference in the mean value of the convolved signal during the applied stimulus and a baseline value obtained prior to stimulus onset.

Results

We investigated several spatial and temporal characteristics of stimulation via a chronically implanted UEA in V1 for use as a visual prosthesis. Early experiments consisted of several months of periodic microstimulation at currents up to 96 μA [7]. Data shown here are from later experiments performed with a UEA that had been

implanted for more than 18 months. These data consist of 83 stimulation sessions that span 8 months and include 81 of the 96 electrodes. Stimulus currents up to 300 µA were used.

Effect of simultaneous stimulation of multiple electrodes on response thresholds

Microstimulation was performed on individual electrodes and groups of two, four, and nine contiguous electrodes distributed evenly across the array to assess the functionality over the spatial extent of the array. Responses to systematic stimulation of individual electrodes across the array were tested. Microstimulation of 77 of the 96 electrodes at levels up to 200 µA, however, did not evoke consistent behavioural responses from the animal.

Following single electrode testing, stimulus levels were increased by increasing the number of electrodes that were simultaneously stimulated and the amount of current that was delivered to each of the electrodes of the group. Eight groups of two electrodes were tested and only two produced responses from which psychometric curves could be generated. The threshold currents per electrode for these groups were 268 and 300 µA. The six remaining groups did not evoke responses at levels up to 300 µA.

Stimulation of groups of four electrodes, in contrast, produced consistent behavioural responses across the spatial extent of the array. Thirty-two unique, overlapping groups were chosen for stimulation that tiled 75 percent of the array. Of the 32 stimulated groups, 26 produced consistent responses and psychometric curves were obtained. A total of 55 thresholds from the 32 unique groups were used to generate an average spatial threshold map (Figure 4.2(a)). The average threshold current per electrode

Figure 4.2. Increasing the volume of activated tissue during microstimulation by simultaneously stimulating groups of 4 and 9 contiguous electrodes resulted in an increased percentage of responsive regions across the UEA and lower response thresholds. Data were collected from 566 to 687 days after implantation for plots a-c and 505 days after implantation for plot d. (a) Average psychometric response thresholds to microstimulation of overlapping groups of 4 contiguous electrodes across the UEA. Values for the individual electrodes of this plot, represented by the colored boxes, were calculated by taking the average threshold of all groups common to that particular electrode. 26 of 32 groups produced response thresholds at or below 300 μA. 6 groups did not elicit responses at levels up to 300 μA. 7 electrodes were common to one or more of the 6 unresponsive groups and are represented by black boxes and labeled as no response (NR) electrodes. White boxes represent electrodes that were not stimulated (NS). (b) Average response thresholds to microstimulation of non-overlapping groups of 9 contiguous electrodes. 8 of 8 groups produced response thresholds at or below 300 μA. (c) Nonlinear fits of the Weibull function to the psychometric data from stimulation of groups of 4 and 9 contiguous electrodes across the UEA. Thresholds were taken at the 50% response probability. The mean threshold for all groups of 4 was significantly higher than all groups of 9 electrodes ($p < 0.05$) with values of 204 ± 49 and 91 ± 25 μA (mean $\pm$ std), respectively. (d) Myometric curves for microstimulation of groups of 1, 4 and 9 contiguous electrodes in chronically implanted feline motor cortex. The average rectified EMG value recorded during muscle twitch evoked by stimulation was used as a response metric. Each point on the myometric curves represents the mean of 10 trials at the specified stimulus intensity. The error bars represent the standard error of the mean. At stimulation levels of 200 and 250 μA, a significant ($p < 0.05$) increase in EMG amplitude occurred as the number of electrodes per group increased.
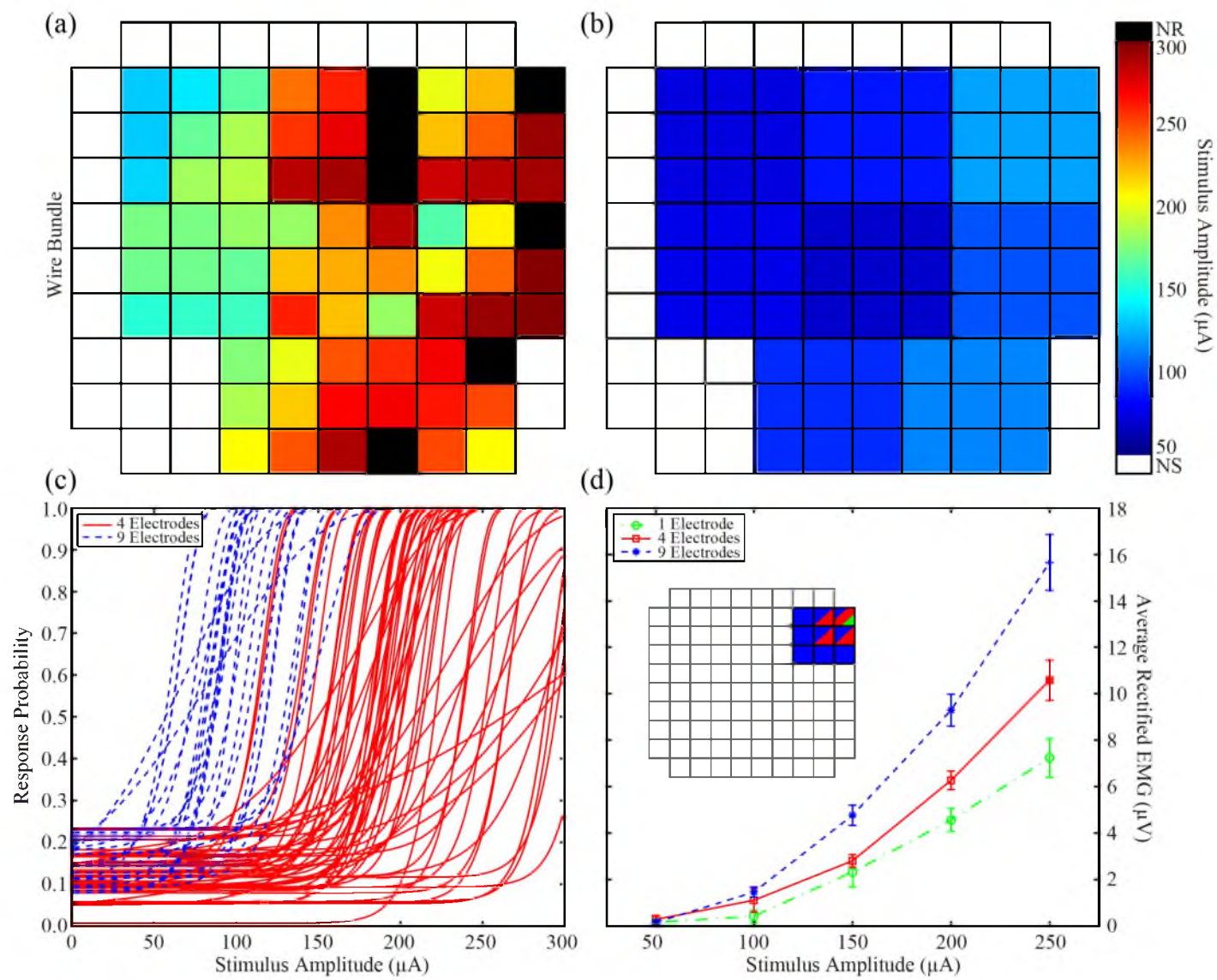
and standard deviation for all groups of four was 204 ± 49 µA. Non-overlapping groups of nine contiguous electrodes were also tested. It was found that increasing the number of stimulated electrodes from four to nine led to a significant ($p<0.05$, Kolmogorov–Smirnov) decrease in response threshold and a corresponding increase in the consistency of the responses across the spatial extent of the array. A total of 25 threshold values from 8 unique groups were used in the calculation of the spatial average (Figure 4.2(b)). One hundred percent or 8 of the 8 unique groups produced consistent responses from which psychometric curves were obtained. The average threshold current per electrode and standard deviation for all groups of nine was 91 ± 25 µA. Nonlinear fits of the Weibull function to the raw psychometric data demonstrate that multiple electrode stimulation consistently evoked responses throughout the experiment (Figure 4.2(c)).

To confirm that increasing the spatial extent of cortex being stimulated (i.e. increasing the number of electrodes) lowered the level of current per electrode needed to evoke a response, stimulation was also performed via a UEA in motor cortex of a feline. Data were collected 505 days post-implantation. Muscle twitches were recorded using EMG signals and the average rectified amplitude of the EMG was used as a response measure. An individual electrode and a group of four and nine contiguous electrodes were stimulated using the parameters described in section 2.4. The single electrode and the group of four were contained within the group of nine electrodes to minimize any variance in threshold based on spatial location. Stimulation was applied to each of the groups in a repetitive sequence over time to minimize the influence of anesthesia depth on the measured responses. Myometric curves were generated for each electrode group relating stimulus intensity to response amplitude. The EMG responses showed a

significant increase (p<0.05) in amplitude as the number of electrodes per group

increased for stimulus amplitudes of 200 and 250 µA (Figure 4.2(d)). These results are

similar to those observed in the macaque, and support the finding that simultaneous

stimulation of groups of electrodes of a chronically implanted UEA decreases the amount

of current required to generate robust physiological and behavioural responses.

Effect of pulse duration on response thresholds

A strength-duration curve was determined for one group of four contiguous

electrodes to serve as a comparison with other studies and provide a metric for optimizing

stimulation in terms of safety and efficacy. Threshold currents were measured at various

pulse durations ranging from 0.15 to 0.8 ms (Figure 4.3(a)). Other stimulation parameters

were held constant at the values given in section 2.4. Chronaxie and rheobase were

estimated by fitting the following hyperbolic function to the data:

$$I * t = I_{rh} * (t + \tau_{SD})$$ (1)

where I = threshold current, I_{rh} = rheobase current, t = pulse duration, and τ_{SD} =

chronaxie. This equation was found to provide the best fit for strength-duration data [41].

The chronaxie and rheobase estimated by the fit and the corresponding 95% confidence

intervals were 0.16 ± 0.06 ms and 102 ± 13 µA, respectively. These values are

comparable to those provided by other neural stimulation studies [3, 6, 8, 41-43] as

shown in Table 4.1. A linear trend ($R^2 = 0.97$) was observed between threshold charge

density and pulse duration (Figure 4.3(b)). Stimulation using a pulse duration of 0.2 ms

resulted in a threshold charge density less than 2 mC cm^{-2} for this particular group of four
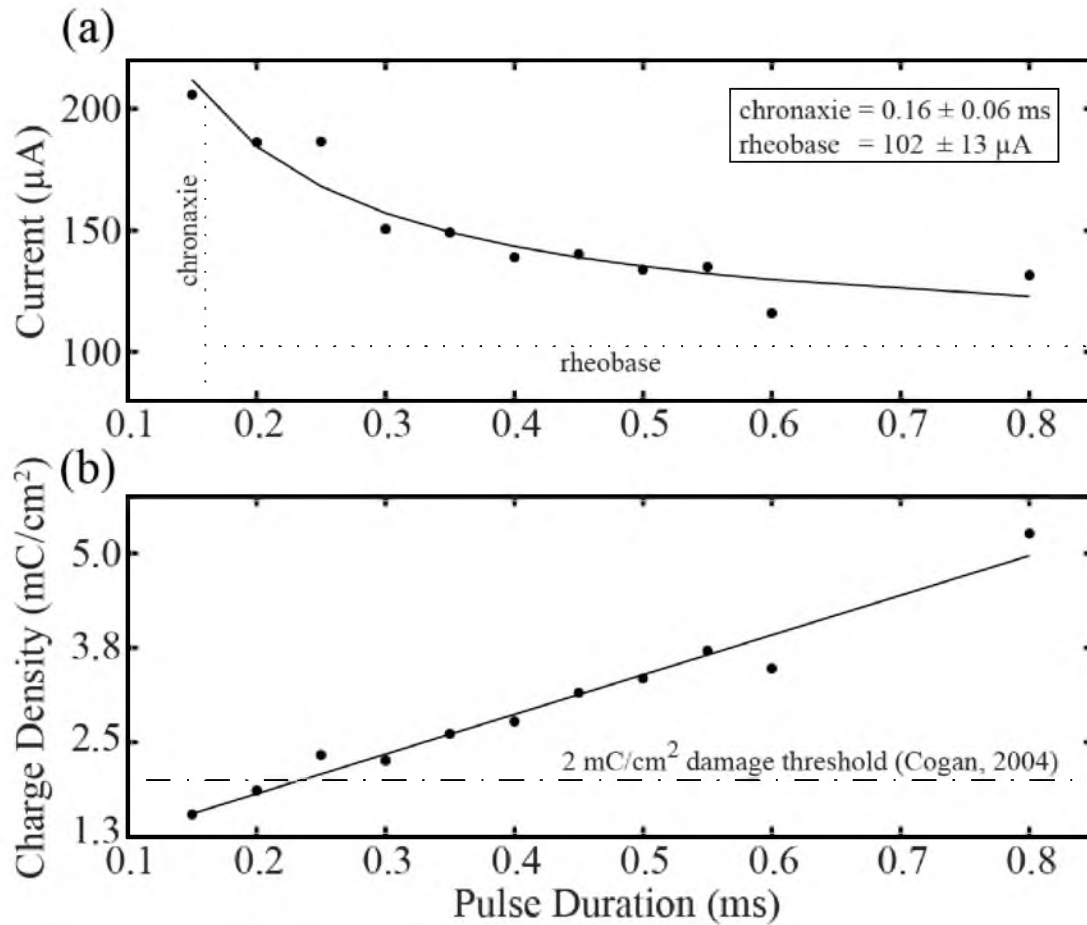
Figure 4.3. Strength-duration curves for a group of 4 contiguous electrodes. Electrodes were stimulated using 40 symmetric biphasic cathodic-first pulses with increasing pulse durations at a frequency of 200 Hz. Response thresholds for current and charge density were measured. (a) The relationship between pulse duration and threshold current was estimated using the following hyperbolic function: $I * t = I_{rh} * (t + \tau_{SD})$, where I = threshold current, t = pulse duration, I_{rh} = rheobase current, and τ_{SD} = chronaxie. Chronaxie and rheobase were calculated to be 0.16 ± 0.06 ms and 102 ± 13 µA, respectively. (b) A linear relationship existed between pulse duration and threshold charge density. Pulse durations of 0.2 ms or less were determined to be safe to tissue and electrode according to a study by Cogan et al. (2004).

Table 4.1. Summary of chronaxie/rheobase data from select neural stimulation studies

Citation	Model System	Electrode Location	Electrode Type	Chronaxie (ms)	Rheobase (μA)
Davis et al. (2012)[a]	**Macaque**	**V1**	**Intracortical**	**0.16**	**102**
Bartlett et al. (2005)	Macaque	V1	Intracortical	0.23	75[b]
Tehovnik et al. (2004)	Macaque	V1	Intracortical	0.13-0.24	NR[c]
Schmidt et al. (1996)	Human	V1	Intracortical	0.22[b]	9.1[b]
Ronner et al. (1983)	Feline	V1	Intracortical	0.22	160
Dobelle et al. (1974)	Human	V1	Surface	0.35[b]	1800[b]
Mogyoros et al. (1996)	Human	Median nerve	Surface	0.67	1270

[a]Current study
[b]Estimation based on data provided in figure/table
[c]Not reported

contiguous electrodes. Throughout the study, 56 percent of all contiguous groups of four electrodes and 100 percent of all contiguous groups of nine electrodes had threshold charge densities below this value. Charge densities less than 2 mC cm^{-2} were determined to be safe to activated iridium microelectrodes and did not appear to decrease neuronal populations in the surrounding cortical tissue [44].

Stability of response thresholds over time

Thresholds were monitored over time from 566 to 789 days post-implantation for groups of four and nine electrodes (Figure 4.4). Thresholds were measured 5 ± 2 times (mean ± std) for each of 11 groups spanning an average of 125 ± 78 days. Groups of four electrodes demonstrated a significant increase in threshold of 0.7 ± 0.3 μA day^{-1}

(weighted average ± 95% confidence interval). Groups of nine electrodes showed a smaller increase of 0.2 ± 0.1 µA day^{-1}. The root-mean-squared-error about the linear trend for groups of four and nine was 33 and 21 µA, respectively.

One group of four electrodes was stimulated 7.5 times more frequently and at higher levels than the other groups of four (Figure 4.4, solid line). This group was stimulated using an average charge density of 2.9 mC cm^{-2} and a maximum of 7 mC cm^{-2}. The remaining groups of four electrodes were stimulated using a combined average charge density of 1.9 mC cm^{-2} and a maximum of 2.9 mC cm^{-2}. Groups of nine electrodes were stimulated with a combined average charge density of 0.9 mC cm^{-2} and a maximum of 1.5 mC cm^{-2}. The increase in threshold for the high stimulation group of four was not found to be significantly different from the other groups of four ($p = 0.6$, ANOVA).

Functional status of the electrodes and implant sites

Electrode impedances before each stimulation session, electrode voltage-time traces during stimulation sessions, and behavioural visual thresholds to photic stimuli that excited regions of V1 where the UEAs were implanted were monitored to verify functionality and help identify damage to electrodes or tissue.

The mean impedance of the electrodes, as measured using a 1 kHz sine-wave 10 nA constant current signal, showed an initial increase above pre-implantation values from approximately 2 to 12 weeks after implantation. The combined average impedance during this period was 492 ± 46 kΩ (mean ± SEM). This increase was followed by a gradual decrease towards pre-implantation values (Figure 4.5(a)). A similar pattern was observed in chronic UEA implants in feline cortex [45]. The mean impedance and standard error of the electrodes at the start of the current study 562 days after implantation was 57 ± 2 kΩ.
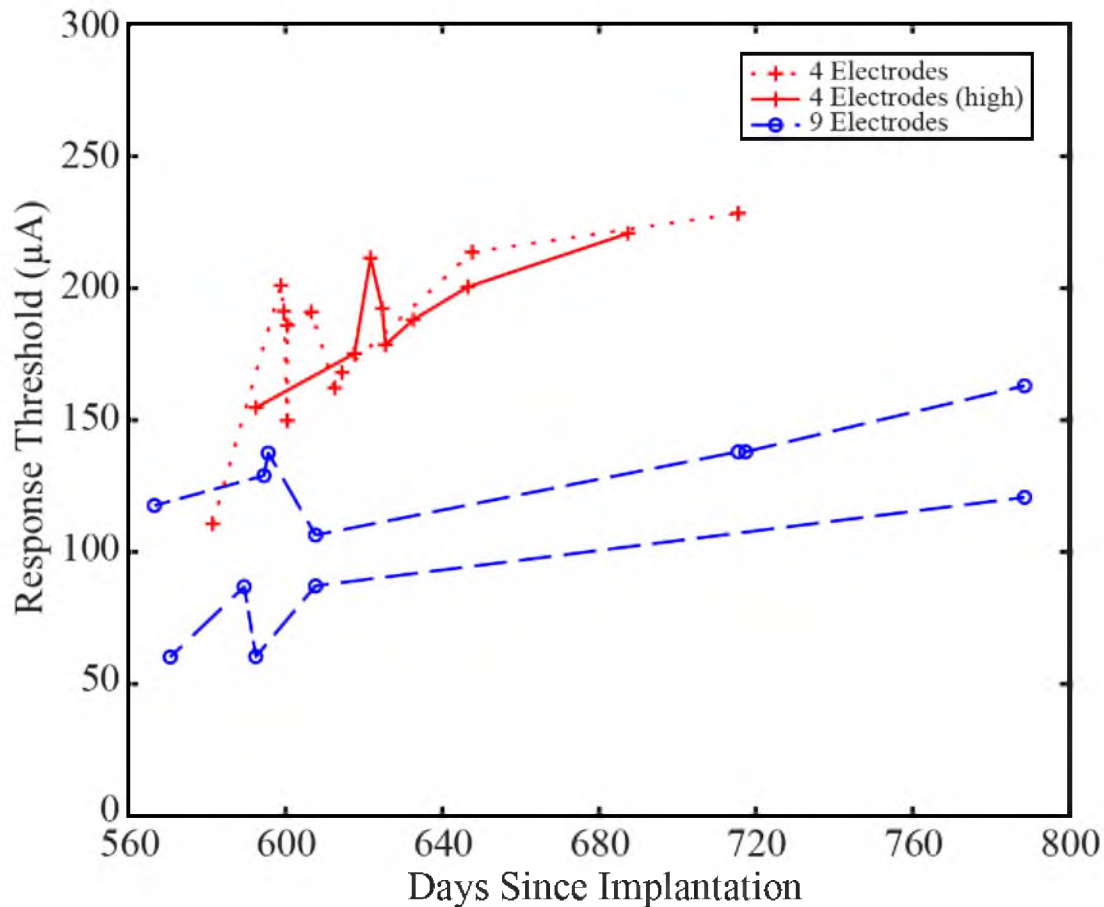
Figure 4.4. Thresholds for 4 groups of 4 and 7 groups of 9 contiguous electrodes were monitored over time. Two curves from each group are shown. Groups of 4 electrodes showed a significant increase in threshold of 0.7 ± 0.3 μA day^{-1} (weighted average $\pm$ 95% confidence interval). Groups of 9 electrodes showed a significant increase of 0.2 ± 0.1 μA day^{-1}. The average root-mean-squared-error about the linear trend was 33 and 21 μA for groups of 4 and 9, respectively. The group of 4 electrodes shown with a solid line was stimulated 7.5 times more frequently and at higher levels than other groups. An average charge density of 2.9 mC cm^{-2} with a maximum of 7 mC cm^{-2} was delivered to this group throughout the course of experimentation. An average charge density of 1.9 mC cm^{-2} with a maximum of 2.9 mC cm^{-2} was delivered to the 3 remaining groups of 4. The groups of 9 were stimulated using an average charge density of 0.9 mC cm^{-2} and a maximum of 1.5 mC cm^{-2}. The increase in threshold for the high stimulation group of 4 was not found to be significantly different from the other groups of 4 ($p = 0.6$, ANOVA).
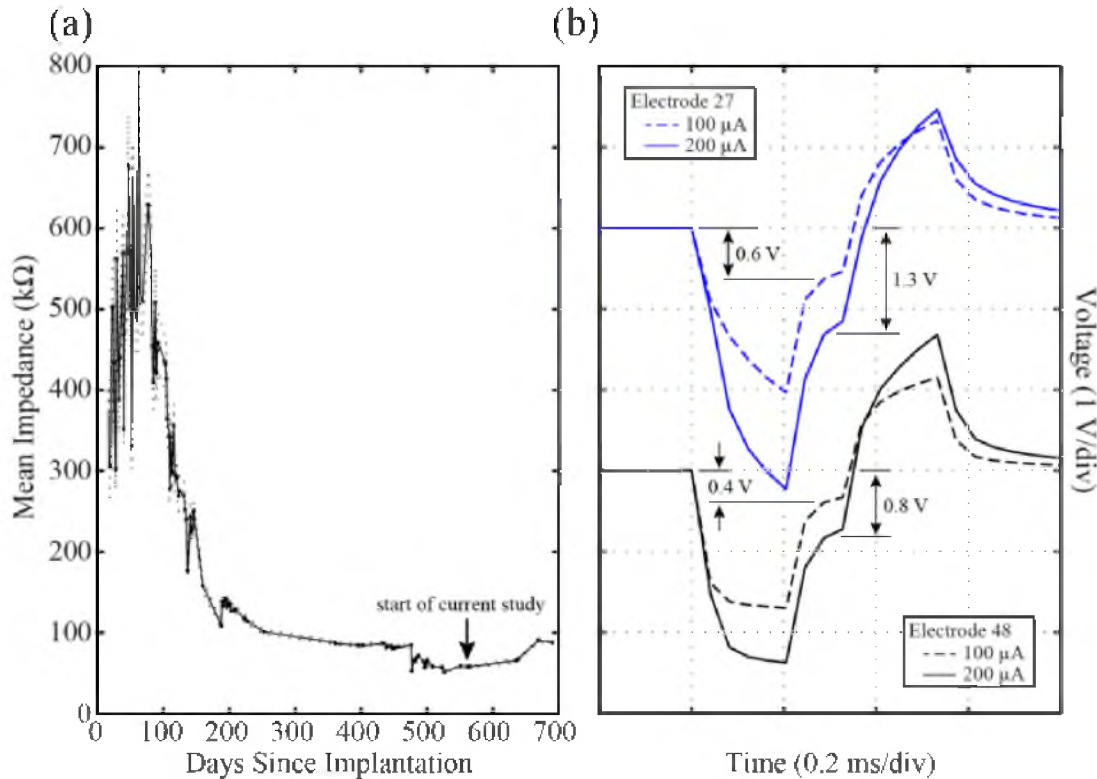
Figure 4.5. Electrode impedances measured before stimulation sessions and voltage traces acquired during stimulation sessions confirm the functionality of the implant and do not indicate significant device damage. (a) Mean impedances of all array electrodes demonstrate an initial increase followed by a gradual decrease over time. The start of the current study, approximately 18 months post-implantation, is indicated with an arrow. No significant changes in impedance occurred after this point in time (p = 0.4, ANOVA) as a result of stimulation. (b) Voltage traces during 100 and 200 μA constant current stimulation for 2 electrodes. These electrodes show a maximum cathodic voltage excursion that is under the generally regarded safe limit of -0.6 V for a stimulus current of 100 μA and exceeds this limit for 200 μA. Both electrodes provided consistent behavioral responses to stimulation throughout the study.

No significant changes from this value were observed for the remainder of the study (p = 0.4, ANOVA).

Effective stimulation currents for some groups of four electrodes produced a maximum cathodic voltage excursion (E_{mc}) that exceeded the generally regarded safe limit of -0.6 V [39, 44]. It was possible, however, to reduce these voltages to safe levels by increasing the number of electrodes to nine. Voltage traces in response to biphasic

current pulses of 100 and 200 μA for two electrodes are shown in Figure 4.5(b). The

upper traces are from an electrode that was stimulated using high charge density levels as

described in section 3.3. Impedances measured using a small-signal 1 kHz sine-wave for

these two electrodes were 59 and 79 kΩ for the upper and lower traces, respectively. E_{mc}

can be approximated with the voltage during the inter-phase interval of each trace. This

value exceeds the safety limit for both electrodes when using a 200 μA stimulus and is

within this limit for a 100 μA stimulus. Both electrodes were in groups of four and nine

that provided consistent behavioural responses to stimulation throughout the course of the

study.

Before implantation, dark-adapted thresholds to photic stimuli were measured in

the approximate location of visual space representing the region of cortex where the UEA

was implanted and were found to range from 250 to 550 μcd m^{-2}. Ten months after

implantation, thresholds for the visual field locations represented by the cortex where the

array was implanted were measured and ranged from 420 to 490 μcd m^{-2}. Twenty-five

months after implantation and following stimulation at levels up to 300 μA, thresholds

for stimuli presented at the same locations ranged from 370 to 470 μcd m^{-2}. These values

are similar to human thresholds [7] and indicate that cortical function was not impaired

by the implantation and chronic presence of the UEA. Further, no behavioural evidence

of epileptiform activity occurred in response to electric stimulation, and the animal never

exhibited signs of neurological deficiencies or other behavioural abnormalities

throughout the course of experimentation.

Spatial discrimination of phosphenes

Data were collected for saccades made to electrical stimulation of three groups of nine contiguous non-overlapping electrodes. These data were obtained to confirm that electrical stimulation was producing visual percepts that the animal could spatially discriminate. Data from this task were collected 790 to 804 days post-implantation and show saccades to both photic and electric stimuli (Figure 4.6).

These data demonstrate that the animal was able to discriminate the location of three separate visual percepts produced by electrical stimulation of three groups of nine contiguous electrodes. The distance between these groups of electrodes was 1.6 ± 0.3 mm (mean $\pm$ std) on the array, and the corresponding separation in visual space, based on the measured receptive field locations, was 1.0 ± 0.2 degrees. The mean electric saccade centres showed a significant separation ($p<0.05$, MANOVA), and the locations in visual space corresponded with the locations where the visual percepts would be expected to appear based on the map of receptive fields. The average distance to target for the photic saccades was 0.6 degrees, and the average standard deviation of the scatter of saccade endpoints was 0.5 degrees. For electric saccades, the average distance to target was 2.9 degrees, and the average standard deviation of the scatter was 1.0 degree. The scatter of endpoints for electric saccades was 2.0 times greater than for photic saccades. This decrease in electric saccade precision was also observed in a related study [5].

Discussion

In this work, we investigated several spatial and temporal characteristics of V1 microstimulation using a chronically implanted UEA in a behaving macaque monkey. After 2 years of implantation, consistent behavioural responses to microstimulation were
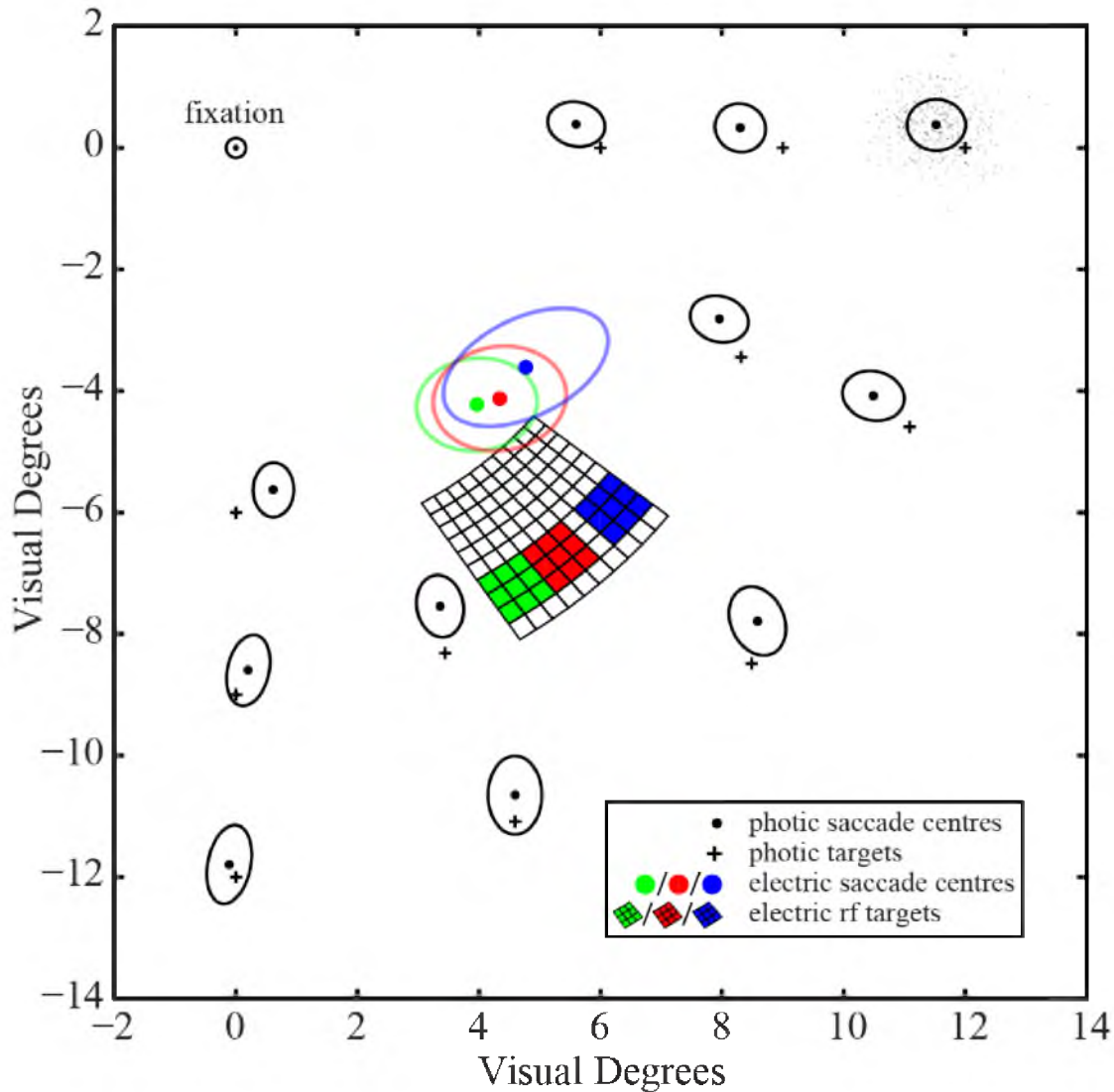
Figure 4.6. Saccades to electrical stimulation of 3 groups of 9 contiguous electrodes demonstrate discrimination of 3 spatially distinct percepts. The mean saccade centres to photic targets are depicted as black dots bounded by black ellipses that represent the Mahalanobis distance of the scatter. An example of the photic saccade scatter is shown in the upper-right corner. Each photic centre is near the corresponding photic target shown as a black plus. The mean saccade endpoints to microstimulation (electric targets) are represented with colored dots and are bounded by colored ellipses. Colors match the estimated target locations depicted with the inset plot of the UEA. A non-linear, least-mean-square method was used to position the inset UEA by minimizing the distances between the actual receptive field centres and the coordinate transforms of each electrode into visual space. The mean electric saccade centres showed a significant separation (p<0.05, MANOVA).

obtained over the spatial extent of the array by activating larger volumes of cortical tissue through stimulation of groups of contiguous electrodes. It was found that increasing the size of the contiguous groups reduced the threshold current and charge density delivered through each electrode to levels generally considered safe [44]. In addition, no behavioural signs of epileptiform activity occurred in response to multiple electrode stimulation, and neither stimulation nor the presence of the UEA in V1 impacted the behavioural photic thresholds to light stimuli that excited regions of V1 where the UEA was implanted.

Stimulation thresholds in a chronically implanted UEA

Early microstimulation experiments performed approximately three months after the implantation of the UEA yielded behavioural responses to stimulation of individual electrodes with threshold currents ranging from 18 to 76 μA [7]. More than a year after these experiments, we show that simultaneous stimulation of groups of electrodes using currents ranging from 57 to 300 μA was required to produce consistent behavioural responses. Additionally, threshold currents for several electrode groups were found to increase with time. Other chronic microstimulation studies have reported increases in thresholds or a loss of functional electrodes with time [8, 11]. Many V1 microstimulation studies have not reported an increase, but these studies were performed with either acute electrode placement or with chronic implantation of no more than 4 months [6, 9, 10, 46, 47]. This observed increase in stimulation thresholds over the course of the study may have resulted from alteration of the implanted tissue or the electrode array.

Studies have shown that a glial sheath develops around chronically implanted penetrating microelectrodes and that this sheath may serve as a resistive barrier to the

flow of current [48, 49]. Contraction of this sheath as it ages, as well as, movement of the

tissue in relation to the rigid array of electrodes might lead to extrusion of the array or the

formation of a fluid barrier between the electrode surface and tissue. This fluid layer

could provide a low impedance return path for injected current during stimulation,

effectively shunting current away from the target tissue and causing an increase in

stimulation thresholds. Microstimulation itself can affect the surrounding tissue, which

might also lead to an increase in thresholds. Levels used to evoke behavioural responses

during V1 microstimulation have ranged from 2 to 200 μA [6-10, 46, 47] with charge

densities as high as 7.7 mC cm^{-2} [6]. Continuous stimulation as low as 0.2 mC cm^{-2} was

found to induce a loss of cortical neurons from within a radius of 150 μm of the electrode

tips [50]. It is unknown if or how this neuronal loss would affect stimulation-evoked

percepts. Many V1 microstimulation studies have exceeded this level of stimulation [5-7,

46]. The total duration of stimulation applied in these studies, however, was typically

much less than the continuous stimulation paradigms that are found in studies assessing

tissue safety. We applied up to 300 μA and 3 mC cm^{-2} on some of our electrodes to evoke

responses. One group of four electrodes was repeatedly stimulated with an average

charge density of 2.9 mC cm^{-2}. This group did not show a significantly larger increase or

demonstrate a larger variation in threshold with time when compared with other groups

of electrodes.

A SIROF UEA implanted in cat sensorimotor cortex for over 300 days exhibited

decreased impedances and an increased charge storage capacity with implant time [51]. It

was suggested that these changes might be caused by leakage of electrolyte under the

parylene insulation of the electrodes, leading to an overall increase in surface area and

thus an overestimation of charge density during microstimulation. The surface area of SIROF UEA electrodes can vary significantly from 500 to 4000 μm^2, adding another component of uncertainty to the estimation of charge density. The maximum safe charge density during stimulation of iridium microelectrodes can range from 0.4 to 4 mC cm^{-2} [44, 51-53]. The variance in this value can be attributed to differences in the electrode fabrication, the parameters of stimulation used in testing, and the conditions under which the stimulation was applied. Seven hours of intracortical microstimulation in feline sensorimotor cortex was shown to damage the electrodes at levels above 2 mC cm^{-2} [44]. These electrodes were constructed from iridium microwire, the tips were composed of activated iridium oxide film, and anodically biased biphasic pulses with a width of 400 μs were used for stimulation. With the same parameters of stimulation that were used in our experiments, but under acute conditions in physiological phosphate buffered saline, the maximum safe charge density for a SIROF UEA was estimated to be 2 mC cm^{-2} [52]. Levels that exceeded this value were needed to evoke percepts on some of our electrodes. The impedances and the voltage traces during stimulation of these electrodes, however, did not exhibit any obvious changes over time.

It is likely that the observed increase in stimulation thresholds over the course of the study is related to the chronic presence of the UEA in tissue or to changes that resulted at the electrode-tissue interface due to microstimulation. Even when stimulating at high current levels, we did not observe any catastrophic failures in the ability to evoke visual percepts. However, continuous chronic stimulation at these levels might eventually result in a failure to evoke percepts through alterations to the implanted tissue or the electrode array. One way to minimize these alterations might be to increase the surface

area of the electrodes by exposing more of the electrode tip during the manufacturing process. This would likely degrade spatial resolution acutely, but it would also decrease charge density and might improve chronic performance. In spite of the increasing thresholds, we show that every group of electrodes that evoked behavioural responses initially was able to evoke consistent responses throughout the duration of the study at levels that are unlikely to cause device failure. Further, repeated stimulation and the chronic presence of the UEA in tissue have not adversely affected the animal's vision or overall health.

Microstimulation using multiple electrodes

In this study, we showed that simultaneous stimulation of contiguous groups of microelectrodes was needed to produce consistent primate behavioural and feline motor responses and that the threshold level of stimulation per electrode decreased as electrode number increased. It appears, therefore, that a tradeoff between resolution and safety exists for this device under chronic conditions for use as a visual prosthesis. The question arises: What are the features of the percepts produced during multiple electrode stimulation using a chronically implanted UEA? Few studies have attempted to characterize the percepts evoked during stimulation of multiple microelectrodes in V1. One study in a human patient showed that two distinct phosphenes could be generated by simultaneously stimulating two nearby electrodes with a separation of 500 μm or more using currents near 50 μA [6]. This study also showed that simultaneous stimulation of multiple electrodes could be used to form simple visual patterns, such as a vertical line of phosphenes, and that less current was required to produce a visual percept when compared to stimulation of the individual constituent electrodes. Studies have looked at

the effective spread of current during microstimulation and found that the radius of activated tissue is proportional to the square root of the total current applied during stimulation [54]. At currents less than 100 μA, such as those used in many acute microstimulation experiments, the radius of activated tissue is predicted to be less than 500 μm and confined to a hypercolumn in V1. For our study, the average threshold for stimulation of groups of four and nine contiguous electrodes was 204 and 91 μA, respectively. Using these thresholds, the estimated current spread would be near or greater than the inter-electrode separation of 400 μm of the UEA. Due to the overlap in effective current between stimulated electrodes, the individual percepts during multiple electrode stimulation are likely to combine to form a single larger and possibly amorphous percept. In addition to the passive spread of current, the complex neuronal structure of V1 may introduce even more complexity to the resulting percept when stimulating multiple electrodes. Our results from the memory saccade experiment support the idea of a spatially diffuse and amorphous percept. We found that the scatter of saccades to electric targets during stimulation of nine contiguous electrodes was 2.0 times greater than that for photic targets. In a related chronic study, the scatter of electrically-evoked saccades during single electrode stimulation was found to be 2.5 times greater than for photic saccades [5]. One explanation for this difference may be that electrically-evoked saccades are inherently more imprecise than saccades to photic stimuli. It may also be that electrically-evoked percepts are more amorphous and spatially diffuse than the punctate photic stimuli used to guide saccades. In spite of the decreased saccade precision to electrically-evoked percepts, we were still able to show discrimination when stimulating separate groups of nine contiguous electrodes using a chronically implanted

UEA. The complex spatio-temporal nature of the percepts generated during multiple electrode stimulation of V1, however, is still not understood. Experiments to explore these characteristics appear to be the next logical step towards the development of a cortically-based visual prosthesis.

Conclusion

We have demonstrated several features associated with the chronic functionality of an array of penetrating microelectrodes implanted in V1 for use in a vision prosthesis. We have shown that this device is capable of evoking reliable visual percepts two years after implantation, and that photic thresholds, electrical thresholds, and impedances remained substantially stable over the course of the study. We have also shown that the subject can spatially discriminate the location of these visual percepts when separate regions of the array are stimulated. In order to reliably evoke visual percepts at safe current levels, it was necessary to expand the volume of cortex that was stimulated. This will likely reduce electrically-evoked visual acuity. However, it was still possible to evoke multiple spatially distinct phosphenes with a resolution comparable to the current epi-retinal prostheses. The spatial variance of saccades to electrically-evoked visual percepts suggests that these percepts may be spatially extended and amorphous rather than spatially restricted and punctate. To gain an in-depth understanding of the correlation between the spatio-temporal characteristics of cortical stimulation via multiple microelectrodes and the evoked visual percepts, it may be necessary to move into human experiments where a verbal description of the visual percepts is possible.

References

[1]   K. D. Frick, and A. Foster, "The magnitude and cost of global blindness: an increasing problem that can be alleviated," *Am. J. Ophthalmol.*, vol. 135, no. 4, pp. 471-6, Apr, 2003.

[2]   G. S. Brindley, and W. S. Lewin, "The visual sensations produced by electrical stimulation of the medial occipital cortex," *J. Physiol.*, vol. 196, no. 2, pp. 479-93, Feb, 1968.

[3]   W. H. Dobelle, and M. G. Mladejovsky, "Phosphenes produced by electrical stimulation of human occipital cortex, and their application to the development of a prosthesis for the blind," *J. Physiol.*, vol. 243, no. 2, pp. 553-76, Dec, 1974.

[4]   D. A. Pollen, "Some perceptual effects of electrical stimulation of the visual cortex in man," *The Nervous System*, vol. 2, pp. 519-28, 1975.

[5]   D. C. Bradley *et al.*, "Visuotopic mapping through a multichannel stimulating implant in primate V1," *J. Neurophysiol.*, vol. 93, no. 3, pp. 1659-70, Mar, 2005.

[6]   E. M. Schmidt *et al.*, "Feasibility of a visual prosthesis for the blind based on intracortical microstimulation of the visual cortex," *Brain*, vol. 119 (Pt 2), pp. 507-22, Apr, 1996.

[7]   K. Torab *et al.*, "Multiple factors may influence the performance of a visual prosthesis based on intracortical microstimulation: nonhuman primate behavioural experimentation," *J. Neural. Eng.*, vol. 8, no. 3, pp. 035001, Jun, 2011.

[8]   J. R. Bartlett *et al.*, "Psychophysics of electrical stimulation of striate cortex in macaques," *J. Neurophysiol.*, vol. 94, no. 5, pp. 3430-42, Nov, 2005.

[9]   E. A. DeYoe *et al.*, "Laminar variation in threshold for detection of electrical excitation of striate cortex by macaques," *J. Neurophysiol.*, vol. 94, no. 5, pp. 3443-50, Nov, 2005.

[10]   E. J. Tehovnik, and W. M. Slocum, "Depth-dependent detection of microampere currents delivered to monkey V1," *Eur. J. Neurosci.*, vol. 29, no. 7, pp. 1477-89, Apr, 2009.

[11]   P. J. Rousche, and R. A. Normann, "Chronic intracortical microstimulation (ICMS) of cat sensory cortex using the Utah Intracortical Electrode Array," *IEEE Trans. Biomed. Eng.*, vol. 7, no. 1, pp. 56-68, Mar, 1999.

[12]   P. J. Rousche, and R. A. Normann, "A method for pneumatically inserting an array of penetrating electrodes into cortical tissue," *Ann. Biomed. Eng.*, vol. 20, no. 4, pp. 413-22, 1992.

[13]   J. Kaas, and C. Collins, "The Primate Visual System," C. Press, ed., pp. 265-9, Boca Raton, FL: CRC Press, 2004.

[14]   P. K. Campbell *et al.*, "A silicon-based, three-dimensional neural interface: manufacturing processes for an intracortical electrode array," *IEEE Trans. Biomed. Eng.*, vol. 38, no. 8, pp. 758-68, Aug, 1991.

[15]   R. A. Normann *et al.*, "A neural interface for a cortical vision prosthesis," *Vision Res.*, vol. 39, no. 15, pp. 2577-87, Jul, 1999.

[16]   J. Baker *et al.*, "Multi-scale recordings for neuroprosthetic control of finger movements," *Conf. Proc. IEEE Eng. Med. Biol. Soc.*, pp. 4573-7, 2009.

[17]   N. Hatsopoulos *et al.*, "Cortically controlled brain-machine interface," *Conf. Proc. IEEE Eng. Med. Biol. Soc.*, vol. 7, no. 1, pp. 7660-3, 2005.

[18]   M. D. Linderman *et al.*, "Neural recording stability of chronic electrode arrays in freely behaving primates," *Conf. Proc. IEEE Eng. Med. Biol. Soc.*, vol. 1, pp. 4387-91, 2006.

[19]   M. Velliste *et al.*, "Cortical control of a prosthetic arm for self-feeding," *Nature*, vol. 453, no. 7198, pp. 1098-101, Jun 19, 2008.

[20]   S. J. Kim *et al.*, "Electrophysiological mapping of cat primary auditory cortex with multielectrode arrays," *Ann. Biomed. Eng.*, vol. 34, no. 2, pp. 300-9, Feb, 2006.

[21]   P. J. Rousche, and R. A. Normann, "Chronic recording capability of the Utah Intracortical Electrode Array in cat sensory cortex," *J. Neurosci. Methods,* vol. 82, no. 1, pp. 1-15, Jul 1, 1998.

[22]   T. Hillman *et al.*, "Cochlear nerve stimulation with a 3-dimensional penetrating electrode array," *Otol. Neurotol.*, vol. 24, no. 5, pp. 764-8, Sep, 2003.

[23]   S. J. Kim *et al.*, "Selective activation of cat primary auditory cortex by way of direct intraneural auditory nerve stimulation," *Laryngoscope,* vol. 117, no. 6, pp. 1053-62, Jun, 2007.

[24]   D. McDonnall *et al.*, "Selective motor unit recruitment via intrafascicular multielectrode stimulation," *Can. J. Physiol. Pharmacol.,* vol. 82, no. 8-9, pp. 599-609, Aug-Sep, 2004.

[25]   E. M. Maynard *et al.*, "A technique to prevent dural adhesions to chronically implanted microelectrode arrays," *J. Neurosci. Methods,* vol. 97, no. 2, pp. 93-101, Apr 15, 2000.

[26]   D. J. Warren *et al.*, "High-resolution two-dimensional spatial mapping of cat striate cortex using a 100-microelectrode array," *Neuroscience,* vol. 105, no. 1, pp. 19-31, 2001.

[27]   P. A. House *et al.*, "Acute microelectrode array implantation into human neocortex: preliminary technique and histological considerations," *Neurosurg. Focus,* vol. 20, no. 5, pp. 1-4, 2006.

[28]   C. J. Keller *et al.*, "Heterogeneous neuronal firing patterns during interictal epileptiform discharges in the human cortex," *Brain,* vol. 133, no. Pt 6, pp. 1668-81, Jun, 2010.

[29]   C. A. Schevon *et al.*, "Propagation of epileptiform activity on a submillimeter scale," *J. Clin. Neurophysiol.,* vol. 27, no. 6, pp. 406-11, Dec, 2010.

[30]   C. A. Schevon *et al.*, "Microphysiology of epileptiform activity in human neocortex," *J. Clin. Neurophysiol.,* vol. 25, no. 6, pp. 321-30, Dec, 2008.

[31]   C. A. Schevon *et al.*, "Spatial characterization of interictal high frequency oscillations in epileptic neocortex," *Brain,* vol. 132, no. Pt 11, pp. 3047-59, Nov, 2009.

[32]   A. Waziri *et al.*, "Initial surgical experience with a dense cortical microarray in epileptic patients undergoing craniotomy for subdural electrode implantation," *Neurosurgery,* vol. 64, no. 3, pp. 540-5, Mar, 2009.

[33]   L. R. Hochberg *et al.*, "Neuronal ensemble control of prosthetic devices by a human with tetraplegia," *Nature,* vol. 442, no. 7099, pp. 164-71, Jul 13, 2006.

[34]   S. P. Kim *et al.*, "Neural control of computer cursor velocity by decoding motor cortical spiking activity in humans with tetraplegia," *J. Neural Eng.,* vol. 5, no. 4, pp. 455-76, Dec, 2008.

[35]   C. L. Ojakangas *et al.*, "Decoding movement intent from human premotor cortex neurons for neural prosthetic applications," *J. Clin. Neurophysiol.,* vol. 23, no. 6, pp. 577-84, Dec, 2006.

[36]   W. Truccolo *et al.*, "Primary motor cortex tuning to intended movement kinematics in humans with tetraplegia," *J. Neurosci.*, vol. 28, no. 5, pp. 1163-78, Jan 30, 2008.

[37]   C. E. Vargas-Irwin *et al.*, "Decoding complete reach and grasp actions from local primary motor cortex populations," *J. Neurosci.*, vol. 30, no. 29, pp. 9659-69, Jul 21, 2010.

[38]   S. Shushruth *et al.*, "Comparison of spatial summation properties of neurons in macaque V1 and V2," *J. Neurophysiol.*, vol. 102, no. 4, pp. 2069-83, Oct, 2009.

[39]   S. F. Cogan, "Neural stimulation and recording electrodes," *Annu. Rev. Biomed. Eng.*, vol. 10, pp. 275-309, 2008.

[40]   T. S. Davis *et al.*, "A minimally invasive approach to long-term head fixation in behaving nonhuman primates," *J. Neurosci. Methods*, vol. 181, no. 1, pp. 106-10, Jun 30, 2009.

[41]   I. Mogyoros *et al.*, "Strength-duration properties of human peripheral nerve," *Brain*, vol. 119 (Pt 2), pp. 439-47, Apr, 1996.

[42]   S. F. Ronner, and B. G. Lee, "Excitation of visual cortex neurons by local intracortical microstimulation," *Exp. Neurol.*, vol. 81, no. 2, pp. 376-95, Aug, 1983.

[43]   E. J. Tehovnik *et al.*, "Microstimulation of V1 delays the execution of visually guided saccades," *Eur. J. Neurosci.*, vol. 20, no. 1, pp. 264-72, Jul, 2004.

[44]   S. F. Cogan *et al.*, "Over-pulsing degrades activated iridium oxide films used for intracortical neural stimulation," *J. Neurosci. Methods*, vol. 137, no. 2, pp. 141-50, Aug 30, 2004.

[45]   R. A. Parker *et al.*, "The functional consequences of chronic, physiologically effective intracortical microstimulation," *Prog. Brain Res.*, vol. 194, pp. 145-65, 2011.

[46]   M. Bak *et al.*, "Visual sensations produced by intracortical microstimulation of the human occipital cortex," *Med. Biol. Eng. Comput.*, vol. 28, no. 3, pp. 257-9, May, 1990.

[47]   D. K. Murphey, and J. H. Maunsell, "Behavioral detection of electrical microstimulation in different cortical visual areas," *Curr. Biol.*, vol. 17, no. 10, pp. 862-7, May 15, 2007.

[48]   J. P. Frampton *et al.*, "Effects of glial cells on electrode impedance recorded from neuralprosthetic devices in vitro," *Ann. Biomed. Eng.*, vol. 38, no. 3, pp. 1031-47, Mar, 2010.

[49]   R. W. Griffith, and D. R. Humphrey, "Long-term gliosis around chronically implanted platinum electrodes in the Rhesus macaque motor cortex," *Neurosci. Lett.*, vol. 406, no. 1-2, pp. 81-6, Oct 2, 2006.

[50]   D. McCreery *et al.*, "Neuronal loss due to prolonged controlled-current stimulation with chronically implanted microelectrodes in the cat cerebral cortex," *J. Neural. Eng.*, vol. 7, no. 3, pp. 036005, Jun, 2010.

[51]   S. R. Kane *et al.*, "Electrical performance of penetrating microelectrodes chronically implanted in cat cortex," *Conf. Proc. IEEE Eng. Med. Biol. Soc.*, vol. 2011, pp. 5416-9, 2011.

[52]   S. Negi *et al.*, "In vitro comparison of sputtered iridium oxide and platinum-coated neural implantable microelectrode arrays," *Biomedical materials*, vol. 5, no. 1, pp. 15007, Feb, 2010.

[53]   J. D. Weiland *et al.*, "In vitro electrical properties for iridium oxide versus titanium nitride stimulating electrodes," *IEEE Trans. Biomed. Eng.*, vol. 49, no. 12 Pt 2, pp. 1574-9, Dec, 2002.

[54]   E. J. Tehovnik *et al.*, "Phosphene induction and the generation of saccadic eye movements by striate cortex," *J. Neurophysiol.*, vol. 93, no. 1, pp. 1-19, Jan, 2005.

CHAPTER 5

CONCLUSION

This dissertation has provided an in-depth evaluation of the safety and efficacy of

V1 microstimulation via chronically implanted Utah Electrode Arrays (UEAs) in

macaque monkeys. Safety was evaluated by monitoring the stability of photic thresholds

and neural recordings over time and in response to stimulation. Photic thresholds for the

visual field locations represented by the cortex where the arrays were implanted were

found to be similar both before and after array implantation and microstimulation at

currents up to 96 µA. High-resolution visuotopic mapping of V1 was obtained by

measuring the receptive field locations using both the multi-unit activity and local field

potential signals across the UEA over a period of several months. It was found that

microstimulation did not result in functional impairment of the UEAs or the neural tissue

as indicated by the stability of both the photic thresholds and receptive field recordings

[1]. Similar results were observed from chronically implanted UEAs in the primary motor

cortex of cats. In these animals, microstimulation was performed at a level sufficient to

evoke EMG activity in the limb muscles. After chronic microstimulation, these UEAs

were still able to record action potentials and evoke EMG activity [2]. A further

assessment of safety comes from the observation that repeated stimulation and the

chronic presence of the UEA in tissue did not result in seizures or adversely affect the

animals' overall health.

Regarding efficacy, it was shown that shortly after implantation of the UEAs microstimulation was able to evoke phosphenes on a small number of individual electrodes using currents less than 100 μA [1]. After approximately one year of implantation, it was no longer possible to evoke visual percepts via individual electrodes. Increasing the spatial extent of microstimulation by simultaneously stimulating groups of four and nine contiguous electrodes, however, resulted in the ability to evoke visual percepts over time. A trend toward increasing levels of microstimulation was also observed. These spatial and temporal changes in stimulation thresholds may be related to gliotic encapsulation of the electrodes or other tissue responses to a foreign body. In spite of these changes, however, two years after implantation it was shown that discrimination of visual percepts with a resolution of approximately one degree could be achieved. This level of discrimination is comparable to the current epi-retinal prosthesis by Second Sight [3]. This dissertation demonstrates chronic perceptual functionality and provides evidence for the feasibility of a UEA-based vision prosthesis for the blind. There are, however, several problems that must be addressed before such a system can progress to a clinically-relevant prosthetic device.

<div align="center">Future Work</div>

Threshold levels for detection of microstimulation of V1 with the UEA were found to increase with time. Early after the implantation, percepts could be evoked with single electrode stimulation using currents below 100 μA. Near the end of the study, however, multiple contiguous groups of electrodes were required to evoke percepts at currents up to 300 μA. Other chronic microstimulation studies have reported increases in thresholds or a loss of functional electrodes with time [4, 5]. Many V1 microstimulation

studies have not reported an increase, but these studies were performed with either acute electrode placement or with chronic implantation of no more than 4 months [6-10]. This increase in threshold is likely related to device design and the complex interactions of the electrodes with the tissue. Optimization of the neural interface for better biocompatibility and stability, therefore, is needed to improve chronic performance. Studies have looked at ways to improve biocompatibility by treating the surfaces of microelectrodes with different coatings to minimize the foreign body response (FBR) [11-15]. Electrically conductive polymers combined with biomolecules for cell adhesion are being tested. Results demonstrate improved cell growth and adhesion, which may translate to a decreased FBR and improved longevity [11]. Electrodes coated with carbon nanotubes are being characterized for their ability to improve neural recordings, as well as, the delivery of charge during stimulation [13, 14]. Carbon nanotubes increase conductivity and charge injection capacity for stimulation. They also offer methods for the attachment of biomolecules that could be used to decrease FBR. One group has found that reducing the surface area of penetrating microelectrodes results in significantly less persistent macrophage activation, decreased blood brain barrier leakiness, and reduced neuronal cell loss, all features of the FBR [16]. Another way to improve biocompatibility might be to eliminate the concept of penetrating electrodes altogether. Revisiting the idea of surface stimulation and focusing on the optimization of electrodes to deliver charge from the surface might provide a way to improve chronic performance. Surface stimulation would also allow for the placement of electrodes in difficult to reach areas of cortex like the saggital sulcus where parafoveal and peripheral vision in humans is located. MicroECoG grids, like those by Ad-Tech Medical Instrument Corporation, are surface grids that

consist of platinum microwires embedded in a silicone substrate. These microECoG grids can be fabricated in a variety of configurations with microwire diameters ranging from 45 to 150 μm, inter-electrode spacing of one through several millimeters, and up to a total of 64 electrodes. They are designed to be placed under the dura and closely approximate the surface of the cerebral cortex. These types of grids have been chronically implanted in human patients and have been used to make recordings of local field potentials for decoding various speech and movement tasks [17, 18]. Microstimulation with the UEA to restore foveal vision and surface stimulation for the restoration of peripheral vision could be an optimal combination for achieving a high-resolution, functional V1 prosthesis.

Although there is a significant body of work to support the concept of V1 microstimulation for use as a prosthesis [1, 4, 6-10, 19-21], it is still unknown if complex spatio-temporal patterns of microstimulation can lead to visual percepts that can effectively provide useful information to the visually deprived brain. Even though we can reliably evoke visual percepts with V1 microstimulation in macaque monkeys, it has not been possible to get these animals to discriminate between patterns of microstimulation. It is also impossible to get macaque monkeys to report the qualities and subtle variations of microstimulation-evoked visual percepts. Future work must include experiments to understand the spatio-temporal nature and subtle qualities of patterned microstimulation. Experiments must be performed that determine the ability of subjects to identify objects on a table or to discriminate letters on a screen. It will also be important to understand if there is a component of learning associated with the performance of these types of tasks. Because of the complex and subjective nature of these experiments, they would be better conducted in human patients where verbal descriptions of the visual percepts can be

recorded. It is likely that performing experiments in human patients will result in a significant advance in our understanding of patterned cortical microstimulation and in the development of a cortically-based visual prosthesis.

Currently, visual prostheses based on electrical stimulation of the visual pathways are at best able to provide a very simple visual experience by evoking patterns of phosphenes. This limited degree of vision restoration is still useful to blind individuals. It would be better, however, if it were possible to restore a much richer visual experience that approximated natural vision rather than using unnatural phosphenes to paint crude pixelated images. To achieve this goal, it would be necessary to selectively activate individual neurons within neural circuits of the visual pathway with high spatial and temporal precision. This may be possible with a technique known as optogenetics. Optogenetics introduces into neurons light-sensitive proteins that regulate ion conductance and allow optical excitation or inhibition of specific neuron types with different wavelengths of light. This technique has been applied in many behavioral and physiological studies in rodents [22-26]. For this technique to be successfully implemented in the development of a visual prosthesis in humans, extensive testing must first be performed in nonhuman primate models. Viral vectors with cell-specific promoters for the different retinal and cortical cell types would need to be developed. Different opsins with absorbance spectra that enable differential and simultaneous neural activation would need to be delivered by these vectors. Photonic hardware would be needed to provide optical stimulation to retina and cortex with great spatial, temporal, and wavelength specificity. In order to provide naturalistic vision, biomimetic algorithms would also be necessary to translate video images to control signals for the photonic

hardware. This work would require the efforts of a multidisciplinary team working in parallel. With testing and validation performed chronically in nonhuman primates, there would be a clear path to human applications. Fortunately, some of this work has already begun, and some groups are beginning to test these methods in the cortex of behaving nonhuman primates [27, 28]. If an optogentic-based visual prosthesis could be achieved, the impact would revolutionize the treatment of blindness. This would likely make it possible to restore high acuity naturalistic vision with detailed color and texture. It would also provide a tool to map the functions of the neural circuitry underlying visual processing as it progresses from the retina to the cerebral cortex.

Interfacing with the nervous system to restore sight to the blind represents an emerging and promising frontier in modern science. Sensory neural prosthetic approaches have already allowed thousands of deaf patients to hear sounds and acquire language abilities. Current visual prosthetic approaches have enabled blind patients to recognize individual alphanumeric characters and to achieve limited visual navigation. Although these results are exciting, there is still much progress to be made. In spite of the many challenges, however, the future of visual prosthetics will unquestionably provide a life changing experience to thousands of individuals that are affected by the debilitating disease of blindness.

References

[1]   K. Torab *et al.*, "Multiple factors may influence the performance of a visual prosthesis based on intracortical microstimulation: nonhuman primate behavioural experimentation," *J. Neural. Eng.*, vol. 8, no. 3, pp. 035001, Jun, 2011.

[2]   R. A. Parker *et al.*, "The functional consequences of chronic, physiologically effective intracortical microstimulation," *Prog. Brain Res.*, vol. 194, pp. 145-65, 2011.

[3]   M. S. Humayun *et al.*, "Interim results from the international trial of Second Sight's visual prosthesis," *Ophthalmology,* vol. 119, no. 4, pp. 779-88, Apr, 2012.

[4]   J. R. Bartlett *et al.*, "Psychophysics of electrical stimulation of striate cortex in macaques," *J. Neurophysiol.,* vol. 94, no. 5, pp. 3430-42, Nov, 2005.

[5]   P. J. Rousche, and R. A. Normann, "Chronic intracortical microstimulation (ICMS) of cat sensory cortex using the Utah Intracortical Electrode Array," *IEEE Trans. Biomed. Eng.,* vol. 7, no. 1, pp. 56-68, Mar, 1999.

[6]   M. Bak *et al.*, "Visual sensations produced by intracortical microstimulation of the human occipital cortex," *Med. Biol. Eng. Comput.,* vol. 28, no. 3, pp. 257-9, May, 1990.

[7]   E. A. DeYoe *et al.*, "Laminar variation in threshold for detection of electrical excitation of striate cortex by macaques," *J. Neurophysiol.,* vol. 94, no. 5, pp. 3443-50, Nov, 2005.

[8]   D. K. Murphey, and J. H. Maunsell, "Behavioral detection of electrical microstimulation in different cortical visual areas," *Curr. Biol.,* vol. 17, no. 10, pp. 862-7, May 15, 2007.

[9]   E. M. Schmidt *et al.*, "Feasibility of a visual prosthesis for the blind based on intracortical microstimulation of the visual cortex," *Brain,* vol. 119 (Pt 2), pp. 507-22, Apr, 1996.

[10]   E. J. Tehovnik, and W. M. Slocum, "Depth-dependent detection of microampere currents delivered to monkey V1," *Eur. J. Neurosci.,* vol. 29, no. 7, pp. 1477-89, Apr, 2009.

[11]   X. Cui *et al.*, "Surface modification of neural recording electrodes with conducting polymer/biomolecule blends," *J. Biomed. Mater. Res.,* vol. 56, no. 2, pp. 261-72, Aug, 2001.

[12]   J. J. Pancrazio, "Neural interfaces at the nanoscale," *Nanomedicine,* vol. 3, no. 6, pp. 823-30, Dec, 2008.

[13]   R. A. Parker *et al.*, "The use of a novel carbon nanotube coated microelectrode array for chronic intracortical recording and microstimulation," *Conf. Proc. IEEE Eng. Med. Biol. Soc.,* 2012.

[14]   C. M. Voge, and J. P. Stegemann, "Carbon nanotubes in neural interfacing applications," *J. Neural. Eng.,* vol. 8, no. 1, pp. 011001, Feb, 2011.

[15]   R. Wadhwa *et al.*, "Electrochemically controlled release of dexamethasone from conducting polymer polypyrrole coated electrode," *J. Control. Release,* vol. 110, no. 3, pp. 531-41, Feb 21, 2006.

[16]   J. L. Skousen *et al.*, "Reducing surface area while maintaining implant penetrating profile lowers the brain foreign body response to chronically implanted planar silicon microelectrode arrays," *Progress in Brain Research,* vol. 194, pp. 167-80, 2011.

[17]   S. Kellis *et al.*, "Decoding spoken words using local field potentials recorded from the cortical surface," *Journal of neural engineering,* vol. 7, no. 5, pp. 056007, Oct, 2010.

[18]   S. S. Kellis *et al.*, "Human neocortical electrical activity recorded on nonpenetrating microwire arrays: applicability for neuroprostheses," *Neurosurgical focus,* vol. 27, no. 1, pp. E9, Jul, 2009.

[19]   D. C. Bradley *et al.*, "Visuotopic mapping through a multichannel stimulating implant in primate V1," *J. Neurophysiol.,* vol. 93, no. 3, pp. 1659-70, Mar, 2005.

[20]   T. S. Davis *et al.*, "Spatial and temporal characteristics of V1 microstimulation during chronic implantation of a microelectrode array in a behaving macaque," *J. Neural. Eng.,* vol. 9, no. 6, pp. 065003, Dec, 2012.

[21]   P. H. Schiller *et al.*, "New methods devised specify the size and color of the spots monkeys see when striate cortex (area V1) is electrically stimulated," *Proc. Natl. Acad. Sci. USA,* vol. 108, no. 43, pp. 17809-14, Oct 25, 2011.

[22]   A. R. Adamantidis *et al.*, "Neural substrates of awakening probed with optogenetic control of hypocretin neurons," *Nature,* vol. 450, no. 7168, pp. 420-4, Nov 15, 2007.

[23]   R. D. Airan *et al.*, "Temporally precise in vivo control of intracellular signalling," *Nature,* vol. 458, no. 7241, pp. 1025-9, Apr 23, 2009.

[24]   A. M. Aravanis *et al.*, "An optical neural interface: in vivo control of rodent motor cortex with integrated fiberoptic and optogenetic technology," *Journal of neural engineering,* vol. 4, no. 3, pp. S143-56, Sep, 2007.

[25]   V. Gradinaru *et al.*, "Optical deconstruction of parkinsonian neural circuitry," *Science,* vol. 324, no. 5925, pp. 354-9, Apr 17, 2009.

[26]   H. C. Tsai *et al.*, "Phasic firing in dopaminergic neurons is sufficient for behavioral conditioning," *Science,* vol. 324, no. 5930, pp. 1080-4, May 22, 2009.

[27]   I. Diester *et al.*, "An optogenetic toolbox designed for primates," *Nature neuroscience,* vol. 14, no. 3, pp. 387-97, Mar, 2011.

[28]   X. Han *et al.*, "Millisecond-timescale optical control of neural dynamics in the nonhuman primate brain," *Neuron,* vol. 62, no. 2, pp. 191-8, Apr 30, 2009.